J-910900-3

Development and Tests of Small Fused Silica Models of Transparent Walls for the Nuclear Light Bulb Engine

NASA Contract No. SNPC-70

UNITED AIRCRAFT CORPORATION

United Aircraft Research Laboratories

EAST HARTFORD, CONNECTICUT

United Aircraft Research Laboratories

UNITED AIRCRAFT CORPORATION

EAST HARTFORD, CONNECTICUT

J-910900-3

Development and Tests of Small Fused Silica Models of Transparent Walls for the Nuclear Light Bulb Engine

NASA Contract No. SNPC-70

REPORTED BY Paul G. Vogt
Paul G. Vogt

APPROVED BY James W. Clark
James W. Clark, Chief
Fluid and Systems Dynamics

DATE September 1970

NO. OF PAGES 92

COPY NO. 28

FOREWORD

An exploratory experimental and theoretical investigation of gaseous nuclear rocket technology is being conducted by the United Aircraft Research Laboratories under Contract SNPC-70 with the joint AEC-NASA Space Nuclear Propulsion Office. The Technical Supervisor of the Contract for NASA is Captain C. E. Franklin (USAF). Results of portions of the investigation conducted during the period between September 16, 1969 and September 15, 1970 are described in the following eight reports (including the present report) which comprise the required first Interim Summary Technical Report under the Contract:

1. Klein, J. F. and W. C. Roman: Results of Experiments to Simulate Radiant Heating of Propellant in a Nuclear Light Bulb Engine Using a D-C Arc Radiant Energy Source. United Aircraft Research Laboratories Report J-910900-1, September 1970.

2. Jaminet, J. F. and A. E. Mensing: Experimental Investigation of Simulated-Fuel Containment in R-F Heated and Unheated Two-Component Vortexes. United Aircraft Research Laboratories Report J-910900-2, September 1970.

3. Vogt, P. G.: Development and Tests of Small Fused Silica Models of Transparent Walls for the Nuclear Light Bulb Engine. United Aircraft Research Laboratories Report J-910900-3, September 1970. (present report)

4. Roman, W. C.: Experimental Investigation of a High-Intensity R-F Radiant Energy Source to Simulate the Thermal Environment in a Nuclear Light Bulb Engine. United Aircraft Research Laboratories Report J-910900-4, September 1970.

5. Bauer, H. E., R. J. Rodgers and T. S. Latham: Analytical Studies of Start-Up and Dynamic Response Characteristics of the Nuclear Light Bulb Engine. United Aircraft Research Laboratories Report J-910900-5, September 1970.

6. Latham, T. S. and H. E. Bauer: Analytical Studies of In-Reactor Tests of a Nuclear Light Bulb Unit Cell. United Aircraft Research Laboratories Report J-910900-6, September 1970.

7. Palma, G. E. and R. M. Gagosz: Optical Absorption in Transparent Materials During 1.5 Mev Electron Irradiation. United Aircraft Research Laboratories Report J-990929-1, September 1970.

8. Krascella, N. L.: Analytical Study of the Spectral Radiant Flux Emitted from the Fuel Region of a Nuclear Light Bulb Engine. United Aircraft Research Laboratories Report J-910904-1, September 1970.

Report J-910900-3

Development and Tests of Small Fused Silica Models of Transparent Walls for the Nuclear Light Bulb Engine

TABLE OF CONTENTS

TABLE OF CONTENTS (Continued)

Report J-910900-3

Development and Tests of Small Fused Silica Models of Transparent Walls for the Nuclear Light Bulb Engine

SUMMARY

A program was conducted to develop and test small fused silica models of transparent walls for the nuclear light bulb engine. The principal objectives were (1) to develop fabrication techniques for constructing models using thin-walled fused silica tubing, (2) to arrive at model configurations which provide satisfactory vortex flow patterns, and (3) to test these models in a thermal environment similar to that in the engine.

The transparent wall in the engine surrounds the fuel region and separates it from the annular propellant duct. A vortex, driven by a transparent buffer gas, is employed to isolate the fuel from the wall. The wall is internally cooled and has provision for circumferential injection of buffer gas to drive the vortex.

Fused silica models having axial coolant tubes (i.e., coolant tubes aligned with the axis of the vortex) were fabricated using tubes with wall thicknesses down to 0.005 in. A potting technique based on the use of silicone rubber sealant (RTV) was the most effective of three methods developed for joining the tubes to coolant manifolds at the ends of the model. These axial-coolant-tube models were tested using the UARL 1.2-megw r-f induction heater where an argon plasma was used as a source of thermal radiation (analogous to radiation from the fuel in the engine, although at lower flux levels). By using improved methods for circumferential gas injection with resultant improvements in the vortex flow, the amount of heat deposited in the transparent walls by conduction and convection was reduced to 30 percent of that in previous tests. The maximum radiation flux levels used were limited by overheating of the water-cooled copper injectors due to all three modes of heat transfer, rather than by any limitations of the transparent walls. Significant increases in radiation flux can be obtained by modifying the vortex injector configuration to increase its cooling capability. Improvement in the flow pattern within the models also can be obtained which will result in a further reduction in the levels of conduction and convection heat transfer to the model inner walls.

In related work, fused silica tubes having 0.005-in. wall thicknesses were also formed into shapes suitable for circumferential-coolant-tube models by sagging straight tubes into a mold at elevated temperatures. Optical transmission characteristics of arrays of coolant tubes were measured, and procedures for predicting heat transfer rates and stresses in the tubes were developed.

RESULTS AND CONCLUSIONS

1. Significant progress was made in the development of small, internally cooled, fused silica models similar to the transparent walls of the nuclear light bulb engine. The following are the major fabrication results achieved:

   a. Axial-coolant-tube models were fabricated with a range of inside diameters between 0.846 and 1.55 in. using fused silica tubing having individual internal diameters of 0.040 in. to 0.050 in. and wall thicknesses down to 0.005 in. A potting technique, based on a silicone rubber sealant (RTV), was developed for joining the tubes to manifolds at the ends of the model.

   b. Fused silica tubes with wall thicknesses down to 0.005 in. were formed using an oven sagging method into shapes suitable for use as circumferential coolant tubes. Straight tubes were sagged into ceramic molds in a process requiring short times in the oven at 2400 F.

2. Flow visualization tests using lucite models with water and dye led to the following major results:

   a. An array of copper hypo-tube injectors positioned such as to provide injection as nearly circumferentially as possible along the periphery of the model resulted in an apparent reduction in the turbulence due to injection, compared with several other methods tested. These injector tubes had large ratios of tube length-to-diameter and were either flush with the wall or projected into the vortex flow slightly.

   b. An improved flow pattern was obtained by sealing the gaps between the axial coolant tubes, thus eliminating radially outward flow into the annulus surrounding the model.

3. Tests with axial-coolant-tube models in the 1.2-megw r-f induction heater resulted in the following levels of performance:

   a. The maximum power deposited in the r-f discharge in these tests was approximately 36 kw. The maximum radiation fluxes at the transparent wall were on the order of 1.0 kw/in.^{2} (compared with 151 kw/in.^{2} in the engine).* These maximum values were limited by localized melting

*The maximum total heat flux deposited in the transparent-wall models in these tests was on the order of 25 percent of the flux deposited in the transparent wall of the engine.

of the copper hypo-tube vortex injectors rather than by any limitation of the transparent wall. To obtain further increases, it will be necessary to protect the injectors from conduction and convection heating entirely, and to improve the removal of heat deposited by absorption of radiation.

b. The average value of the power deposited in the transparent-wall coolant tubes divided by the total power in the r-f discharge, Q_C/Q_T, was reduced to approximately 0.15, compared with 0.53 in previous tests. This reduction was the result of an improved method of vortex injection which reduced the turbulence level and thus reduced conduction and convection heating of the model.

c. The average value of the power deposited in the injector tubes divided by the total power in the r-f discharge, Q_{INJ}/Q_T, increased to approximately 0.10, compared with 0.02 in previous tests. Approximately 0.006 to 0.01 of this increase is due to absorption of radiation in the increased amount of opaque material (copper) used in the hypo-tube injectors, compared with the previous injectors (holes drilled in injection manifolds, rather than an array of tubes). The remaining increase in power deposition is attributed to the combined effects of conduction, convection, and direct r-f heating.

d. The average value of power radiated through the model coolant tubes divided by the total power in the r-f discharge, $(Q_{ANN} + Q_{RAD})/Q_T$, was about the same (0.30) as in previous tests. To increase the fraction of radiated power, higher pressures and/or higher discharge temperatures must be obtained.

e. The average value of power deposited in the end walls and exhaust thru-flow ducts divided by the total power in the r-f discharge, $(Q_{EW} + Q_{TF})/Q_T$, increased to about 0.45, compared with 0.15 in previous tests. This increase is an indirect result of the reduction in the turbulence level near the model peripheral wall (i.e., energy that previously was conducted and convected to the peripheral wall is now conducted and convected to the end wall and thru-flow duct).

SECTION I

INTRODUCTION

Research directed toward determining the feasibility of the nuclear light bulb type of gaseous core nuclear rocket engine is being conducted by the United Aircraft Research Laboratories under Contract SNPC-70 administered by the joint AEC-NASA Space Nuclear Propulsion Office. In this engine concept, heat is transferred from gaseous fissioning uranium fuel through an internally cooled transparent wall to hydrogen propellant seeded with tungsten. A transparent buffer gas (neon) is injected at the inner surface of the transparent wall to form a vortex which isolates the fuel from the wall. Because of the high temperatures obtainable in the gaseous fuel, engines of this type can theoretically provide specific impulses of 1500 to 3000 sec and thrust-to-weight ratios greater than one. The concept is also attractive because the physical barrier between the fuel and propellant offers the possibility of perfect containment of fuel and fission products. A reference version of this engine has been designed and consists of a cluster of seven unit cavities similar to the one shown schematically in Fig. 1. Additional details of the nuclear light bulb concept are discussed in Ref. 1.

This report describes the present status of the transparent-wall model program. The primary objective of this program is to develop and test small internally cooled transparent walls similar to those which may be employed in a nuclear light bulb engine. A summary of the physical dimensions and operating conditions of the models employed in the tests is given in Table I. Also shown in Table I are corresponding physical dimensions and operating conditions for the reference nuclear light bulb engine. As noted in Table I, the transparent wall structure for each unit cavity is 1.604 ft in diameter by 6.0 ft long. The size of the structure combined with the requirements for a thin wall, internal cooling, and buffer-gas injection make most types of transparent-wall structures unsuitable. The bursting stress due to coolant pressure drop in a 6.0 ft length precludes use of a single concentric tube or coiled structure. The most suitable structure would consist of a number of small diameter, thin-walled tubes (refer to Table I) formed in a circumferential arrangement with provision for buffer-gas injection as shown in section A-A of Fig. 1.

The walls of the engine, as presently envisioned, will be made from high purity fused silica. High purity (consequently, high transmission) is necessary to minimize the thermal radiation deposition in the walls. Refer to Table II of Ref. 2 for the transmission characteristics of fused silica. The opacity of the transparent wall in the ultraviolet portion of the spectrum is the primary factor governing radiant heat deposition in the transparent wall. Substitution of single-crystal beryllium oxide for fused silica as the transparent-wall material might result in a significant

reduction in the ultraviolet cutoff wavelength and a corresponding increase in permissible fuel radiating temperature (Ref. 3). Also, synthetic quartz crystals have been successfully grown with ultraviolet cutoffs down to 0.147 micron (Ref. 4). However, the difficulty in growing single-crystal beryllium oxide or quartz as well as the handling and forming operations required to put them in a usable form preclude their use at the present time. Another method for reducing the wall heat deposition is to seed the coolant vortex buffer gas with a material (e.g., oxygen) which absorbs in the ultraviolet portion of the spectrum, yet passes thermal radiation in portions of the spectrum where the wall has high transmission characteristics (Ref. 3).

The walls of the engine must be internally cooled to remove heat deposited by radiation, conduction and convection. Hydrogen will be employed as the wall coolant due to its high heat capacity and radiation transmission at low temperatures. The walls must be thin (approximately 0.005 in.) to conduct the heat to the coolant with a suitable wall temperature drop. The inner wall temperature must be high enough (about 800 C) to allow thermal annealing to reduce coloration opacity due to neutron damage, yet low enough to maintain high wall strength and minimize devitrification (which normally occurs in fused silica at temperatures above 1100 C). Therefore, the temperature of the wall must be maintained between relatively narrow limits. However, results of recent experiments described in Ref. 5 indicate that ionizing radiation and optical bleaching of the fused silica may enable a greater wall temperature difference (ΔT of approximately 900 R (500 C)) to be used. In the engine calculations (Ref. 3), the allowable temperature difference across the wall was assumed to be 200 R (111 C). The total heat deposited in the wall as noted in Table I is about equally divided between heating from the propellant region and heating from the fuel region. Re-radiation from the propellant region was neglected since the temperature along most of the propellant duct length is considerably less than the radiating temperature of the gaseous nuclear fuel. It is anticipated that the temperature at the exit of the propellant passage will be equal to 80 percent of the radiating temperature from the nuclear fuel.

The walls of the engine will also have provision for tangential injection to create a vortex flow which provides a buffer layer between the nuclear fuel and the transparent walls. The use of a buffer layer serves three purposes: (1) it minimizes heat deposition in the walls by conduction and convection, (2) it minimizes both wall heat deposition and wall discoloration by fission fragments from the nuclear fuel, and (3) it minimizes the possibility of condensation of the low-vapor-pressure nuclear fuel on the transparent wall. Neon will probably be employed as the buffer gas due to its high density for improving the stability of the vortex flow and its high transparency to thermal radiation from the fuel region. As noted in Fig. 1, the injected buffer flow spirals towards the end walls of the unit cavity and down the end walls in the secondary-flow region toward the centerline. This flow pattern is typical of a radial-inflow vortex. After leaving the unit cavity, heat

is removed from the buffer flow to condense both the nuclear fuel and a major portion of the entrained fission products. The buffer flow and condensed nuclear fuel will be recycled during engine operation.

The region outside of the transparent wall contains seeded hydrogen propellant flow. The innermost flow will consist of an unseeded buffer layer of hydrogen along the transparent wall to keep the seeds (tungsten particles) off the wall. Deposition of tungsten on the fused silica wall could result in a chemical reaction with, or devitrification of, the wall.

The main text of this report describes the basic techniques developed for fabrication of fused silica models (Section III) and the results of tests employing these models (Section IV). A summary of the physical properties of fused silica is given in Section II. The Appendixes describe measurements of the optical transmission characteristics of thin-wall fused silica tubes (Appendix A), procedures used in heat transfer and stress analyses (Appendix B), and the vortex flow parameters (Appendix C).

SECTION II

PHYSICAL CHARACTERISTICS OF FUSED SILICA

Fused silica (also known as fused quartz) is made either by heating high purity, naturally occurring quartz crystals to a temperature of approximately 1800 C to produce an amorphous condition or, by chemically reacting silicon compounds with oxygen. Transparent fused silica, typical of that used in this program, nominally has a purity of 99.97 to 99.98 percent SiO_2. Alumina (AL_2O_3) is the major impurity, usually accounting for about two-thirds of the total impurity content. Higher purity fused silica (e.g., General Electric Type 151 or Corning Type 7940) nominally has a 99.997 percent SiO_2 content.

Chemical Reaction

Most acids, metals, chlorine, and bromine are unreactive with fused silica at room temperature. Hydrofluoric acid is reactive with fused silica at all temperatures. Carbon and some metals reduce fused silica and basic oxides, carbonates, sulfates, etc., react with it at elevated temperatures.

Devitrification

Fused silica will undergo devitrification at elevated temperatures. When fused silica devitrifies, as described in Ref. 6, the original product is β or high cristobalite. Nucleation occurs on the surface or at an interface between the fused silica and some other material, such as a metal. A devitrified surface while still hot will appear clear, just as it appeared prior to heating. On cooling, a hazy film develops on the surface. This haze develops as the surface cools below about 250 C and consists of a maze of very fine cracks. These cracks are the results of a large volume change in the devitrified layer. Completely devitrified fused silica falls apart, like ashes from a fire, upon handling. The rate of devitrification depends upon the temperature and whether foreign material is in contact with the fused silica. Above 1000 C the devitrification rate increases with increasing temperature. At 1450 C, appreciable devitrification can occur in a relatively short time. When it is desired to use fused silica for prolonged times at temperatures in excess of 1000 C, it is advisable to maintain the devitrified fused silica at an elevated temperature to supress the surface cracking. Contamination of fused silica which also leads to higher devitrification rates can be in just about any form. Alkaline salt solutions or vapors are particularly bad. Handling of the fused silica with bare

hands deposits sufficient alkali from perspiration to leave clearly defined fingerprints upon devitrification. Also, drops of water allowed to stand on the surface may collect enough contamination from the air to promote devitrified spots and water marks.

Dissociation

Heating of fused silica to temperatures above approximately 1350 C causes the SiO_2 to undergo dissociation (or sublimation). Consequently, when flame-working fused silica, one observes a band of haze (or smoke) forming just outside of the intensely heated region. This haze or smoke forms presumably by the process of SiO recombining with oxygen from the air (and perhaps water) and condensing as extremely small particles of amorphous SiO_2. The haze can be removed from the surface by a gentle heating in the oxy-hydrogen flame. Dissociation is greatly enhanced when fused silica is heated in a reducing atmosphere. For example, the proximity of graphite during heating will cause rapid dissociation of the SiO_2.

Optical Transmission

Clear fused silica has one of the best transmission characteristics commercially available. In the wavelength range from 0.30 to 2.5 microns it is virtually 100 percent transparent to all radiation (Ref. 6). Its ultraviolet cutoff at 50 percent transmission ranges from 0.17 to 0.21 microns (for 1-cm thickness) depending upon the purity of the fused silica. Its infrared cutoff at 50 percent transmission is 3.55 microns. Some fused silica has an absorption band from 2.6 to 2.9 microns, due to the presence of water (hydroxyls) in the fused silica. The magnitude of the absorption is dependent upon the quantity of water present. Irradiation of fused silica by high-energy radiations (such as X-rays, gamma rays, neutrons, and electrons) will induce certain absorption bands in some materials. For instance, in Corning 7940 grade fused silica, absorption bands will occur at 0.165 and 0.215 microns (Ref. 7). However, when absorptions are induced, they can be bleached by heating (Ref. 5).

Electrical Properties

Fused silica has excellent electrical properties which remain relatively constant with temperature. The electrical resistivity is on the order of 10^{17} ohms/cc between 25 C and 1000 C. One of the unique properties is the extremely low dissipation factor (less than 0.0001 at 20 C, and 1 MHz). The dissipation factor is an

indication of the amount of r-f power which would be picked up by the material. The higher the dissipation factor, the higher the r-f power deposition. Thus, the low dissipation factor of fused silica makes it suitable for use in an r-f environment.

Mechanical Strength

Fused silica has good mechanical strength. Its compressive strength is greater than 160,000 psi, and its nominal tensile strength is greater than 7000 psi. Tensile strengths, however, of 1 or 2 x 10^6 psi have been measured in the laboratory, but these are flaw-free values. Under normal manufacturing and handling, the prevention of microscopic surface flaws is essentially impossible. The surface flaws produce stress concentrations and, hence, the normal values of tensile strength for commercial fused silica are in the range of 10,000 to 20,000 psi, and vary only slightly with composition (Ref. 8). A value of 7000 psi is considered the standard nominal value for the tensile strength of fused silica used in this program. Components were designed with a safety factor of 7, i.e., for a 1000 psi maximum working stress. The modulus of elasticity is approximately 10^7 psi. Fused silica is one of the most perfectly elastic materials known. Fibers of this material used as galvanometer suspensions sustain large angles of deflection (twist) and yet return the instrument reading to zero after the deflection.

Thermal Properties

Fused silica has an extremely low coefficient of thermal expansion, 0.55 x 10^{-6} cm/cm/deg C (0 - 300 C). This makes it possible to subject fused silica to extremely large temperature gradients and heating rates. It can be heated rapidly to above 1500 C and then plunged into water without cracking. The softening point of fused silica has been variously reported from 1500 to 1670 C. The softening point varies due to the differences in the definition of the softening point as well as to the method of fusion. Materials having a low softening point usually contain appreciable quantities of water as hydroxyl groups. The higher softening points occur in materials which are essentially water-free. The annealing and strain points of fused silica have been determined as 1140 C and 1070 C, respectively. The effect of water content of the fused silica on the annealing and strain points is not as great as on the softening point.

SECTION III

BASIC FABRICATION TECHNIQUES EMPLOYED IN PROGRAM

This section describes the techniques employed in the fabrication of fused silica axial-coolant-tube transparent-wall models. These techniques include drawing and cutting of fused silica tubes, fabricating model manifolds and injectors, and connecting the tubes to the manifolds. The primary model components consist of coolant tubes, manifolds, and injectors and are discussed separately. Several types of models (described later) are illustrated in Fig. 2 to show the location of the various model components. In addition, discussion of the techniques employed in the fabrication of circumferential-coolant-tube segments and recommendations for future fabrication development are also presented.

Fused Silica Coolant Tubes

Drawing

Fused silica tubing, used for model coolant tubes, is drawn either vertically upward (updrawn), vertically downward (downdrawn), or horizontally (Velbo or Danner) from molten fused silica (Ref. 9). Many factors --- drawing speed, temperature control, mechanical vibrations, etc. --- influence the quality of the drawn tubing. Typical variations found in drawn fused silica tubing are shown in Fig. 3. Two tubes drawn to a nominal 0.050-in.-ID by 0.060-in.-OD (0.005-in. wall) specification are shown in Figs. 3(a) and 3(b). Tube B, which was judged to be dimensionally unsuitable for use in a model, is 42 percent larger than the nominal diameter and its diameter varies considerably along the tube length. A suitable tube (i.e., tube A) has diameter variations within approximately 10 percent of the nominal value over the length required for a model (usually 6 in.). The smallest sized tubing commercially available off-the-shelf is 0.0394-in.-ID by 0.0787-in.-OD (1-mm-ID by 2-mm-OD), which has a wall thickness of 0.020 in. (Ref. 6). Smaller tubes (i.e., thinner walls) are drawn from larger tubing on request. Since the demand for these thinner-walled tubes is small, the techniques for properly drawing these tubes are not widely developed. Figure 3(c) shows the cross-sectional views of three tubes. The nominal 0.005-in.-wall tube is highly out-of-round. The techniques developed to date have resulted in commercial availability of tubing with close tolerances and wall thicknesses down to 0.010 in. As the need increases, fused silica tubing with wall thicknesses down to 0.005 in. with close tolerances will also become commercially available.

Cutting

Cutting fused silica tubing without chipping or cracking the ends is a delicate operation. This is especially true when a number of thin-wall tubes lying side-by-side are to be cut at once. Movement of the tubes during the cutting process will result in breakage. To reduce this problem, a procedure has been used to keep the tubes stationary during the cutting process. This procedure consists of encapsulating the fused silica tubes with wax and then cutting after the wax solidifies. This procedure is shown in Fig. 4(a) for tubes connected to an injector manifold (see following description of vortex injectors) and in Fig. 4(b) for tubes not attached. The wax (a mixture of beeswax and rosin) is heated to its melting point (150 F) and then poured between the glass plates and around the fused silica tubes (Fig. 4(a)). The wax is not allowed near the ends of the tubes, otherwise capillary action will cause the wax to fill the tubes. The wax solidifies upon cooling to room temperature. The solid block was then cut as shown in Figs. 4(a) and 4(b) with a diamond wheel (Norton No. D220-N50M-1/16 1AIR). After cutting, the solid block is heated on a hot plate to remove the wax. Any remaining wax is removed with trichloroethylene solvent. The only difference between this procedure and that used for loose tubes (Fig. 4(b)) is that masking tape is used to hold down the tubes and wax flakes are placed on the tubes before heating to more accurately control the wax flow. This procedure of cutting has been successfully applied to tubes with wall thicknesses down to 0.005 in.

Cleaning

The cleaning procedure used in this program involves washing the fused silica in a 10 percent hydrofluoric acid solution at room temperature for 3 to 5 minutes. This is then followed by several rinses in distilled water, removal of the excess water and rapid drying.

Procedure for Measurement of Wall thickness

It is important that the tubes have a uniform wall thickness since local variations could result in "hot spots" where the wall is thick or structurally weak areas where the wall is thin. Thus, an accurate measurement of the wall thickness is desirable. A more accurate procedure of measuring the wall thickness than was used previously (Ref. 10) was developed. This procedure consists of using a microscope and a dial indicator (Fig. 4(c)). First, a sample of the tube was cut into 2-in. lengths. One tube segment at a time was mounted on a vee block and measured as shown in Fig. 4(c). The measurement was made using a 100x microscope mounted on a height gage and focused on the tube. A dial indicator with 0.00005-in. divisions was mounted on another height gage. The cross-hairs of the microscope were aligned with the inner wall of the tube and then the dial indicator was zeroed on

a flat surface ridgidly connected to the microscope. The microscope was raised by adjusting the height gage vertical locator until the cross-hairs were aligned with the outer wall of the tube as shown in section A-A of Fig. 4(c). The reading on the dial indicator corresponds to the tube wall thickness. This procedure has been successfully applied to tubes with 0.005-in. nominal wall thickness.

Typical Dimensions and Tolerances as Received From Vendors

The dimensional characteristics of samples of drawn tubing measured as described above are shown in Table II. Tubes were obtained from several vendors and were of both commercial and high purity grades. The nominal wall thicknesses specified were 0.005 in., 0.010 in., and 0.020 in. For a given vendor, the average/nominal values of the 0.005-in. wall thickness tubing are greater than those values of the 0.010-in. tubing, as might be expected. However, the 0.005-in. wall thickness tubes recently obtained from Vendor II show improved values of average/nominal and standard deviation about the average compared with that previously obtained. These new values may be lower partly due to the small number of samples tested. However, improvements in the dimensional quality of the fused silica tubing can be expected as experience is gained by the vendors in their drawing techniques.

Axial-Coolant-Tube Manifold Configurations

The manifolds for the models (see Fig. 2(b)) were designed to hold the fused silica tubes in a desired location and act as headers and collectors of the tube coolant fluid. The tubes are located axially between two manifolds around the manifold centerline to form an "axial-coolant-tube" model. Two general types of manifold designs were investigated: individual-hole and annular-groove manifolds. Both types have a 0.650-in.-dia hole in the center for the location of the end wall (discussed in Section IV) and a maximum diameter somewhat less than 2.26 in. to enable installation for testing in the 1.2-megw r-f induction heater (also discussed in Section IV).

Individual-Hole Manifold

This manifold design has holes individually drilled around a 1.26-in.-ID circle into which the tubes are placed. The holes have a diameter of 0.073-in. with a 0.019-in. gap between. This design is shown in Figs. 5(a) and 5(b). These manifolds were initially made of aluminum, due to its lightness and machinability, but later versions were made of copper due to the desire to solder the copper vortex injectors to the manifolds (see Section IV). Also, due to its higher thermal conductivity, copper is more easily cooled. Various hole diameters were used to hold

different diameter fused silica tubing. Holes for the injectors were located at 120-deg intervals between the holes for the fused silica tubes (Fig. 5(a)). This type of manifold was used because it presented a large amount of surface area for the sealant to provide a good bond with the fused silica tubes (see next subsection on sealing methods). Due to the large undesirable gaps between the tubes inherent with this design and because improvements were made in the sealing technique, a new manifold having annular grooves was fabricated.

Annular-Groove Manifold

This manifold design (Fig. 5(c)) employs three annular grooves located at the desired model diameter (e.g., 0.846, 0.934, 1.26, and 1.55-in.-ID). Manifolds are shown in Fig. 5(c) for the largest and smallest model inner diameters. The grooves, which are 0.064-in. wide, permit close spacing of the fused silica tubes with gaps between tubes due only to a thin layer of sealant necessary between the tubes. The vortex injector tubes are located either in holes provided in the manifold (as explained above) or on the outside of the manifold if the model inner diameter is too small. At the small model diameters (e.g., 0.846 and 0.934-in.-dia) the vortex injector tubes have a higher thermal deposition due to their close proximity to the plasma compared with the larger diameters (e.g., 1.26 and 1.55-in.-dia). The manifolds shown in Fig. 5(c) are typical of those tested during the present program (see Section IV).

Fused Silica Coolant-Tube Sealing Methods

Three methods were employed in sealing the fused silica tubes to the manifolds used in this and previous programs (Refs. 2 and 10). These methods do not represent all the possible methods of sealing, but they cover the three methods found most satisfactory. The potting method was used exclusively during this present program.

Shrink-Tubing Method

The first method (discussed in Ref. 2) uses shrink-tubing to connect axial fused silica tubes to manifolds. The teflon tubing shrinks upon heating and forms a flexible sealed connection between the fused silica and copper manifold. A photograph of a model fabricated using this method is shown in Fig. 6(a). This design provides for removal and replacement of individual coolant or injector tubes should damage occur. The copper manifold could be reused many times so that only replacement of individual fused silica and teflon tubing was necessary for a new model. In addition, this design could easily be adapted to thinner-wall tubes for testing adjacent to higher-intensity light sources. Work was discontinued due to the

difficulty encountered in uniformly heating the teflon tubing and obtaining suitable shrinking and sealing. Use of an oven would have helped to more uniformly shrink the tubing, but, other more promising methods were investigated first.

Fusing Method

The second method involves fusing the coolant tubes into fused silica manifolds (see Fig. 6(b)). First, the ends of the coolant tubes were heated to the softening point (1670 C) and then pushed into a fused silica manifold which has also been heated, but to a higher temperature. A pulse of air was applied through the tubes at the time they were pushed into the manifold. This process of "blowing" the coolant tubes into the manifolds produced a completely fused structure. An end view of an open manifold with the coolant tubes fused to it is shown in Fig. 6(b). Successful application of this method required precise control of both the coolant tube and manifold temperatures. Models having 0.020-in. wall thicknesses were fabricated using this method. The results of tests with these models are given in Ref. 2. Additionally, several transparent-wall models having 0.010-in. wall thickness were fabricated using this technique. However, careful inspection of some of these models after fabrication showed that small cracks existed in some coolant tubes near the point where the coolant tube joined the coolant manifold. It is believed that these cracks resulted from thermal stresses induced in the model due to the differences in the rate of cooling for coolant tubes and coolant manifolds. The thin-walled coolant tubes cool very rapidly relative to the thick-walled coolant manifold. Although it was sometimes possible to repair the cracked tubes by reheating the model to the fusion temperature, it was generally concluded that, without more precise control of the heating and cooling process, the technique of fusing was impractical at this time for use in fabricating models with 0.010- and 0.005-in. wall thickness.

Potting Method

The third method uses a potting compound to seal the fused silica coolant tubes to the manifold. Numerous silicone rubber and epoxy sealants were used. Pourable, self-leveling silicone rubber (RTV manufactured by the General Electric Co.) was found to have the best combination of adhesive, temperature, and electrical characteristics of the materials tested. It was also found that curing the silicone rubber at temperatures of approximately 200 F was necessary to achieve a leak-tight seal between the coolant tubes and the manifold. An end view of a manifold with the potted fused silica coolant tubes is shown in Fig. 6(c). The sealant was applied with a no. 16 hypodermic needle attached to a specially designed plenum. The hypodermic needle was necessary to force the sealant into the corners of the channel and between the tubes. The plenum consists of a 1/2-in.-ID steel pipe fitted with a plunger and air feed line on one end and a fitting for the needle on the other end. When the plenum is filled with sealant, air pressure applied to the plunger causes a steady flow of

sealant through the needle. Results of previous tests with models made using this method are given in Ref. 10; results of tests during this present program are given in Section IV.

Circumferential-Coolant-Tube Segments

The reference engine shown in Fig. 1 uses circumferentially shaped fused silica tubes for the transparent-wall structure. Axial-coolant-tube models use straight fused silica tubes as supplied by the vendor and are relatively easy to fabricate. However, axial-coolant-tube models are considered only a first step in the overall transparent-wall development program. Eventually, circumferential-coolant-tube models will be used to simulate the transparent walls of the full-scale engine. As part of the current program, various methods have been investigated for fabricating circumferential-coolant-tube segments.

Coiled Fused Silica Method

This method (described in Ref. 10) consists of fusing a cut-and-shaped fused silica coil to form manifold tubes. First, a closely wound fused silica coil (Fig. 7(a)) was cut in half as shown in Fig. 7(b). The coil was about five inches long and, if it was not fused together around the circumference, it was tacked together along the entire length with grading glass. The ends of the cut coil were heated, bent, and "blown" into fused silica manifold tubes as shown in Fig. 7(c). The manifolds were slit to allow the coil to be fused in the same manner as described previously. The circumferential coolant tubes had 0.040-in.-ID by 0.080-in.-OD dimensions and the manifold tubes had 0.240-in.-ID by 0.320-in.-OD dimensions. Three 120-deg segments were combined to form the circumferential-coolant-tube model configuration shown in Fig. 7(d). Peripheral-wall vortex injector tubes could be located between the manifold tubes at 120-deg intervals. It is also possible to pot the cut-and-shaped fused silica coil into copper manifold tubes, similar to potting of the axial-coolant-tube models. This potting method, explained in the section on sealing methods, would eliminate the distortion of the fused silica manifold tubes caused by the fusing method. Use of this method has been discontinued due to the problem of obtaining satisfactory coils and due to the development of a more promising sagging method.

Sagging Fused Silica Method

This method consists of heating fused silica tubes located over a mold and allowing them to sag to the contour of the mold. The procedure used is illustrated in Fig. 8. To form the lower mold, modelling clay (plasticine - Harbutt's Plasticine Lt'd.) was placed inside the aluminum form shown in Fig. 8(a). A grooved roller

was rolled over the form to make ridges in the modelling clay. The aluminum container was placed over the form and a castable ceramic (Ceramacast 511)* was poured over the plasticine. The ceramic, which was obtained as a powder, was mixed with water (20 percent water by volume) to obtain a pourable solution. The container and contents were then vibrated on a shaker to remove bubbles for 15 to 20 min. After approximately 20 min, the ceramic had hardened sufficiently so that any remaining bubbles would not be removed by vibration. The container and contents were dried for approximately 12 hrs at room temperature and then for another 2 hrs in an oven at 660 R. Then, the ceramic mold was removed from the container and baked approximately 2 hrs at 2460 R to harden and remove any remaining moisture. The completed lower mold is shown in Fig. 8(a). The upper mold was fabricated in the same manner as the lower mold except that the plasticine was not grooved. The upper mold with its form is shown in Fig. 8(b). The molds were placed in an oven to preheat to approximately 2400 F. Clean fused silica tubes were then placed between the upper and lower molds as shown in Fig. 8(c). This operation required care and speed since the molds were removed from the oven for a short time to properly locate the tubes on the molds. The molds were preheated so that they would not act as heat sinks, which would increase the time required for the tubes to sag. It is desirable to have the tubes exposed to the high temperature for as short a time as possible to keep devitrification to a minimum. Thus, as soon as the tubes were located between the molds, the molds with the tubes as shown in Fig. 8(c) were placed back into the oven. In a few minutes, the weight of the upper ceramic mold combined with the high temperature sagged the fused silica tubing to the shape of the ceramic mold contour.

Difficulties were encountered during initial tests, mainly because of a need for additional weights to be placed on the upper mold as the tubes began to sag. This is due to the greater surface area of the tubes taking up the weight as the tubes sag around the upper mold. Thus, initial tests took up to 2 hours before the tubes had sufficiently sagged. This resulted in excessive devitrification of the fused silica tubes where they had come in contact with the ceramic molds.

Many tubes can be sagged simultaneously with the exact same contours by this method. This method is also applicable to tubes having almost any diameter and wall thickness.

Vortex Injector Configurations

Peripheral-wall vortex injection is one of the features of the transparent walls in the reference engine shown in Fig. 1. Accordingly, vortex injectors were included in the design of models which simulate these transparent walls. Various types of

*Available from Aremco Products, Inc., Briarcliff Manor, N. Y. 10510.

injectors were investigated and incorporated into the model designs. The following is a discussion of the vortex injectors used in the program. The ultrasonically drilled fused silica tube and the drilled copper tube injectors were previously described in Refs. 2 and 10, respectively, and are summarized below to show the development of the vortex injectors. The copper hypo-tube injector design was used exclusively during this present program and is listed chronologically. The fused silica hypo-tube injector (Fig. 9(d)) has been fabricated during this program but has not yet been used in tests.

The ultrasonically drilled fused silica tube injectors made of 0.080-in.-ID by 0.160-in.-OD fused silica tubes (Fig. 9(a)) were originally employed in the all-fused-silica axial-coolant-tube model tests (Ref. 2). These injectors had 0.012-in.-dia holes ultrasonically drilled at an angle to give nearly tangential injection. The number of holes varied depending upon the particular configuration employed. The holes were ultrasonically drilled because standard drilling would result in chipping and cracking of the fused silica tubes. Fused silica was used originally to enable fusion to the fused silica manifolds in the all fused silica models (see Fig. 2(a)). When the manifolds were changed to metal, a drilled copper tube injector was designed.

It was found that by using copper tube injectors the injector could be soldered to the copper manifolds, thus forming a rigid structure. The injectors were made from 0.1275-in.-ID by 0.1875-in.-OD copper tubes having 0.020-in.-dia holes drilled at an angle to give nearly circumferential injection. The number of holes varied according to the particular configuration employed. A typical drilled copper tube injector is shown in Fig. 9(b) and a complete model with these injectors is shown in Fig. 2(b). The length-to-diameter ratio (L/D) of the holes was approximately 2. This low value resulted due to the larger hole diameter compared with the ultrasonically drilled hole previously discussed. A discussion of tests employing axial-coolant-tube models with drilled copper tube injectors is given in Ref. 10. Tests made during this present program (see Section IV) indicated that considerable turbulence in the flow was caused by the protrusion of the injector tubes into the vortex flow. The turbulence results in a large convective heat flux on the injectors, which were only cooled by the injected argon flow, and would result in eventual injector failure.

Accordingly, an improved method of injection using hypo-tube injectors was developed. The copper hypo-tube injector design (Fig. 9(c)) consisted of a copper manifold tube with attached copper hypo tubes acting at the vortex injectors. There were approximately 100 0.010-in.-ID by 0.020-in.-OD copper hypo tubes for each manifold tube. The manifold tube was first cut and then the hypo tubes were installed and soldered to provide a leak-tight seal. The hypo tubes were then bent as a group to give circumferential injection. A complete model with these injectors

is shown in Fig. 2(c). This type of injector provided an exceptionally good flow pattern since its L/D ratio after the bend was approximately 16. This injector also allowed the relatively large manifold tube to be located outside the model coolant tubes with only the small hypo tubes protruding inside the coolant tubes. Copper hypo tubes were soldered to the vortex injector manifold to provide water coolant flow during hot flow tests.

The fused silica hypo-tube injectors (Fig. 9(d)) used drawn fused silica hypo tubes instead of the copper hypo tubes mentioned above. This is expected to reduce the heating of the injectors caused by r-f electrical loading and radiant heating. Approximately 100 0.010-in.-ID by 0.020-in.-OD fused silica hypo tubes were potted with silicone rubber into a cut, copper manifold tube. The fused silica hypo-tube injector is shown in Fig. 9(d). The 0.1275-in.-ID by 0.1875-in.-OD copper manifold tube could easily be replaced with a fused silica tube of comparable size to further eliminate excess heating. This injector has not yet been used in axial-coolant-tube model tests but it appears promising for further investigation.

Recommendations for Future Development of Fabrication Techniques

It is recommended that the fused silica coolant tubes in the axial-coolant-tube models be fused together to provide complete separation between the fuel region and the propellant region. Flow interaction between these regions will likely lead to fuel and/or propellant seed deposition on the transparent walls. The fusing method must not effect the tube diameter or wall thickness and it should not alter the transmission of the model to any appreciable degree. Thus, it is suggested that a method such as laser welding of the fused silica tubes be studied. This method was initially attempted at UARL without a filler material. A small fused silica rod, upon melting, could act as the filler material and thus maintain the tube dimensions. The laser beam power (approximately 40 watts) and traverse speed would present the only variables. It is believed that the laser is ideally suited to this application (Ref. 11).

It is recommended that the fused silica tubes for the circumferential-coolant-tube models be fabricated by using the sagging technique. Initial difficulties encountered from devitrification resulting from extended periods at elevated temperatures could be eliminated by using an improved procedure of weighting the tubes and

by sagging in an oven with an inert atmosphere. Due to the requirement of having many tubes each with the same shape as well as a high degree of transparency, oven sagging appears to be promising for tubes of any diameter and wall thickness.

SECTION IV

FUSED SILICA MODEL TEST PROGRAM

The primary objective of the test program is to subject fused silica models to an environment similar to that expected for the transparent walls of a nuclear light bulb engine. This section describes the cold-flow and hot-flow tests conducted during the present program. The description includes the fused silica models, principal equipment, procedures used during the tests and the major results. Recommendations for future tests are also presented.

Description of Principal Equipment and Procedures

Cold-Flow Tests

Principal Equipment

Two lucite chambers were used in cold-flow tests with water to simulate the hot-flow tests with argon in the 1.2-megw r-f induction heater. The chambers each consisted of a tube for simulating the model configuration and a surrounding lucite box which, when filled with water, presented an undistorted view of the test sections. The chambers are shown in Fig. 10(a). The larger chamber (2.26-in.-ID lucite model) is shown positioned for testing. During a test, light from the lamp is collimated and reflected vertically downward through a slit. The slit is aligned with the centerline of the model tube to show a cross-section of the flow pattern inside the model tube. The flow pattern was observed by injecting dye (uranine concentrate powder in water) into the flow. The flow control panel was used to regulate the injected flow during the test. A variety of injector configurations were investigated with the chambers.

The smaller chamber consisted of a 1.26-in.-ID lucite tube which had provision for three vortex injectors to be located at 120-deg intervals around the periphery. This chamber was used to simulate a 1.26-in.-ID axial-coolant-tube model. The lucite tube was grooved at the 120-deg intervals and the injector tubes were placed into these grooves so that the injector would more closely simulate the protrusion into the vortex flow of the axial-coolant-tube model injectors. The injectors in this simulator extended through the chamber walls and were sealed by O-rings to enable injector rotation during testing. Thus, the effect of injection angle on the flow pattern could be investigated. Lucite end walls were easily removable from the chamber between tests to enable various end-wall and thru-flow diameters to be investigated.

The larger chamber consisted of a 2.26-in.-ID fused silica tube which represented the innermost fused silica coolant tube (i.e., the test chamber boundary) in the 1.2-megw r-f induction heater. The same models tested in hot-flow tests could be tested using this simulator. The end walls and thru-flow ports had diameters of 0.625-in. and 0.180-in., respectively, and were the same as those used in the hot-flow tests. This chamber had provision for flow to be passed over the outside of the model to simulate the propellant flow so that the disturbance of the flow pattern due to the numerous coolant and injector tubes, and the spacing between the tubes, could be investigated.

Test Procedures

The chamber containing the model simulator to be tested was first positioned in front of the light source as shown in Fig. 10(a). The lamp was turned on and the water injection flow was begun. Dye was injected from the chamber end walls. The slit was positioned to produce the clearest cross section of a particular flow pattern. The injection flow was then varied until the most well-defined dye pattern was observed. At this point, the flow rates and pressures were measured and photographs were taken. With each change in variables (e.g., injection angle, end wall or thru-flow diameter, vortex injector configuration, etc.) data and photographs were taken.

Hot-Flow Tests

Principal Equipment

The UARL 1.2-megw r-f induction heater is described in Refs. 10 and 12. Photographs of the resonator section are shown in Fig. 11(a). The resonator section and load are located within a 56-in.-dia cylindrical aluminum test tank. The resonator section consists of two arrays of ten vacuum capacitors; each array is connected to a single-turn, 3.06-in.-ID r-f work coil. A pair of concentric water-cooled fused silica tubes (approximately 39-in. long) located within the r-f coils form the outer boundary of the test chamber (see Fig. 11(a)). These inner and outer fused silica tubes have wall thicknesses of 0.060 and 0.170 in., respectively. The innermost diameter of the tubes is 2.26 in. (58 mm). The annulus between the tubes is used for water coolant.

The discharge is started using an auxiliary d-c arc which provides the initial ionization level necessary for sustained coupling with the r-f power. A 3-kw d-c arc is drawn between two movable electrodes along the centerline of the test chamber. The starter assembly is described in Ref. 2.

The arrangement of the various panels for controlling the operation of the 1.2-megw r-f induction heater is shown in Fig. 11(b). The annular coolant flow control panels and the d-c arc starter control are also shown. A high-pressure 450-psi system using a positive displacement pump can supply up to 20 gpm of cooling water. This system was used to cool the transparent wall model during the tests. A 180-psi system employing centrifugal pumps can supply up to 100 gpm of cooling water. This system was used to cool the test chamber wall during the tests. The laboratory water system was used to cool the test chamber end walls and the water-cooled components of the r-f heater.

To provide end-wall simulation similar to that of the full-scale engine, a symmetrical pair of end walls were used to form the axial boundary of the test chamber. The end walls supported the axial-coolant-tube models as shown in Fig. 12. A 0.180-in.-dia thru-flow port was located on the centerline of each 0.625-in.-OD end wall to allow removal of the hot exhaust gases (see Fig. 12(a)). The copper end walls were internally water-cooled to remove the heat deposited from the hot plasma. The end walls were attached to the test tank such that the end-wall faces were located 2 in. apart. A bench mockup showing the relative location of the end walls and model is shown in Fig. 12(b).

Test Equipment and Instrumentation

The equipment used in the hot-flow tests is shown in Fig. 10(b). There are five viewports in the 1.2-megw r-f resonator tank cover for observation during testing. The radiometer, which is shown in position, was turned out of the way to enable photographs to be taken with the still camera, which was rotated to a horizontal position. Continuous visual observation was made through the two side viewports. The control panel was used to regulate the argon injection and exhaust flows and the model water coolant flow. This equipment was located adjacent to the control panels shown in Fig. 11(b).

Test Procedures

The model to be tested was first installed on a bench on one end wall as shown in Fig. 12. The end wall and model were installed as a unit into the 1.2-megw r-f induction heater test chamber. By being attached to the end wall, the model was restrained from movement and possible breakage while being installed for testing. The model was given a final leak check by pressurizing with the model coolant water to 20 psig. If the model leaked more than a few drops a minute (usually due to a broken coolant tube or a poor seal in the potted region) then it was removed for repair. But, if the model did not leak (as in most instances), then the coolant flows (e.g., annular, end wall, r-f electrical, etc.), r-f power and recorders were started. A low injected argon flow rate (approximately 0.002 lb/sec) was

established. Then, the d-c arc and the r-f coil voltage were simultaneously initiated to produce the r-f discharge. When the discharge was established (usually within 2-3 sec) the r-f coil voltage, injection flow rate, and chamber pressure parameters were individually increased. These parameters were maintained constant during the time data runs were taken. The data were recorded by strip chart recorders and by hand in as short a time as possible (usually within 30 sec) to ensure that any change in the parameters did not influence the data. The data consisted of temperatures, flow rates, pressures, photographs with various neutral density filters, and radiation measurements. Upon completion of the test the r-f coil voltage would be turned off, and the flows would be stopped. The model would be removed and inspected.

Test Results

A major objective of the tests conducted during this program has been to reduce the level of turbulence inside the model by improving the method of vortex injection. Turbulence in the buffer gas layer adjacent to the transparent wall can result in excessive conduction and convection heat transfer from the hot plasma to the transparent wall. Previous tests (Ref. 13) indicated that poor flow patterns were produced in models with injectors in which the length of the injection hole divided by its diameter, L/D, was less than 5. A poor flow pattern is one having no well-defined recirculation cells (see Appendix C) and indicates the presence of undesirable turbulence. The approach used was to first study several different methods of injection by observing the flow characteristics obtained in cold-flow water vortex tests. The most promising of these injection methods was then incorporated into models for hot-flow tests.

Cold-Flow Tests

The lucite simulators (described previously) were used in tests to study the effects of various parameters on the flow patterns within the model. For these tests, dye injected from both end walls into the water permitted direct visual observation of the flow pattern in and around the model. This method was used to qualitatively determine the conditions that resulted in the most desirable flow pattern.

Tests Using 1.26-In.-ID Simulator

Tests were conducted using the 1.26-in.-ID lucite tube simulator during which the following model parameters were independently investigated: (1) flow injection angle, (2) injection area, (3) end-wall diameter, (4) thru-flow port diameter, (5) number of thru-flow ports, and (6) injection flow rate. It was found that a change of a few degrees (approximately 5 to 10 deg) in injection angle did not

noticeably affect the flow pattern. Neither did a change in injection area of up to 50 percent visibly effect the flow pattern. However, a noticeably improved flow pattern was obtained when the clearance (approximately 0.250 in.) between the end wall periphery and the model inner diameter was eliminated, thereby eliminating flow into the regions behind the end walls. (The clearance was simulated initially because it existed in the configurations used in 1.2-megw r-f induction heater tests; see Fig. 25 of Ref. 10.)

Drilled copper injectors (see Fig. 9(b) described in Section III) similar to those used in the hot flow tests described in Ref. 10 were used for the initial series of water tests. These injectors each had 23 injection holes with diameters of 0.020 in. A photograph of a typical dye pattern obtained with this injection configuration is shown in Fig. 13(a). The concentrated vortex core shown for β_t = 23 was the most well defined dye pattern observed for this injection configuration (β_t is the secondary flow parameter, defined in Appendix C, and is an indication of the type of flow pattern created by the vortex injectors). At higher flow rates (lower β_t) the dye pattern became more diffuse, apparently due to turbulence. At lower flow rates (higher β_t), the pattern approached solid-body rotation.

In subsequent tests, fused silica injectors shown in Fig. 9(a), each having 14 injection holes with diameters of 0.012 in., were used. In these tests, a much more desirable flow pattern was obtained. One possible reason for this improvement is that the injection hole L/D was approximately 2 for the copper injectors and was approximately 5 for the fused silica injectors. Based on these observations, copper injectors with smaller injection hole diameters and fewer injection holes were tested. These injectors had from 14 to 50 0.012-in.-dia holes over a 2-in. length. The L/D of these tubes was approximately 5, compared with approximately 2 for the previous injectors, and should have resulted in improved flow patterns. However, no noticeable improvements were observed. In fact, the flow patterns in all tests with copper injector tubes were poorer than those obtained with fused silica injectors (see Ref. 2), even for approximately the same length-to-diameter ratio ($L/D \approx 5.0$) and for the same number of injector holes. This difference may be attributed to the straighter and smoother holes obtained from ultrasonically drilling the fused silica tubing. During all of these tests, eddies were shed from the vortex injector tubes due to their penetration into the flow (see Fig. 13(a)). The diameter of the eddies was approximately equal to the penetration depth (one-half the injector tube diameter).

A second 1.26-in.-ID lucite tube slit axially in three locations (120-deg apart) was used to investigate another injection method. Hypo tubes (100 0.010-in.-ID by 0.020-in.-OD), connected at one end to supply tubes, were inserted into the slits

(see sketch in Fig. 13(b)). By using these hypo tubes as the vortex injectors, the larger copper tubes could be moved out of the flow region and used only as supply tubes. This injection method eliminated two problems previously encountered. The hypo-tube injectors were flush with the wall and thus the eddies were eliminated; also, each hypo tube provided a straight, smooth hole with a very large L/D (approximately 55). A photograph of a typical dye pattern obtained with this injection scheme is shown in Fig. 13(b). Recirculation cells were observed for a fairly wide range of flow rates. Thus, the hypo-tube injectors appear to produce the most desirable flow characteristics observed to date.

2.26-In.-ID Simulator

Tests were conducted using the 2.26-in.-ID fused silica tube simulator to study the effects on the flow pattern of model coolant tube spacing and wall roughness due to the presence of the coolant tubes. In some tests simulated propellant flow was injected around the model to simulate the conditions present in the 1.2-megw r-f heater during propellant heating tests (see Ref. 10). A 0.934-in.-ID axial-coolant-tube model was used in these tests and is shown in Fig. 13(c). There were 48 0.050-in.-ID by 0.060-in.-OD fused silica tubes in the model. The three injectors each consisted of 100 0.010-in.-ID by 0.020-in.-OD copper hypo tubes soldered to a 0.187-in.-OD copper manifold tube. A photograph of a typical dye pattern obtained with this injection scheme is shown in Fig. 13(c). The value of β_t is lower than in Figs. 13(a) or 13(b) due primarily to the different model diameter. The recirculation cells appear more diffuse in Fig. 13(c) than those of Fig. 13(b), due in part to the distortion of light caused by a multiple number of tubes, to the gaps between the coolant tubes allowing radially outward flow, and to the wall roughness. It should be noted that the injectors still protruded somewhat into the flow and that a gap existed between the injectors and adjacent coolant tubes (compare Fig. 13(c) with Fig. 13(b)). Rotating flow, existing in the space between the model coolant tubes and the 2.26-in.-dia tube was caused by the vortex flow moving radially outward between the coolant tube gaps. This flow outside of the model is undesirable because it would disturb the seeded propellant flow and result in seed deposition on the model. It was found that part of the simulated propellant flow at higher propellant flow rates (i.e., propellant flow rates greater than the vortex flow rates) passed radially inward and exhausted through the thru-flow ports rather than out the propellant exhaust duct. Thus, it is necessary to seal the gaps between the coolant tubes to effectively separate the fuel region from the seeded propellant region and thus, in the engine, to reduce the fuel and seed deposition on the tubes.

Hot-Flow Tests

Results of previous tests (Ref. 10) indicated that heating of the transparent wall was due primarily to conduction and convection from the plasma. The objectives of the subsequent tests were to decrease the heat deposition due to conduction and convection and to increase the total operating discharge power level. Two different axial-coolant-tube configurations used in previous tests are shown in Fig. 14. The configuration shown in Fig. 14(a) consists of a manifold with individual holes for mounting the fused silica coolant tubes and injectors. Use of an individual hole for each coolant tube provides a good sealant bond between tube and manifold. A second type of manifold (Fig. 14(b)) with annular grooves instead of individual holes was also used in previous tests after a suitable sealant potting technique was developed. This permitted the axial coolant tubes to be positioned such that the gaps between adjacent tubes were essentially eliminated. These gaps were undesirable since they allowed some of the vortex flow inside of the model to flow radially outward into the surrounding chamber. This flow radially outward added to the convective heat loading of the transparent wall.

Test Configuration

The configuration shown in Fig. 14(c) was the first tested in the present program. It consists of an annular manifold with straight copper hypo-tube injectors. Approximately 100 0.010-in.-ID by 0.020-in.-OD copper hypo tubes, 0.187-in. long, were placed side-by-side in each injector manifold tube. The length-to-diameter ratio of the individual injection holes was approximately 18. This injection method produced substantially improved injection flow characteristics compared with the drilled holes used previously (see Fig. 9(b)). A configuration having curved injection tubes (Fig. 14(d)) was also fabricated. It was believed that curving the injection tubes would help to align the injection flow tangentially with the vortex flow and lead to reduced turbulent mixing. The hypo-tube length after the bend was 0.187 in. to maintain a high length-to-diameter ratio. To further reduce the disturbance of the flow due to the presence of the injectors, an offset annular manifold like that shown in Fig. 14(e) was also used in some tests.

Description of Typical Test

A photograph of the 0.934-in.-ID axial-coolant-tube offset annular-manifold model tested in the 1.2-megw r-f induction heater is shown in Fig. 15(a). The axial-coolant-tube manifolds were located 3.0 in. apart instead of 5 in. (the distance used in Ref. 10). This change was based on the results of water vortex tests. Copper coolant hypo tubes were soldered directly to the hypo-tube injectors, as shown in Fig. 15(a). The axial-coolant-tube offset is clearly seen in Fig. 15(b). The hypo-tube injectors are hidden in this view behind the axial-coolant-tube

manifold, but are shown schematically in Fig. 14(e). The 0.934-in.-ID axial-coolant-tube model is shown installed in the 1.2-megw r-f induction heater in Fig. 16(a). A photograph of the plasma discharge during a typical test condition is shown in Fig. 16(b). Due to multiple reflections from the axial coolant tubes, the shape of the discharge is not readily apparent.

Photographs of the model during the start-up phase of a typical hot-flow test (Fig. 17(a)) are shown in Fig. 17(b). The sequence was taken with a movie camera at a speed of 24 frames per sec. The plasma discharge is initiated (t = 0) with a d-c arc. The discharge is faintly visible after 0.083 sec. The discharge is shown fully established in the last photograph (t = 0.292 sec). During the tests care must be taken to prevent excessively large flow rates or else the discharge will become unstable and the argon will breakdown outside of the model. This phenomenon is shown in Fig. 17(c). The sequence was taken at a framing speed of 500 frames per sec. The discharge is first in its normal operating mode (t = 0). Approximately 0.004 sec later, gas breakdown occurred in the gap between the model coolant tubes and the 2.26-in.-ID fused silica coolant tube (first photo in Fig. 17(c)). The discharge is shown behind the model in the first photograph. The next photograph shows the discharge in front of the model at t = 0.006 sec. The third and fourth photographs also show the discharge behind and in front of the model, respectively. This condition of discharge breakdown outside of the model could usually be avoided by proper choice of flow conditions (e.g., chamber pressure, injected flow rate, and r-f power).

A breakdown of the power losses from a typical test with the 0.934-in.-ID axial-coolant-tube model is shown in Fig. 18. For this test, a total of 28.2 kw was deposited into the plasma discharge; of this, 7.0 kw, or approximately 25 percent, was deposited into the model coolant and 3.18 kw, or 11.3 percent, was deposited into the vortex injector bypass coolant flow. The total power radiated was 6.12 kw, or 21.7 percent, as measured by the radiometer and determined from the annular coolant flow heat balance. The remaining 11.88 kw was deposited in the end-wall coolant and thru-flow exhaust gases.

There are only three parameters to be varied during testing of a given model configuration in the 1.2-megw r-f induction heater. They are: (1) the vortex injection flow rate, (2) the chamber pressure, and (3) the r-f coil voltage. These parameters are not independent. For example, an increase in the injection flow rate causes an increase in the chamber pressure and an increase in the r-f coil voltage. The chamber pressure will increase due to the increased flow being added into a constant volume unless the thru-flow exhaust valve is opened to allow the pressure to remain constant. The increased flow rate causes a decrease in the discharge diameter which results in an increased r-f coil voltage. The relative effect of these parameters on the power breakdown for a typical axial-coolant-tube model test

is shown in Fig. 19. The total power deposited into the plasma for this test series was 18.2 kw. The tests proceeded as follows. The discharge was initiated with the d-c arc at a pressure of 1 atm at a low injection flow rate and r-f coil voltage. After the discharge was initiated the flow rate was increased to 0.0032 lb/sec and the voltage to 3.1 kv. Then, after conditions stabilized, data for Run No. 1 were recorded (see point marked "1" in Fig. 19). The voltage was increased to 3.3 kv and then data for Run No. 2 was taken (point "2" in Fig. 19). The d-c arc starter rods were removed and exhaust plugs were installed in their place. Since the starter rods were located in the thru-flow exhaust ports, installation of the plugs will reduce the thru-flow exhaust which in turn will slightly increase the chamber pressure. In this case the pressure increased to 1.1 atm. Data for Run No. 3 was then taken (point "3", and so on). The increases in flow, pressure, and voltage were continued until the discharge went out after the last data run (data for Run No. 8) at values of 0.0105 lb/sec, 3.7 atm, and 6.7 kv, respectively. It is believed that the discharge extinguished due to too low an r-f coil voltage for the flow conditions present. This belief is substantiated by the experimentally determined operating corridor shown in Fig. 20. The upper bound of this corridor denotes the condition for which gas breakdown outside of the model occurred and the lower bound denotes the condition required for sustaining the discharge. The curves of the total power levels shown in Fig. 20 represent approximate values required for stable operation. The numbers shown in Fig. 20 correspond to the runs in Fig. 19. The last data run (data for Run No. 8) was shown to correspond to 18.2 kw into the plasma, but in Fig. 20 this data run is found above the 20 kw boundary. Thus it is believed that the injection flow rate and/or the chamber pressure were too high for the power setting to maintain a stable discharge. This test represents one of many such tests used to determine the operating corridor as shown in Fig. 20.

Summary of Test Results

A summary of the results of tests of models having inner diameters varying from 0.845 to 1.55 in. is shown in Figs. 21 thru 24. The variation of power deposited into the coolant tubes with total discharge power, Q_C/Q_T, decreased during this present program as compared to previous data from Ref. 10. For example, from Fig. 21, for the 0.934-in.-ID model at a total discharge power of 8 kw the ratio Q_C/Q_T was reduced from 0.75 to 0.15 during this present program. The data from the present program at the higher power levels tend toward higher levels of Q_C/Q_T primarily due to plating on the fused silica coolant tubes resulting from vaporization of the copper hypo-tube injectors. Because of the difficulty encountered in curving the hypo tubes without crimping them, the radius of curvature was larger than desired and they protruded into the plasma region. This was true even with the offset annular model. Thus the limitation in maximum total discharge power during this present program has been due to failure of these copper hypo-tube injectors. Plating on the fused silica coolant tubes causes a larger than normal amount of absorption

of radiation in the coolant tubes and increases the fraction Q_C/Q_T. The values in Fig. 21 include radiation deposited into the water coolant and fused silica tubes. From Table I of Ref. 14, anywhere from 15 to 25 percent of the indicated power deposited into the model coolant tubes can be assumed to be due to the presence of the water. Assuming a value of 20 percent for the radiation deposited into the water coolant and a value of 5 percent for the radiation deposited into the fused silica coolant tubes, then for an indicated value of Q_C/Q_T of 0.15, we find that the value of Q_C/Q_T due to conduction and convection is 0.11 (0.15 - 0.04). Thus the actual amount of power deposited into the coolant tubes by conduction and convection is approximately 75 percent of that shown in Fig. 21.

Some tests were also conducted with three fused silica segments located outside of the model acting as a solid wall to eliminate the flow radially outward. The location of the wall segments is shown in Fig. 14(e). No significant differences were noted in the fraction Q_C/Q_T compared with data from tests without the wall segments. The variation of model diameter in these tests did not appear to effect the test results.

The variation of power deposited into the copper hypo-tube injectors with total discharge power in the axial-coolant-tube model tests is shown in Fig. 22. It is seen that the ratio of the power deposited into the injector tubes divided by the total discharge power, Q_{INJ}/Q_T, increased during this present program compared with previous data from Ref. 10. For example, from Fig. 21, for the 0.934-in.-ID model at a total discharge power of 8 kw, the ratio Q_{INJ}/Q_T was increased from 0.015 to 0.08. This increase in Q_{INJ}/Q_T is partly attributed to the increased amount of copper exposed to the discharge radiation in the hypo-tube injectors, compared with the drilled injectors. The surface area exposed to radiation over a 3 in. length is 1.20 sq in. for the hypo-tube injector shown in Fig. 9(c), but only 0.88 sq in. for the drilled injector tube shown in Fig. 9(b). Thus, the copper hypo-tube injectors received nearly one-third more of the radiation, compared with the drilled copper tube injectors. The increase is also partly attributed to the increased r-f loading on the copper hypo-tube injectors. A test was made of a copper hypo-tube injector under the r-f coils. It was found that approximately 0.4 kw of power was deposited into the injector at a water coolant flow rate of 0.12 gpm and an r-f coil voltage of 3.8 kv. Since the hypo-tube injectors protruded somewhat into the plasma region, as mentioned above, the remainder of the increase in Q_{INJ}/Q_T is attributed to conduction and convection heating.

The variation of power radiated with total discharge power in the axial-coolant-tube model tests is shown in Fig. 23. The power radiated is obtained from the radiation received by the radiometer and the power deposited into the annular coolant, which is assumed to be deposited solely by radiation. The ratio of the power

radiated divided by the total discharge power, $(Q_{ANN} + Q_{RAD})/Q_T$, remained approximately constant. The average value of the ratio $(Q_{ANN} + Q_{RAD})/Q_T$ is approximately 0.3. Part of the reason for this ratio remaining constant can be attributed to the increased radiation taken by the copper hypo-tube injectors, compared with the drilled injectors. For instance, the coolant tube surface area exposed to the radiation in a 0.934-in.-ID model is approximately 9.0 sq in. Thus, using the injection areas from the preceding paragraph, the blockage of radiation due to the hypo-tube injector is 0.133 of the total model surface area, compared with 0.098 for the drilled injector tube. This means that nearly 38 percent more radiation will be deposited into the hypo-tube injectors, compared with the drilled injectors. Thus, for a given total discharge power, the indicated amount of power radiated from the hypo-tube injector model should be increased by about 3 percent, compared with the drilled injector tube model.

The variation of power deposited in the end walls and thru-flow exhaust with total discharge power in the axial-coolant-tube model tests is shown in Fig. 24. It is seen that the ratio of the power deposited in the end walls and thru-flow exhaust divided by the total discharge power, $(Q_{EW} + Q_{TF})/Q_T$, increased during this present program, compared with previous data from Ref. 10. For instance, from Fig. 24, for the 1.26-in.-ID model at a total discharge power of 20 kw the ratio $(Q_{EW} + Q_{TF})/Q_T$ increased from 0.15 to 0.45. This increase in $(Q_{EW} + Q_{TF})/Q_T$ is attributed partly to the decreased turbulence in the vortex injection flow which allows more of the power to be carried away by the exhaust and secondary (end-wall) flows instead of being deposited in the model coolant tubes as in previous tests (Ref. 10).

A summary of the ratio of the component power to the total discharge power for the axial-coolant-tube model tests is shown in Fig. 25. The values of the ratio shown above each column are the average values obtained from Figs. 21 through 24. To increase the percent of the total discharge power being radiated, it will be necessary to decrease the percentages to the end walls and thru-flow ports, and to the injector tubes. This might be accomplished by using smaller injectors, higher pressures, etc.

Figure 26 shows the secondary flow parameter, β_t, as a function of the injection area and the coolant flow rate. Data from both cold-flow and hot-flow tests are also shown for the various diameter models tested. The derivation of β_t as a function of the variables shown is presented in Appendix C. The desired value of β_t is approximately 50 (from Ref. 13). The value of β_t ranged from 7 to 25 for the data obtained during this present program. The values of β_t for a given model configuration (i.e., fixed injection area and model diameter) do not vary much even for an order of magnitude change in flow rate. For instance, the β_t of a 1.26-in.-ID model can be varied only 57 percent (from β_t = 17.5 to 27.5) for an order of magnitude change in flow rate. However, the β_t for the same model at a flow rate of

0.100 lb/sec can be varied 129 percent (from β_t = 17.5 to 40) for an order of magnitude change in injection area. One more variable to be considered is the viscosity of the argon which is used in the calculation of the radial Reynolds number and depends upon temperature. The temperature was assumed to be 685 R for the curves shown in Fig. 26. If the exhaust temperature was assumed to be 10,460 R then the curves (and data points) would be increased by 147 percent. Thus, since theory indicates a desirable value of β_t is approximately 50 and since the experimentally determined values of β_t were less than 20, it can reasonably be assumed the actual exhaust temperature lies somewhere between the two temperatures but probably closer to the 10,460 R temperature. This is actually a very reasonable assumption. For instance, the temperature rise in the exhaust flow in Fig. 18 can be calculated from $(Q_{EW} + Q_{TF})/W_A C_P$ to be approximately 10,000 R.

Difficulties encountered with the injectors during the axial-coolant-tube model hot-flow tests are illustrated in Fig. 27. An ultrasonically drilled fused silica injector previously tested (Ref. 2) is shown in Fig. 27(a). The drilled holes and the location of the overheating are shown for an injector tested to a total discharge power of 24 kw. The round holes appearing in the overheated area were caused by the temperature softening the fused silica tube to a point at which the pressure inside blew open the holes in the tube wall. Typical drilled copper tube injectors previously tested (Ref. 10) are shown in Fig. 27(b) installed in a model. The location of the r-f plasma arc attachment during breakdown outside of the model is shown. Arc attachment causes overheating of the injectors and results in localized melting. The darkened area of the fused silica coolant tubes is due to plating from the copper injector tubes, end walls and tungsten-tipped d-c arc starter rods. Three of the copper hypo-tube injectors tested during this present program are shown in Fig. 27(c). The location of arc attachment during plasma breakdown is shown on the copper manifold tubes since they are located outside of the model. The tips of the hypo-tube injectors were overheated due to their proximity to the plasma. Copper coolant tubes were soldered to each injector, next to the manifold tube, to help cool the injectors. The heat fluxes and energy deposition rates to the injectors were such that this particular geometry was inadequate for cooling the tips of the injectors.

Recommendations for Future Tests

Further tests should be conducted using the lucite model simulators to determine the relative merits of different hypo-tube injector designs. Tests should be made with the fused silica coolant tubes sealed together along their lengths to completely separate the fuel region from the propellant region. A study of the dye patterns will indicate which designs are the most promising for hot-flow tests.

From the results obtained to date, it is evident that the injector tubes must be more adequately protected from overheating due to the plasma. Sealing the models (see recommendations in Section III) would reduce the possibility of plasma breakdown outside the model and would thus eliminate heating due to arc attachment. The conduction and convection heating of the injectors by the plasma could be reduced by locating the injector hypo-tubes as well as the manifold tube behind the offset coolant tubes. The new offset annular model (described in Section III and shown in Fig. 2(d)) will permit injection with straight hypo tubes which will be shielded from the hot plasma. By using straight hypo tubes, the hypo tubes can be shorter and thus present a smaller area for radiation deposition. Fused silica hypo-tube injectors (see Fig. 9(d)) and manifold tubes could be used to further reduce radiation heating. To increase the percent radiation, testing at higher chamber pressures will be required.

Tests should also be conducted to determine the amount of power deposited into the coolant tubes which is due to radiation deposition in the water coolant. This could be accomplished by having a secondary cooling system which would allow a transparent coolant (i.e., argon) to be replaced with water coolant by simply energizing a solenoid valve while the test conditions are maintained constant.

REFERENCES

1. McLafferty, G. H. and H. E. Bauer: Studies of Specific Nuclear Light Bulb and Open-Cycle Vortex-Stabilized Gaseous Nuclear Rocket Engines. United Aircraft Research Laboratories Report F-910093-37, prepared under Contract NASw-847, September 1967. Also issued as NASA CR-1030.

2. Kendall, J. S., W. C. Roman, and P. G. Vogt: Initial Radio-Frequency Gas Heating Experiments to Simulate the Thermal Environment in a Nuclear Light Bulb Reactor. United Aircraft Research Laboratories Report G-910091-17, prepared under Contract NASw-847, September 1968. Also issued as NASA CR-1311.

3. McLafferty, G. H.: Studies of Coolant Requirements for the Transparent Walls of a Nuclear Light Bulb Engine. United Aircraft Research Laboratories Report F-110224-6, March 1967.

4. Ballman, A. A., D. M. Dodd, N. A. Kuebler, R. A. Laudise, D. L. Wood, and D. W. Rudd: Synthetic Quartz with High Ultraviolet Transmission. Applied Optics, Vol. 7, No. 7, July 1968.

5. Palma, G. E.: Optical Absorption in Transparent Materials During 1.5 Mev Electron Irradiation. United Aircraft Research Laboratories Report J-990929-1, prepared under Contract SNPC-70, September 1970.

6. General Electric Company: Fused Quartz Catalog. Form Q16, July 1970.

7. Palma, G. E. and R. M. Gagosz: Optical Absorption in Fused Silica During Irradiation at High Temperature. United Aircraft Research Laboratories Report H-930709-1, prepared under Contract NASw-847, November 1969.

8. Dietz, E. D.: The Glassy State. Science and Technology, November 1968, No. 83, pp. 10-21.

9. Yearick, N. F.: Glass Tubing Manufacturing. Proceedings of the 13th Symposium of the Art of Glassblowing, Sponsored by the American Scientific Glassblowers Society, June 1968, p. 92.

10. Roman, W. C., J. F. Klein, and P. G. Vogt: Experimental Investigations to Simulate the Thermal Environment, Transparent Walls, and Propellant Heating in a Nuclear Light Bulb Engine. United Aircraft Research Laboratories Report H-910091-19, prepared under Contract NASw-847, September 1969.

REFERENCES (Continued)

11. Pfitzer, E. K. and R. Turner: Quartz Working with a CO_2 Laser. Journal of Scientific Instruments (Journal of Physics E), Series 2, Vol. 1, 1968.

12. Roman, W. C.: Experimental Investigation of a High-Intensity R-F Radiant Energy Source to Simulate the Thermal Environment of a Nuclear Light Bulb Engine. United Aircraft Research Laboratories Report J-910900-4, prepared under Contract SNPC-70, September 1970.

13. Travers, A.: Experimental Investigation of Radial-Inflow Vortexes in Jet-Injection and Rotating-Peripheral-Wall Water Vortex Tubes. United Aircraft Research Laboratories Report F-910091-14, prepared under Contract NASw-847, September 1967. Also issued as NASA CR-1028.

14. Mensing, A. E. and J. F. Jaminet: Experimental Investigations of Heavy-Gas Containment in R-F Heated and Unheated Two-Component Vortexes. United Aircraft Research Laboratories Report H-910091-20, prepared under Contract NASw-847, September 1969.

15. Corning Glass Works: Corning Fused Silica Code 7940. Form FS-5, January 4, 1965.

16. Kreith, F.: Principles of Heat Transfer. International Textbook Company, Scranton, Pennsylvania, 1958.

17. Shand, E. B.: Glass Engineering Handbook. McGraw-Hill Book Company, Inc., New York, 2nd Edition, 1958.

18. McAdams, W. H.: Heat Transmission. McGraw-Hill Book Company, Inc., New York, 3rd Edition, 1954.

19. Gould, C. E. and W. M. Hampton: Thermal Endurance of Glass. Journal of the Society of Glass Technology, Vol. 14, p. 188, 1930.

20. Anderson, O. L.: Theoretical Solutions for the Secondary Flow on the End Wall of a Vortex Tube. United Aircraft Research Laboratories Report R-2992-1, prepared under Contract AF 04(611)-7448, November 1961.

21. McLafferty, G. H.: Friction Coefficient Between a Rotating Gas and the Surface of a Containing Tube. United Aircraft Research Laboratories Report M-1686, September 29, 1960.

REFERENCES (Continued)

22. Keyes, J. J., Jr.: An Experimental Study of Gas Dynamics in High Velocity Vortex Flow. Proceedings of the 1960 Heat Transfer and Fluid Mechanics Institute, Stanford University Press, Stanford, California, June 1960.

23. Rodoni, C. A.: An Investigation of the Flow Parameters of a Confined Turbulent Vortex. S. M. Thesis, Department of Aeronautics and Astronautics, Massachusetts Institute of Technology, September, 1969.

LIST OF SYMBOLS

A	Area, sq in. or sq ft
C_p	Specific heat of gas at constant pressure, Btu/lb-deg R
C_v	Specific heat of gas at constant volume, Btu/lb-deg R
C_f	Friction coefficient on the peripheral wall of a vortex tube, dimensionless
C_f^*	Friction coefficient, dimensionless
D	Diameter, in. or ft
d	Diameter of tube, in. or ft
E	Modulus of elasticity, psi
g	Acceleration due to gravity, 32.2 ft/sec^2
h	Heat transfer coefficient of film, Btu/sec-sq ft-deg F
h_j	Height of single injection slot, in. or ft
I	Intensity, arbitrary units
I/I_o	Fraction of light transmitted, dimensionless
K	Constant determined by gas properties, lb/sec-ft^2
K_T	End-wall boundary layer parameter
k	Thermal conductivity, Btu/sec-ft-deg F
L	Length, in. or ft
ℓ_c	Length of coolant tube, in. or ft
M	Mach number
m	Number of sections
P	Pressure, psi

LIST OF SYMBOLS (Continued)

P_B	Bursting pressure, psi
P_D	Chamber pressure, atm or psia
P_r	Prandtl number
Q	Component power or total heat, kw or Btu/sec
Q_{ANN}	Power deposited into annular coolant, kw
Q_{AVG}	Average heat load, Btu/sec
Q_C	Power deposited into coolant tubes, kw
Q_{EW}	Power deposited into end wall coolant, kw
Q_{INJ}	Power deposited into injector tube coolant, kw
Q_j	Total volumetric flow rate injected through peripheral wall, ft^3/sec
Q_m	Total heat in a given section, kw
Q_m''	Heat flux per unit area in a given section, kw/sq in.
Q_{RAD}	Radiated power as measured by radiometer, kw
$Q_{RAD,T}$	Total radiated power ($Q_{RAD} + Q_{ANN}$), kw
Q_s	Secondary flow in one end-wall boundary layer, ft^3/sec
Q_T	Total discharge power ($Q_C + Q_{INJ} + Q_{ANN} + Q_{RAD} + Q_{EW} + Q_{TF}$), kw
Q_{TF}	Power deposited into thru-flow exhaust, kw
R	Gas constant, ft/deg R
r	Radius, in. or ft
Re_r	Radial Reynolds number, dimensionless
Re_t	Tangential Reynolds number, dimensionless

LIST OF SYMBOLS (Continued)

$Re_{t,j}$	Tangential injection Reynolds number based on average injection velocity in vortex tube, dimensionless
$Re_{t,p}$	Tangential Reynolds number based on velocity at peripheral wall of vortex tube, dimensionless
s	Distance measured along tube, in. or ft
T	Temperature, deg R or deg K
t	Time, sec or min
v	Velocity, ft/ sec
W	Flow rate, lb/sec
W_A	Argon weight flow rate or buffer weight flow rate, lb/sec
W_{ST}	Weight flow in one end-wall boundary layer, lb/sec
x	Tube wall thickness, in. or ft
Y	Mach number parameter
α	Thermal expansion, cm/cm/deg C
β_t	Secondary flow similarity parameter, dimensionless
γ	Ratio of specific heats, dimensionless
ΔT	Temperature difference, deg R or deg K
λ	Wavelength, microns
μ	Viscosity, lb/ft-sec

LIST OF SYMBOLS (Continued)

ν	Poisson's ratio, dimensionless
ρ	Density, lb/ft^3
σ_H	Hoop stress in thin-wall tube, psi
σ_T	Total stress in tube, psi
σ_t	Thermal stress in tube, psi

Subscripts

c	Coolant
i	Inner
j	Injection conditions
n	Section
(n-1)	Section preceeding section n
o	Outer
s	Radial stagnation surface
w	Tube wall
1	Periphery of vortex tube

APPENDIX A

TRANSMISSION CHARACTERISTICS OF THIN-WALLED FUSED SILICA TUBES*

The thin-wall transparent models similar to those shown in Fig. 2 distort the light passing through their walls. This distortion is due to refractions and reflections that occur when light passes through the many small-diameter tubes. Tests were conducted in which the fraction of light absorbed in passing through the model walls was measured throughout a wide spectral range. Two experimental arrangements were used; one for measurements in the visible portion of the spectrum, and one for measurements in the ultraviolet portion of the spectrum.

For measurements in the visible portion of the spectrum, the spectral irradiance of a tungsten ribbon lamp was measured both with (I) and without (I_o) the transparent wall model surrounding the lamp. The transparent wall consisted of 0.070-in.-OD fused silica tubing having a nominal wall thickness of 0.005 in. (see Table II for typical wall-thickness variations). The tubing was placed axially around two 1.25-in.-dia rings at each end of the tubes. Throughout the spectral range from 0.35 to 0.85 microns there was no measurable difference in the radiant energy from the source with or without the transparent-wall model surrounding the tungsten ribbon lamp. With the instrumentation used, a difference of one percent in transmission could have been detected. Surface reflection losses, which would have been encountered if the walls were located only between the bulb and the detector, were not encountered because the transparent tubes completely surrounded the lamp.

For measurements in the ultraviolet portion of the spectrum, a different experimental arrangement was used. A sketch of the optical system employed is shown on Fig. 28. A 120-deg segment of the transparent-wall model was used and the emitted energy from a hydrogen discharge lamp was passed through the segment. This arrangement was used because the hydrogen discharge lamp produces a directional beam of light instead of the approximately spherical radiation produced by the tungsten ribbon lamp. The light transmitted was measured using a McPherson 0.5-meter monochromator. Measurements were made both with and without the model segment in the light beam. Since the thin-wall tubes of the model scatter much of the incident light, only a portion of the light from the hydrogen discharge lamp reached the monochromator entrance. The emitted light beam from the hydrogen lamp was approximately 0.25-in. in diameter. The segment of the transparent-wall model was placed

*Tests conducted by A. E. Mensing.

in a chamber that had an argon atmosphere. Lithium fluoride windows were installed in the chamber to permit the passage of the ultraviolet light (lithium fluoride is transparent above 0.115 microns).

Figure 28 presents the variation of intensity (in arbitrary units) with wavelength both with and without the model segment in the light beam. With the model in the beam, the amount of light entering the monochromator was reduced by approximately one order of magnitude. However, it was previously determined that at wavelengths greater than 0.35 microns, a complete model (360-deg segment) transmitted greater than 99 percent of the incident light. Thus, at these wavelengths (i.e., greater than 0.35 microns), the difference in measured intensity with and without the complete model in place is due to scattering. Since scattering is not a loss mechanism, the transparency of the model was determined by taking the ratio (at a wavelength of approximately 0.4 microns) of the intensity with no model to the intensity with the model, and then multiplying the measured intensities at all other wavelengths by this ratio. (This assumes no variation of index of refraction with wavelength.)

Results are presented in Fig. 29 for two different thin-wall models --- one made of commercial grade fused silica with 0.070-in.-OD tubes having a nominal wall thickness of 0.005 in., and one made of high-purity fused silica with 0.080-in.-OD tubes having a nominal wall thickness of 0.020 in. Measurements were made with the commercial grade fused silica model in both vertical and horizontal orientation; the data shown in Fig. 29 show that (1) the 0.005-in.-wall commercial grade fused silica has approximately the same transmission cutoff as the 0.020-in.-wall high-purity fused silica and (2) the transmission cutoff is quite sharp, so that the transmission decreases from about 80 percent to about 20 percent in less than 0.02 microns. The data shown in Fig. 29 are essentially the same as for flat slabs (rather than axial tubes) of equivalent thickness made from the same grades of fused silica (see Ref. 6).

APPENDIX B

HEAT TRANSFER AND STRESS ANALYSES OF FUSED SILICA TUBES

This Appendix presents a discussion of the heat transfer rates and stresses present in the fused silica coolant tubes during the hot-flow tests described in Section IV. In particular, analyses are presented for calculating the temperature distribution along the length of a coolant tube as well as the thermal and mechanical stresses of a coolant tube caused by the proximity of the r-f plasma.

Heat Transfer Analysis

A computer program* was written for calculating the temperature distribution along the length of an internally cooled fused silica tube exposed to a specified heat flux distribution. The tube was assumed to be of length ℓ_c with an inner diameter of d_i and a wall thickness x. The length was divided into m equal sections. The total heat into a given section is

$$Q_m = Q_m'' \frac{\pi}{2} (d_i + 2x) \frac{\ell_c}{m} \tag{B-1}$$

where Q_m'' is the heat flux per unit area at a given section. The factor of 1/2 results because it was assumed the heat is deposited over one-half the tube peripheral area.

The bulk coolant temperature at any section, n, is

$$T_n = \frac{Q_n}{W_c C_p} + T_{(n-1)} \tag{B-2}$$

where $T_{(n-1)}$ is the bulk outlet temperature of the preceeding section (i.e., the bulk inlet temperature of section n). The film temperature differential is

$$(\Delta T_f)_n = \frac{Q_n m}{h_n \pi d_i \ell_c} \tag{B-3}$$

*Program written by H. E. Bauer.

where

$$h_n = 0.023 \cdot \frac{k_n}{d_i} \left(\frac{4W_c}{\pi \mu_n d_i} \right)^{0.8} (Pr_n)^{1/3} \qquad \text{(B-4)}$$

The following linear relations were used for approximating the variation of coolant properties with temperature in Eq. (B-4). These property values are also shown in Fig. 30.

$$k_n = 3.2 \times 10^{-5} + 1.2 \times 10^{-7}\, T_{(n-1)}$$

$$Pr_n = 67.5 - 0.114 T_{(n-1)} \text{ FOR } T_{(n-1)} \leq 550 \text{ R}$$

$$Pr_n = 21.3 - 0.03 T_{(n-1)} \text{ FOR } T_{(n-1)} > 550 \text{ R}$$

$$\mu_n = 6.1 \times 10^{-3} - 1.02 \times 10^{-5}\, T_{(n-1)} \text{ FOR } T_{(n-1)} \leq 550 \text{ R}$$

$$\mu_n = 2.085 \times 10^{-3} - 2.9 \times 10^{-6}\, T_{(n-1)} \text{ FOR } T_{(n-1)} > 550 \text{ R}$$

The temperature difference across the tube wall is

$$(\Delta T_w)_n = \frac{Q_n \times m}{k_w \pi (d_i + x) \ell_c} \qquad \text{(B-5)}$$

where $k_w = 6.75 \times 10^{-5} + 2.55 \times 10^{-7}\, T_n$ (from Fig. 30)

$$T_n = T_{(n-1)} + (\Delta T_f)_{n-1}$$

The following quantities were also specified:

Coolant inlet temperature	(510 R)
Coolant flow rate	(0.00356 lb/sec)
Coolant specific heat	(1 Btu/lb-deg R)
Tube inside diameter	(0.00333 ft)
Tube wall thickness	(0.000833 ft)
Tube length	(0.250 ft)

Number of sections	(10)
Coolant outlet temperature	(program will calculate)
Heat flux per section	(assumed cosine distribution)

The calculation proceeds in a stepwise manner until output values for each section are obtained for the coolant temperature, the inside wall temperature, and the outside wall temperature. A plot of these temperatures for a specific heat flux distribution along the length of a fused silica tube is shown in Fig. 31. A cosine heat flux distribution with an average value of 91.8 Btu/sec-ft^2 was assumed. The average heat flux value of 91.8 Btu/sec-ft^2 represents the total heat flux deposited into the wall of the 1.26-in.-ID axial-coolant-tube model test shown in Table I. An assumed average heat flux value of 70.3 Btu/sec-ft^2 shown in Fig. 32 represents the total heat flux deposited into the wall of the 0.936-in.-ID axial-coolant-tube model shown in Table I. The coolant tubes in this model are divided into three groups with a return flow end cap (see Fig. 15) so that the coolant flow makes two passes (i.e., inlet and return) through the model. These two passes are represented by the two temperature distribution plots placed as shown in Fig. 32. The water coolant temperature, T_c, rises by 58 R (568 R - 510 R) over the entire model. The calculated temperature rise agrees quite well with the measured value of 56 R noted in Fig. 18. This program assumes heat deposition in the coolant only by conduction through the tube wall while in the actual test, some heat is also deposited by radiation. For water coolant the amount deposited due to radiation may be considerable. Thus, the calculated temperature rise of the coolant may be too high due to the energy deposited by radiation.

A heat transfer analysis of the coolant tubes and injector tubes used in axial-coolant-tube models was also made and is shown in Table III. The coolant tubes were made from fused silica and the injector tubes from both fused silica and copper. Both water and argon coolants were used. The tube dimensions, coolant flow rates and assumed temperatures are given in Table III. The equations used (Ref. 16) are

$$\frac{Q}{A} = k_w \frac{\Delta T_w}{x} \qquad \text{(conduction heat capacity)} \qquad \text{(B-6)}$$

where k_w is the tube wall thermal conductivity, ΔT_w is the temperature differential across the wall, and x is the tube wall thickness.

$$\frac{Q}{A} = h_c \Delta T_f \qquad \text{(film convection heat capacity)} \qquad \text{(B-7)}$$

where $h_c = 0.023\ (k_c/d)(4W_c/\pi d\mu_c)^{0.8}(P_{r_c})^{0.4}$, ΔT_f is the temperature differential across the film and

$$Q = W C_p \Delta T_c \qquad \text{(bulk convection heat capacity)} \qquad \text{(B-8)}$$

where ΔT_c is the coolant temperature rise.

The values of the physical constants in Eqs. (B-6), (B-7), and (B-8) were obtained for the temperature specified in Table III from Ref. 16. The results of the three heat capacities for the cases investigated are shown in the last three columns of Table III. The limiting factor with sufficient coolant flow is the conduction heat capacity of the wall material.

Thermal Stress

Fused silica retains its strength and will not deform under load at temperatures approaching the strain point (1343 K), as mentioned in Ref. 17. However, the upper limit for operating temperatures is usually determined by stresses due to the temperature differentials within the fused silica. If one surface of an unrestrained plate of fused silica is maintained at a higher temperature than the other surface, the expansion of the heated surface will cause the plate to bend slightly. If, however, the plate is restrained so that it cannot bend, either by edge clamping or as a result of its shape, as in the case of a tube, internal stresses are developed which are compressive on the warmer side and tensile on the cool side. For this type of constraint, the stresses at the surface can be expressed (refer to Ref. 17) as

$$\sigma_t = \frac{E\alpha\Delta T}{2(1-\nu)} \qquad \text{(B-9)}$$

where ΔT is the temperature difference across wall (uniform gradient assumed), α is the thermal expansion of fused silica, E is the modulus of elasticity, and ν is Poisson's ratio. A clear distinction must be made between the temperature of the fluid in contact with the surface of the fused silica and the true surface temperature. The temperature drop through the films at the surfaces may be several times the temperature difference across the fused silica itself (Ref. 18). Under transient conditions produced by the sudden heating or cooling of one or both of the fused silica surfaces, the stress conditions will differ from those of the steady state discussed

above. The transient stress which can approach a value of twice the steady-state stress will return to the steady state as the temperature conditions are stabilized (Ref. 19).

The thermal stress present in fused silica tubes as calculated from Eq. (B-9) is shown in Fig. 33 as a function of the temperature difference in the material. The solid curve shown includes the effects due to the variations with temperature of the properties in Eq. (B-9). The wall temperature rise assumed in the reference engine (Ref. 3) is shown to be 110 K. The data from the highest power tests for this present program and for previous tests (Ref. 10) as given in Table I are also shown. The design value for thermal stress is usually taken as 1000 psi (Ref. 17) and the nominal tensile stress limit as 7000 psi (Ref. 6). Values of the thermal stress for the calculated temperature distributions are given in Fig. 31 and 32. The thermal stress value in Fig. 31 corresponds to the data point shown in Fig. 33 for the highest power test during the present program (see Table I).

Mechanical Stress

The properties of fused silica under stress differ appreciably from those of metals. Fused silica fails abruptly without measurable yield or permanent deformation. This defines fused silica as a brittle material. Failure always results from a tensile component of stress, even when the load is applied in compression. Fused silica is much stronger under compressive loads than under tensile loads. The spread of breaking stresses obtained from testing a large group of fused silica specimens is much greater than from a corresponding group of metal specimens. As discussed in Ref. 17, fractures of fused silica originate in small imperfections, or flaws, the large majority of which are found at the surface. Since fused silica does not yield, there is no relief of these stresses, and fracture results from the propagation of one of the flaws. Different methods of fabrication and treatment of fused silica produce flaws of different characteristics and sizes.

Hydrostatic tests were conducted to determine the pressure which would cause failure in the fused silica tubes used in axial-coolant-tube models described in Sections III and IV. The fused silica tubes were drawn by a vendor and were tested as received. A photograph of 0.050-in.-ID by 0.060-in.-OD fused silica tubes before and after testing is shown in Fig. 34(a). The tubes were pressurized with water and sealed on each end into end caps with O-rings. The axial alignment of the tubes and the flexibility of the O-ring seals minimized any bending or torsion stresses. Thus, the failure was caused by a hoop or tensile stress. It was noted that in other tests where there was considerable bending stress present, the tubes

failed transverse to their centerline. However, the tubes which failed due to hoop stress failed parallel to the tube centerline with the tube splitting in half (shown in Fig. 34(a)). The hoop stress for a thin-wall tube is given (Ref. 17) as

$$\sigma_H = \frac{P_B D}{2x} \qquad \text{(B-10)}$$

where P_B is the burst pressure, D is the inside tube diameter, and x is the tube wall thickness. A plot of the hoop stress as a function of the burst pressure for various diameter tubes as calculated from Eq. (B-10) is shown in Fig. 34(b). The data from the hydrostatic tests is also shown for the different diameter tests. The results support the choosing of a nominal tensile stress limit of 7000 psi. All of the tubes tested failed at or below the stress level. Also, the stress (i.e., pressure) at tube failure varied considerably more for the 0.05-in.-ID by 0.06-in.-OD drawn, thin-wall tubing than for any of the other tubing tested. This was probably due to the greater variation in wall thickness of this size drawn tube as compared to the larger size tubes.

The total stress in a given tube is equal to the sum of all the component stresses. For the tubes used in the hot flow tests the total stress (neglecting bending, torsion, etc.) is

$$\sigma_T = \sigma_t + \sigma_H \qquad \text{(B-11)}$$

where σ_t is the thermal stress and σ_H is the hoop stress. The pressure difference across the coolant tube wall during the axial-coolant-tube model tests described in Section IV was always less than about 100 psi. Thus, the hoop stress incurred during testing was less than 500 psi (from Eq. (B-10)). The thermal stress for the highest power test is shown to be 470 psi in Fig. 33. Thus, the total stresses for the tests conducted during this program were less than 1000 psi. Thus, the combination of thermal stress and hoop stress encountered by the fused silica coolant tubes during tests conducted in this program (see Section IV) were well within the nominal stress limit.

APPENDIX C

DERIVATION OF VORTEX FLOW PARAMETERS

Radial-Inflow Vortex Flow

The nuclear light bulb concept of the gaseous core nuclear rocket utilizes a radial-inflow vortex to confine the nuclear fuel away from the transparent wall. A summary of the investigations made in the study of radial-inflow vortexes at UARL and elsewhere is given in Ref. 13. As discussed in Ref. 10, the particular radial-inflow pattern of interest for the nuclear light bulb engine is illustrated in Fig. 35(a). It is characterized by a laminar radial stagnation surface across which there is no radial convection. A central recirculation-cell region occurs inside of the radial stagnation surface, and a region of axial flow toward the end walls occurs outside the radial stagnation surface. At the radius of the radial stagnation surface, all of the radial flow passes through the end-wall boundary layers. Previous flow visualization studies in jet-injection vortex tubes (Ref. 13) have shown that the flow is essentially laminar at radii less than that of the radial stagnation surface and is turbulent at larger radii. The turbulence outside of the radial stagnation surface is due in part to wall shear and jet mixing. It is expected that the stabilizing effect of the radial temperature gradient in a nuclear light bulb engine would reduce the turbulence observed in the outer region in these constant-temperature laboratory experiments. The central laminar-flow region would be suitable for fuel containment in the engine, and the axial flow in the outer region would carry away fuel and fission products that diffuse radially outward.

According to the theoretical investigation described in Ref. 20, radial stagnation surfaces and cells occur when the secondary flow resulting from friction on the end walls and the radial gradient of pressure in the vortex is greater than the flow withdrawn through the thru-flow ports at the centers of the end walls. A secondary-flow similarity parameter, β_t, which was introduced in Ref. 20 is

$$\beta_t = \frac{D}{L}\left(\frac{Re_{t,p}^{0.8}}{Re_{t,j}}\right) \qquad (C\text{-}1)$$

where D is the diameter of the vortex tube, L is the length of the vortex tube, $Re_{t,p}$ is the tangential Reynolds number (a measure of the tangential velocity at the periphery of the tube), and Re_r is the radial Reynolds number (a measure of the mass flow withdrawn through the thru-flow ports). The magnitude of the parameter

β_t provides an indication of the type of flow pattern that will occur. The three general types of flow patterns and the corresponding ranges of values of β_t are shown in Fig. 35(b). The flow regime of interest in this investigation is shown at the top of Fig. 35(b); it occurs for values of β_t greater than about 25. Reference 20 also indicates that in this flow regime the radius of the radial stagnation surface increases with increasing β_t. From Ref. 13 the value of β_t from Eq. (B-12) can be written as

$$\beta_t = 2\pi D(\mu)^{0.2}(r_1)^{0.8}\frac{1}{(W)^{0.2}}\left(\frac{Re_{t,p}}{Re_{t,j}}\cdot\frac{1}{A_j}\right)^{0.8} \qquad (C\text{-}2)$$

where μ is the laminar viscosity (temperature-dependent), r_1 is the outer radius of the vortex tube, W_j is the total injected flow rate, and A_j is the total injection area. The only quantity in the determination of β_t which is not known is the ratio $Re_{t,p}/Re_{t,j}$. This ratio, which is equivalent to v_1/v_j, for constant temperature and density flows, is derived below.*

For low Mach numbers, the friction coefficient on the peripheral wall of a vortex tube is given by the following equation from Ref. 21

$$C_f = \frac{W\sqrt{\frac{T}{519}}\,(Y_1 - Y_j)}{LKd\,(P/2121)} \qquad (C\text{-}3)$$

Also, from Ref. 21,

$$K = \frac{2121\,\gamma g\,\pi}{2\sqrt{2g(778)C_p(519)}} \qquad (C\text{-}4)$$

where

$$Y = \sqrt{\frac{\gamma-1}{2}}\left(\frac{1}{M}\right) - (\gamma-1) \qquad (C\text{-}5)$$

*Taken from derivation given in UARL memos by G. H. McLafferty.

$$M = \frac{V}{\sqrt{\gamma g R T}} \tag{C-6}$$

$$\frac{W}{L} = \rho v_j h_j = \frac{P}{RT} v_j h_j \tag{C-7}$$

$$R = 778(C_p - C_v) = 778 C_p \frac{\gamma - 1}{\gamma} \tag{C-8}$$

Substitution of Eqs. (C-4) through (C-7) into Eq. (C-3) gives

$$C_f = \frac{2 v_j h_j}{d\pi} \sqrt{\frac{\gamma - 1}{\gamma} \frac{(778) C_p}{R}} \left(\frac{1}{v_1} - \frac{1}{v_j} \right) \tag{C-9}$$

Substitution of Eq. (C-8) into Eq. (C-9) yields

$$C_f = \frac{2 v_j h_j}{d\pi} \left(\frac{1}{v_1} - \frac{1}{v_j} \right) \tag{C-10}$$

$$\frac{d}{h_j} = \frac{dL}{A_j} = \frac{2}{C_f \pi} \left(\frac{v_j}{v_1} - 1 \right) \tag{C-11}$$

Equation (C-11) is evaluated in Fig. 36(a) using values of friction coefficient determined from the correlation in Fig. 4 of Ref. 21, which was obtained from Ref. 22 for a tangential Reynolds number of approximately 300,000. The curves in Fig. 36(a) for tangential Reynolds numbers other than 300,000 were obtained by assuming that friction coefficient varies as the minus 0.2 power of Reynolds number. This Reynolds number correction was suggested in Ref. 21, but has not been verified experimentally.

The flow injected into the vortex is

$$W_j = \rho v_j A_j = \rho v_1 r_1 \frac{v_j}{v_1} \frac{2A_j}{d} \tag{C-12}$$

The flow passing radially inward through both end-wall boundary layers, according to Ref. 20, is

$$2W_{ST} = 4\pi\mu r_1 K_T Re_t^{0.8} \tag{C-13}$$

Equating these two flows (i.e., equating Eqs. (C-12) and (C-13)) yields

$$\frac{L}{D} = \frac{\pi K_T}{Re_t^{0.2}} \frac{dL}{A_j} \frac{v_1}{v_j} \tag{C-14}$$

Equation (C-14) has been evaluated using a value of K_T of 0.113 (the value for a strong vortex according to Ref. 20), and the results are indicated in Fig. 36(a). The value of v_1/v_j is plotted as a function of several parameters including Re_t in Fig. 2-11 of Ref. 23. The plot shown in Fig. 2-11 is a compilation of existing data and is equivalent to Eq. (C-14). The values of β_t shown in Fig. 13 were determined from Eq. (C-2) and Fig. 36(a).

The variation of friction coefficient with Reynolds number is assumed to be

$$C_f = C_f^* \left(\frac{300{,}000}{Re_t}\right)^{0.2} \tag{C-15}$$

where C_f^* is the value given in Fig. 4 of Ref. 21.

Combining Eqs. (C-11), (C-14), and (C-15),

$$\frac{L}{D} = \frac{2K_T}{C_f^*} \frac{1}{(300{,}000)^{0.2}} \left(1 - \frac{v_1}{v_j}\right) \tag{C-16}$$

The value of K_T to be used in Eq. (C-16) is given in Fig. 6 of Ref. 20. Equation (C-16) has been evaluated using the information from Fig. 4 of Ref. 21 and Fig. 6 of Ref. 20 and the results are given in Fig. 36(b). Thus, for a given value of L/D and V_1/V_j, the ratio of the approximate radius of the radial stagnation surface to the tube radius can be determined.

TABLE I

COMPARISON OF OPERATING CONDITIONS IN FULL-SCALE ENGINE WITH HIGHEST POWER LEVEL MODEL TESTS

	Unit Cavity Full-Scale Engine[a] Reference Engine	MODELS FROM REF. 10		MODELS TESTED DURING PRESENT PROGRAM				
		1.26-in.-ID Axial Coolant-Tube Model	0.95-in.-ID Axial Coolant-Tube Model	1.55-in.-ID Axial Coolant-Tube Model	1.26-in.-ID Axial Coolant-Tube Model	0.934-in.-ID Axial Coolant-Tube Model	0.934-in.-ID Axial Coolant-Tube Offset Model	0.846-in.-ID Axial Coolant-Tube Model
Transparent-wall configuration	Circumferential	Axial	Axial	Axial	Axial	Axial	Axial	Axial
Inside diameter, ft	1.604	0.105	0.079	0.129	0.105	0.078	0.078	0.070
Length between containing end walls, ft	6.0	0.167	0.167	0.167	0.167	0.167	0.167	0.167
Length/Diameter ratio	3.75	1.59	2.11	1.29	1.59	2.12	2.12	2.49
Number of coolant tubes	3000	54	42	69	39	48	48	33
Tube inside diameter, in.	0.050	0.040	0.040	0.040	0.040	0.040	0.040	0.040
Tube outside diameter, in.	0.060	0.050	0.050	0.060	0.060	0.060	0.060	0.060
Tube wall thickness, in.	0.005	0.005	0.005	0.010[f]	0.010	0.010	0.010	0.010
Total tube surface area, ft^2	95.2	0.177[b]	0.137[b]	0.271[b]	0.153[b]	0.188[b]	0.188[b]	0.130[b]
Cylindrical surface area, ft^2	30.2	0.082[b]	0.062[b]	0.101[b]	0.082[b]	0.061[b]	0.061[b]	0.055[b]
Coolant fluid	Hydrogen	Water	Water	Water	Water	Water	Water	Water
Buffer fluid	Neon	Argon	Argon	Argon	Argon	Argon	Argon	Argon
Buffer injection velocity, ft/sec	25[c]	210	211	226	168	60	98	56
Buffer weight flow, lb/sec	2.96	0.012	0.003	0.019	0.010	0.008	0.009	0.006
Chamber pressure, atm abs	500	5.8	2.8	6.3	4.4	6.6	4.9	5.8
Equivalent black-body radiating temperature, R	15,000	-	-	-	-	-	-	-
Radiant energy flux per unit area, Btu/sec-ft^2	24,300	-	-	-	-	-	-	-
kw/$in.^2$	178	-	-	-	-	-	-	-
Total heat flux deposited in wall, Btu/sec-ft^2	490	270	71.5	45	91.8	33	70.3	91.6
Thermal radiation from fuel, Btu/sec-ft^2	218	11[d]	2.5[d]	2.3[d]	4.6[d]	1.6[d]	3.5[d]	4.6[d]
Conduction-Convection from fuel, Btu/sec-ft^2	26	259	(see Ref. 10)	42.7	87.2	31.4	66.8	87
Reradiation from propellant, Btu/sec-ft^2 (neglected)	-	-		-				
Conduction-Convection from propellant, Btu/sec-ft^2	246	0	(see Ref. 10)	0	0	0	0	0
Total heat flux deposited in wall divided by energy flux in fuel region	0.020	0.495[e]	0.623[e]	0.179[e]	0.248[e]	0.131[e]	0.248[e]	0.360[e]

a Data obtained from Refs. 1 and 3
b Based on 3-in. length
c Assumed value of $V_1/V_4 = 0.4$
d Assumed 5 percent of total radiation was deposited in transparent wall and coolant fluid
e Includes heat flux deposited in transparent wall and coolant fluid
f Also tested with 0.005-in. wall thickness

TABLE II

APPROXIMATE DIMENSIONAL CHARACTERISTICS OF FUSED SILICA TUBES USED IN TRANSPARENT-WALL MODELS

Measurements Made by UARL on Samples from Shipments Received from Vendors

Vendor	Grade	Nominal Wall Thickness, in.	Measured Wall Thickness, in.			Average / Nominal	Standard Deviation About Average, in.
			Maximum	Minimum	Average		
I	Commercial	0.005	0.0145	0.009	0.011	2.20	0.0012
		0.010	0.0135	0.007	0.011	1.10	0.0018
II	Commercial	0.005	0.0095	0.0055	0.007	1.40	0.0011
		0.005[a]	0.0060[a]	0.0045[a]	0.0054[a]	1.08[a]	0.0004[a]
III	Commercial	0.005	0.0085	0.0035	0.0061	1.22	0.0011
		0.010	0.010	0.0075	0.009	0.90	0.0007
	High Purity	0.020	0.0185	0.011	0.017	0.85	0.0019
IV	Commercial	0.020	0.026	0.020	0.022	1.10	0.0013

a Most recent supply of tubes obtained from vendor

TABLE III

HEAT TRANSFER ANALYSIS OF MATERIAL USED IN AXIAL-COOLANT-TUBE MODELS

	Tube Inner Diameter, in.	Tube Outer Diameter, in.	Tube Wall Thickness, in.	Number of Tubes	Wall Material	Temp. Drop Across Wall deg F	Coolant Fluid	Coolant Flow lb/sec	Coolant Area ($\times 10^6$) sq. ft	Coolant Temp. Rise deg F	Temp. Drop Across Film . deg F	Film Temp. deg F	Conduction Heat Capacity Btu/sec-ft^2	Film Convection Heat Capacity Btu/sec-ft^2	Bulk Convection Heat Capacity Btu/sec-ft^2
COOLANT TUBES	0.040	0.080	0.020	48	Fused Silica	500[a]	Water	0.417 (3 gpm)	438	100	150	200	83	7484	95,205
								0.139 (1 gpm)						3106	31,735
	0.040	0.060	0.010	48	Fused Silica	500[a]	Water	0.417 (3 gpm)	438	100	150	200	165	7484	95,205
								0.139 (1 gpm)						3106	31,735
	0.050	0.060	0.005	48	Fused Silica	500[a]	Water	0.417 (3 gpm)	653	100	150	200	330	694	63,859
								0.139 (1 gpm)						288	21,129
INJECTOR TUBES	0.080	0.160	0.040	3	Fused Silica	500[a]	Argon	0.030	104	100	150	200	42	151	3614
								0.010						63	1205
								0.030	104	600	800	900	55	326	21,687
								0.010						135	7229
	0.117	0.187	0.035	3	Copper	90[b]	Argon	0.030	224	100	150	200	1940	74	1678
								0.010						30.5	560
								0.030	224	600	800	900	1716	175	10,069
								0.010						72	3356
	0.010	0.020	0.005	3	Copper	90[b]	Water	0.0417 (0.3 gpm)	1.63	100	150	200	13,555	14,369	2,558,282
								0.0139 (0.1 gpm)						5970	852,761

a Assumed thermal stress (σ_t) of 1000 lb/sq in.
b Assumed thermal stress (σ_t) of 10,000 lb/sq in.

FIG. 1

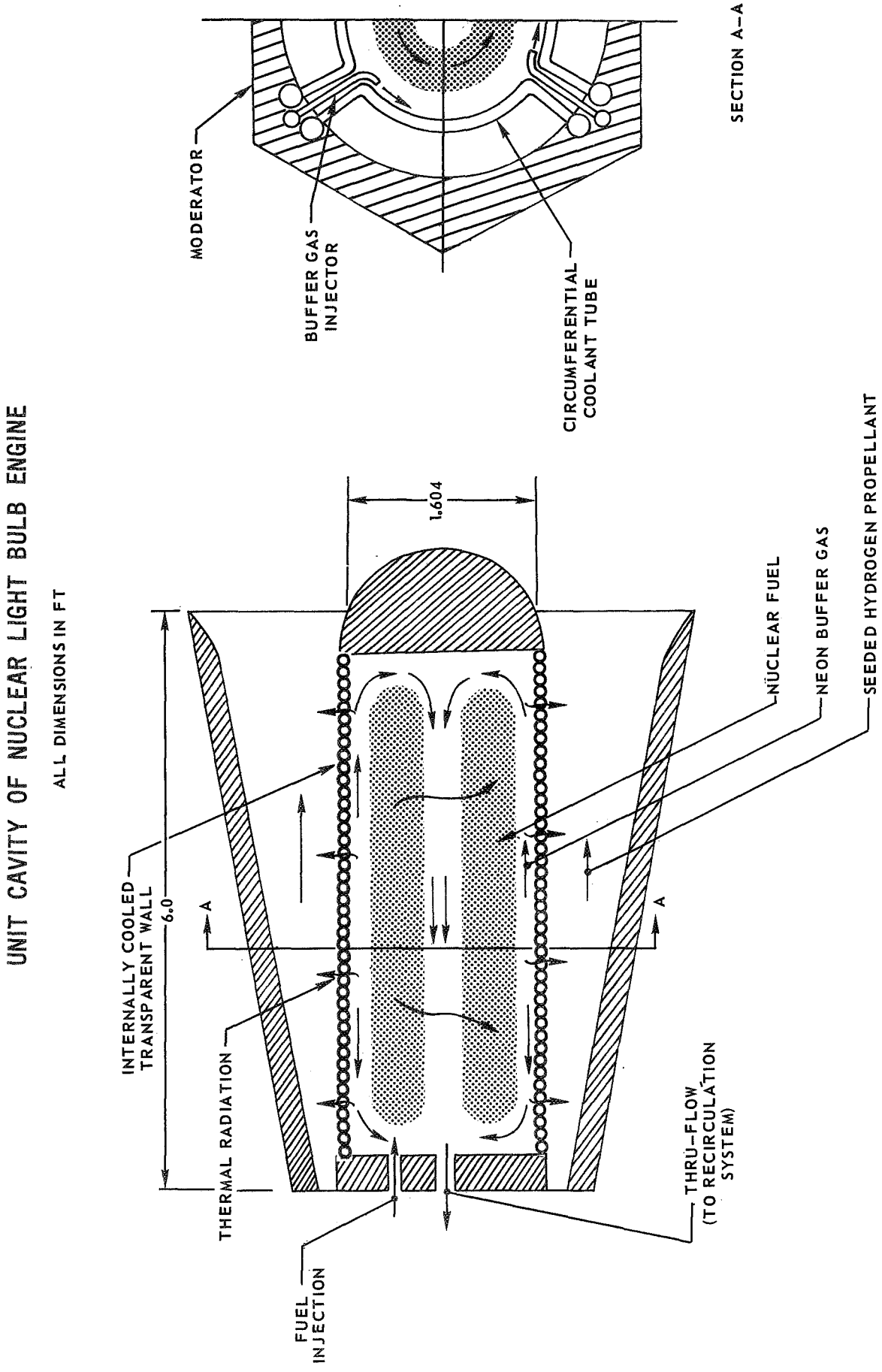
UNIT CAVITY OF NUCLEAR LIGHT BULB ENGINE
ALL DIMENSIONS IN FT
SECTION A-A
MODERATOR
BUFFER GAS INJECTOR
CIRCUMFERENTIAL COOLANT TUBE
1.604
6.0
INTERNALLY COOLED TRANSPARENT WALL
THERMAL RADIATION
FUEL INJECTION
NUCLEAR FUEL
NEON BUFFER GAS
SEEDED HYDROGEN PROPELLANT
THRU-FLOW (TO RECIRCULATION SYSTEM)
A
A

FIG. 2

PHOTOGRAPHS OF SEVERAL TYPES OF AXIAL - COOLANT - TUBE MODELS

(a) FUSED SILICA MODEL

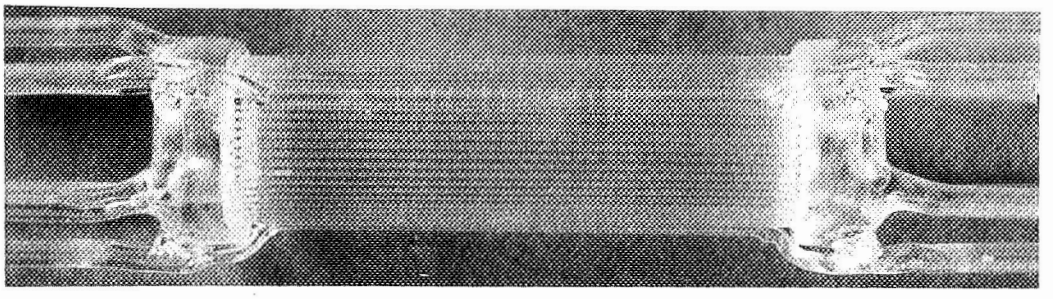

(b) MODEL WITH ANNULAR MANIFOLD AND DRILLED INJECTORS

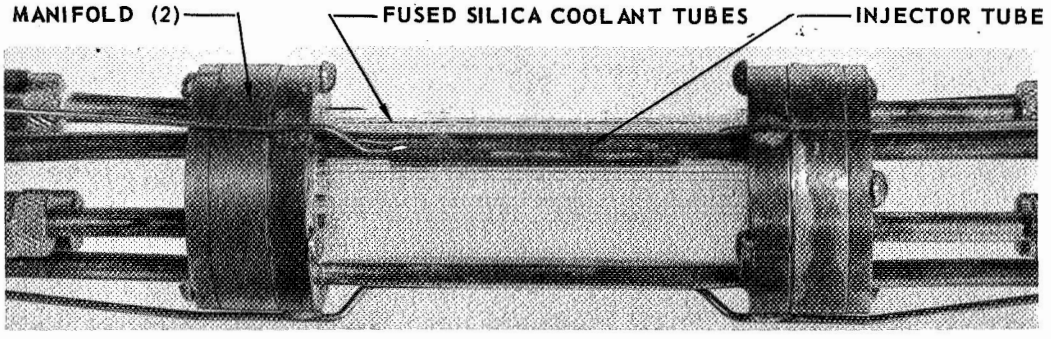

(c) MODEL WITH OFFSET ANNULAR MANIFOLDS AND CURVED HYPO-TUBE INJECTORS

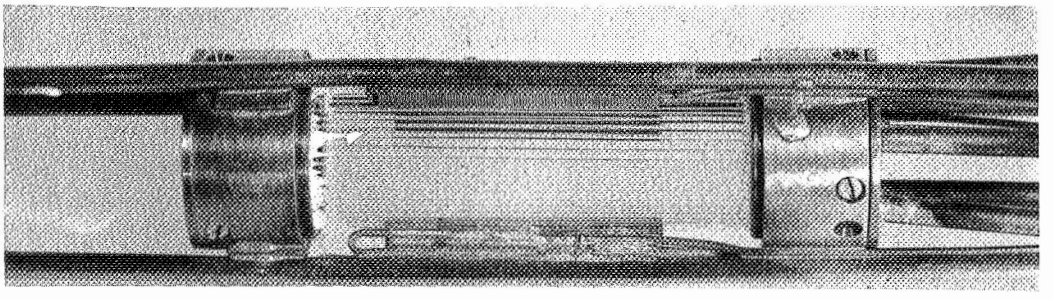

d) MODEL WITH COPPER OFFSET ANNULAR MANIFOLDS AND STRAIGHT HYPO-TUBE INJECTORS

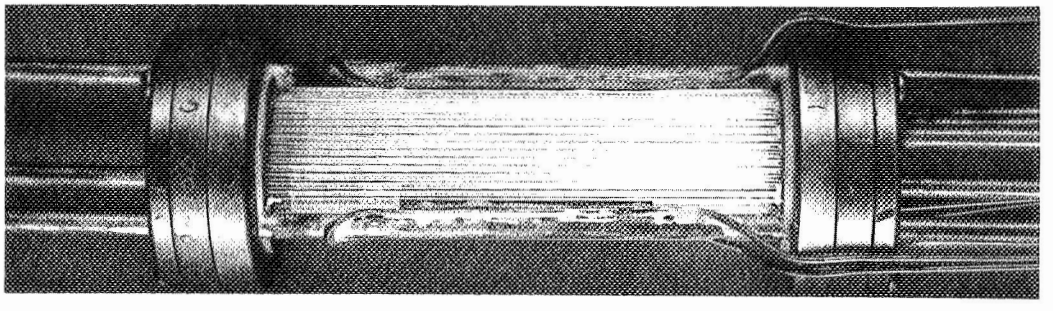

FIG. 3

PHOTOGRAPHS OF DRAWN FUSED SILICA TUBES AS RECEIVED FROM VENDOR

SEE TABLE II FOR DIMENSIONAL CHARACTERISTICS

(a) SIDE VIEW OF NOMINAL 0.050-IN.-ID X 0.060-IN.-OD (0.005-IN. WALL) TUBES

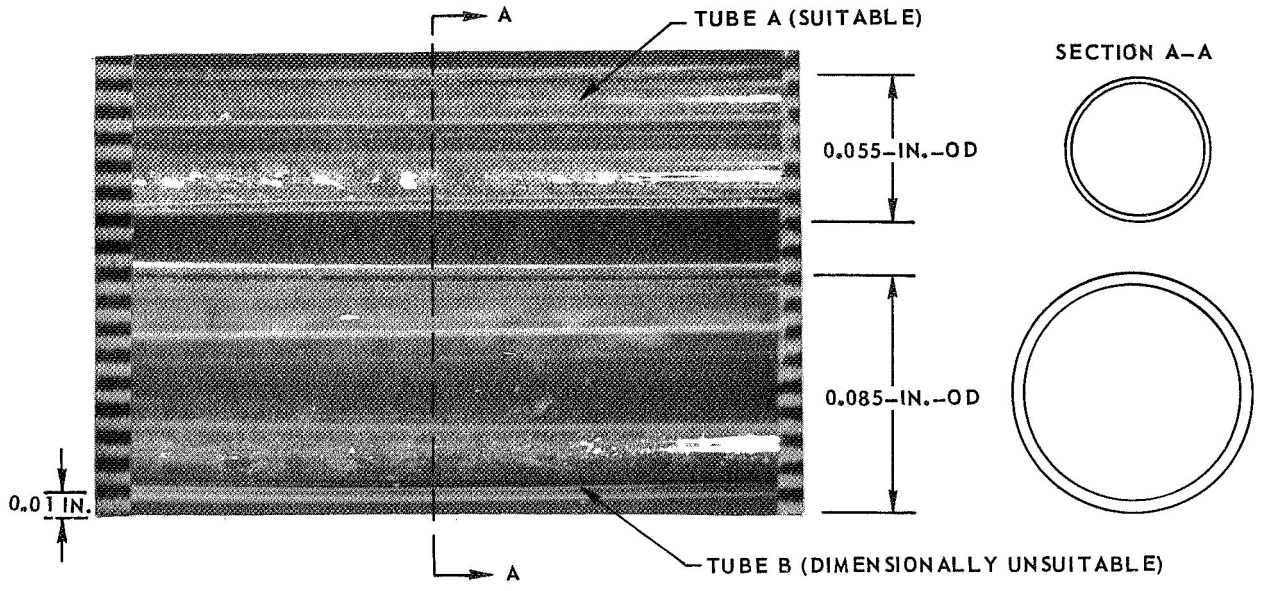

(b) VIEW OF SAME TUBE 3-IN. FROM LOCATION IN (a)

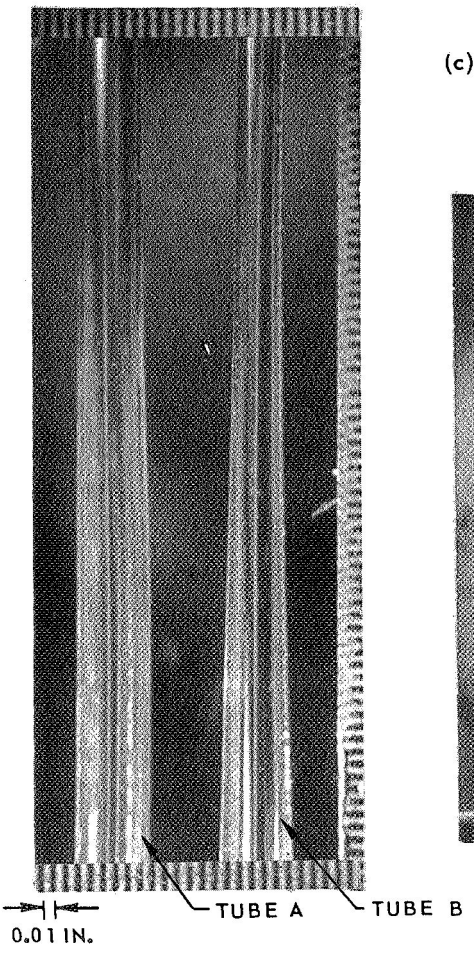

(c) CROSS-SECTIONS OF THREE TUBES WITH DIFFERENT WALL THICKNESSES

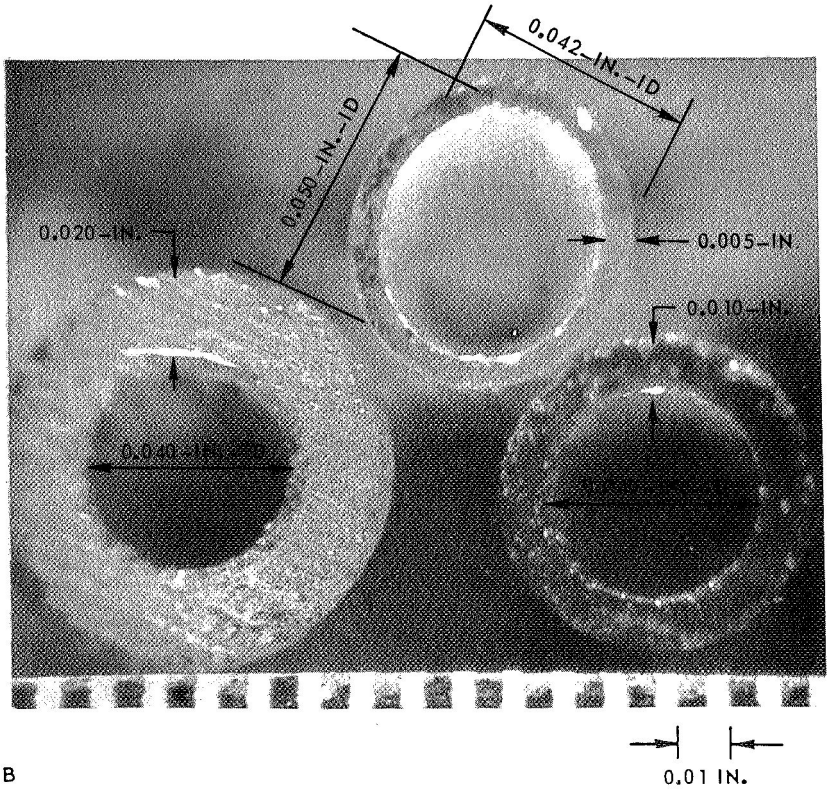

SKETCHES OF EQUIPMENT FOR CUTTING AND MEASURING FUSED SILICA TUBING

METHOD OF TUBE CUTTING

(a) TUBES CONNECTED TO MANIFOLD

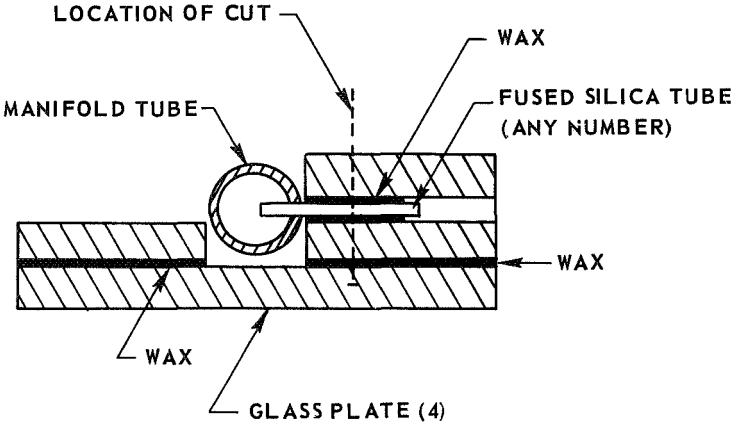

(b) TUBES NOT ATTACHED

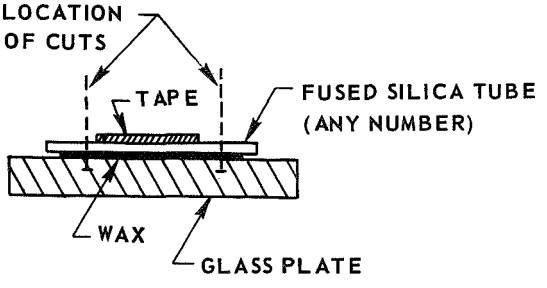

(c) MEASUREMENT OF TUBE WALL THICKNESS

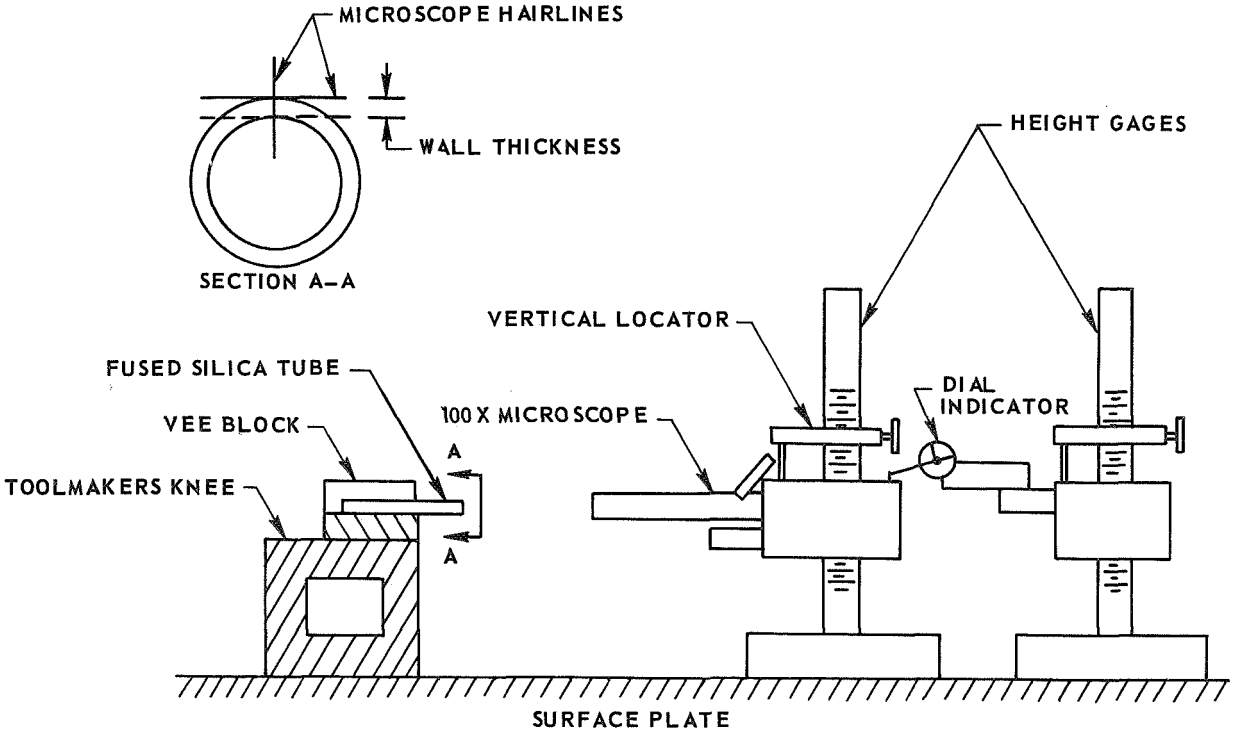

FIG. 5

PHOTOGRAPHS OF MANIFOLD CONFIGURATIONS USED IN AXIAL – COOLANT – TUBE MODELS

(a) INDIVIDUAL–HOLE ALUMINUM MANIFOLDS

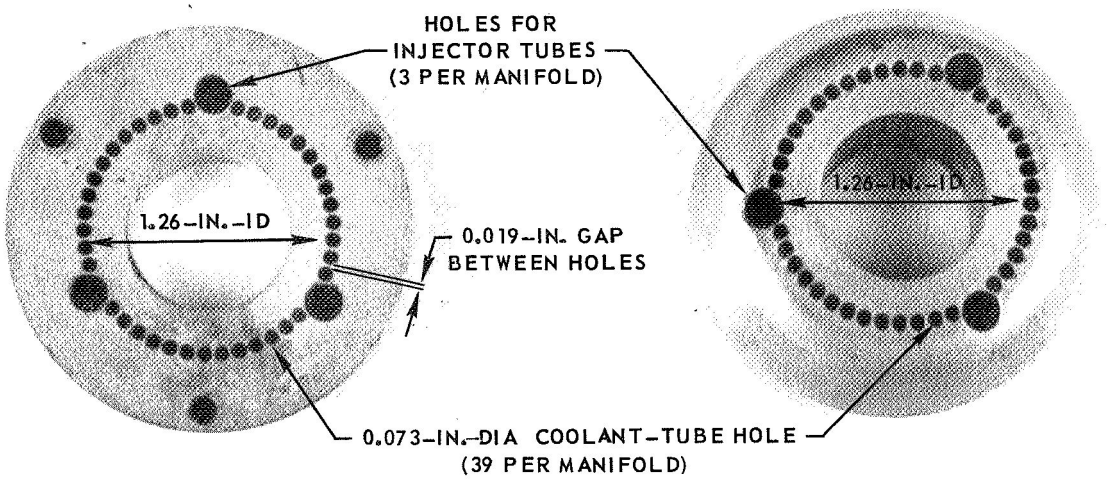

(b) INDIVIDUAL–HOLE COPPER MANIFOLDS

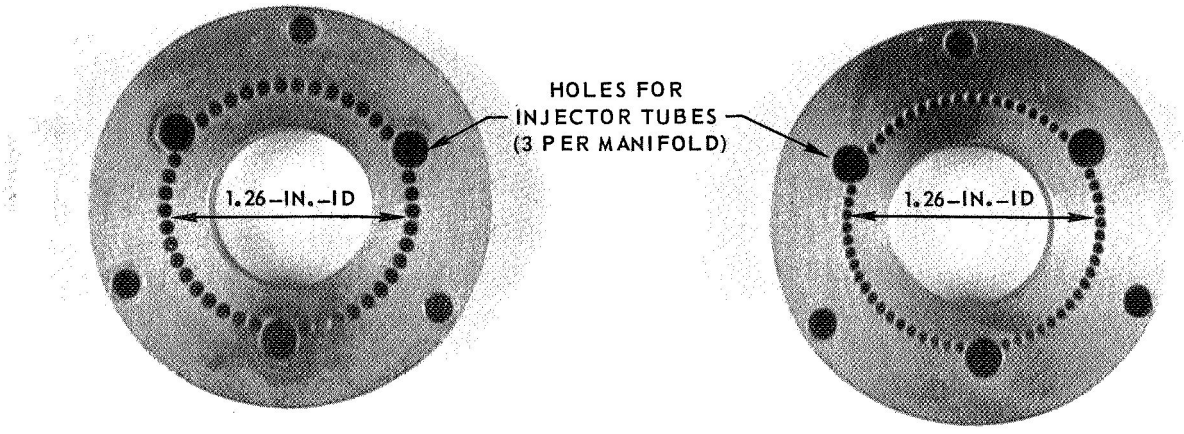

(c) ANNULAR–GROOVE COPPER MANIFOLDS

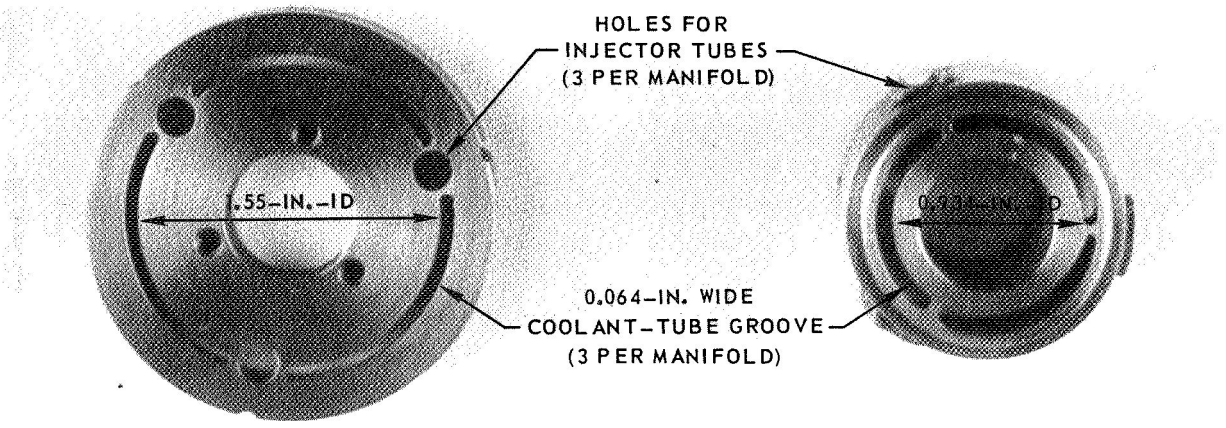

(SAME DESIGN USED FOR 1.26–IN.–ID MODEL)

(SAME DESIGN USED FOR 0.846–IN.–ID MODEL)

PHOTOGRAPHS OF FUSED SILICA COOLANT – TUBE SEALING METHODS EMPLOYED IN AXIAL – COOLANT – TUBE MODELS

(a) SHRINK–TUBING METHOD

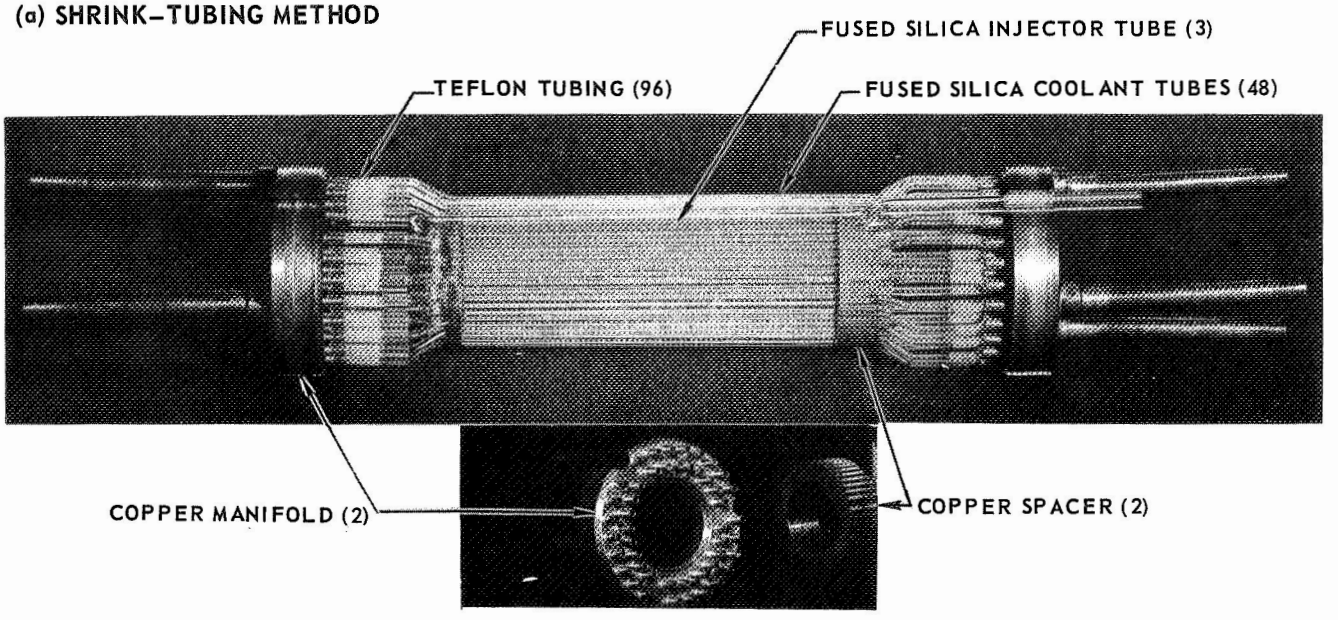

(b) FUSING METHOD

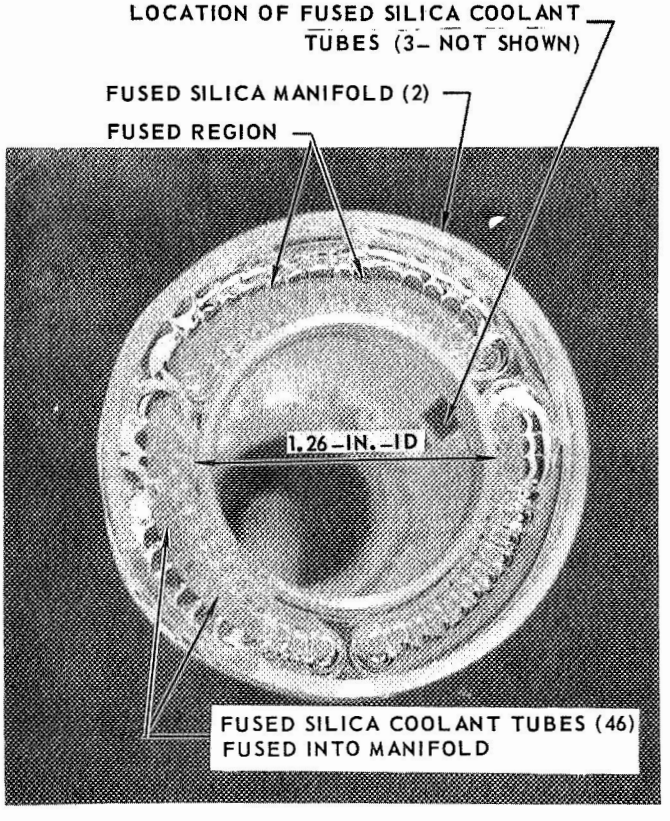

(c) POTTING METHOD

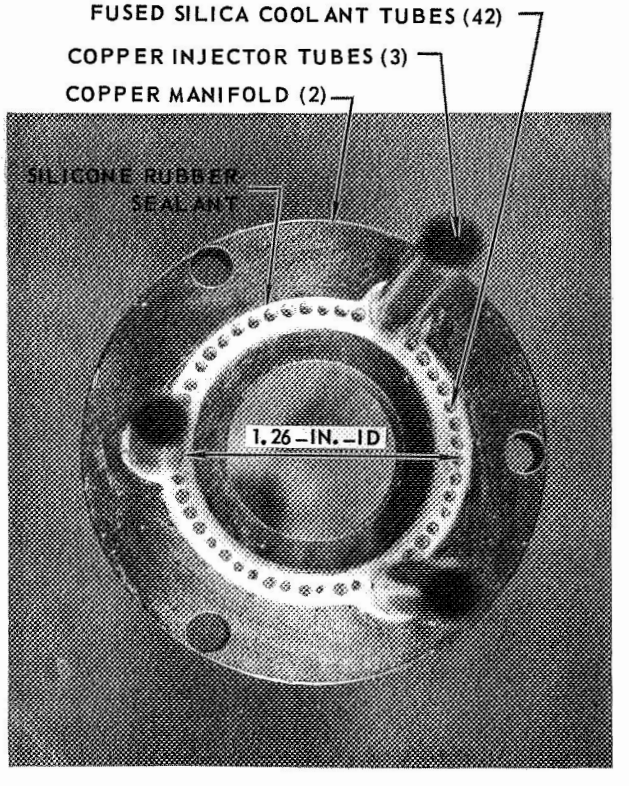

J-910900-3 FABRICATION OF CIRCUMFERENTIAL COOLANT – TUBE SEGMENTS FROM COILED FUSED SILICA TUBING FIG. 7

(a) ORIGINAL FUSED SILICA TUBE

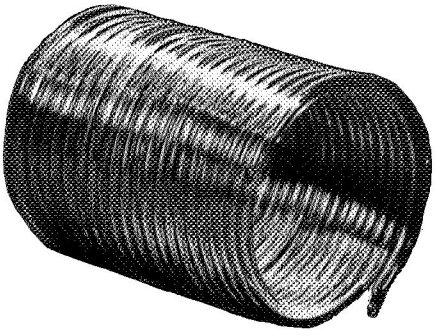

(b) COIL AFTER CUTTING

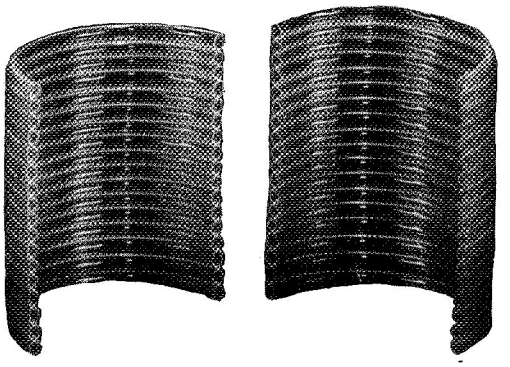

(c) PARTIALLY ASSEMBLED COOLANT TUBE SEGMENTS

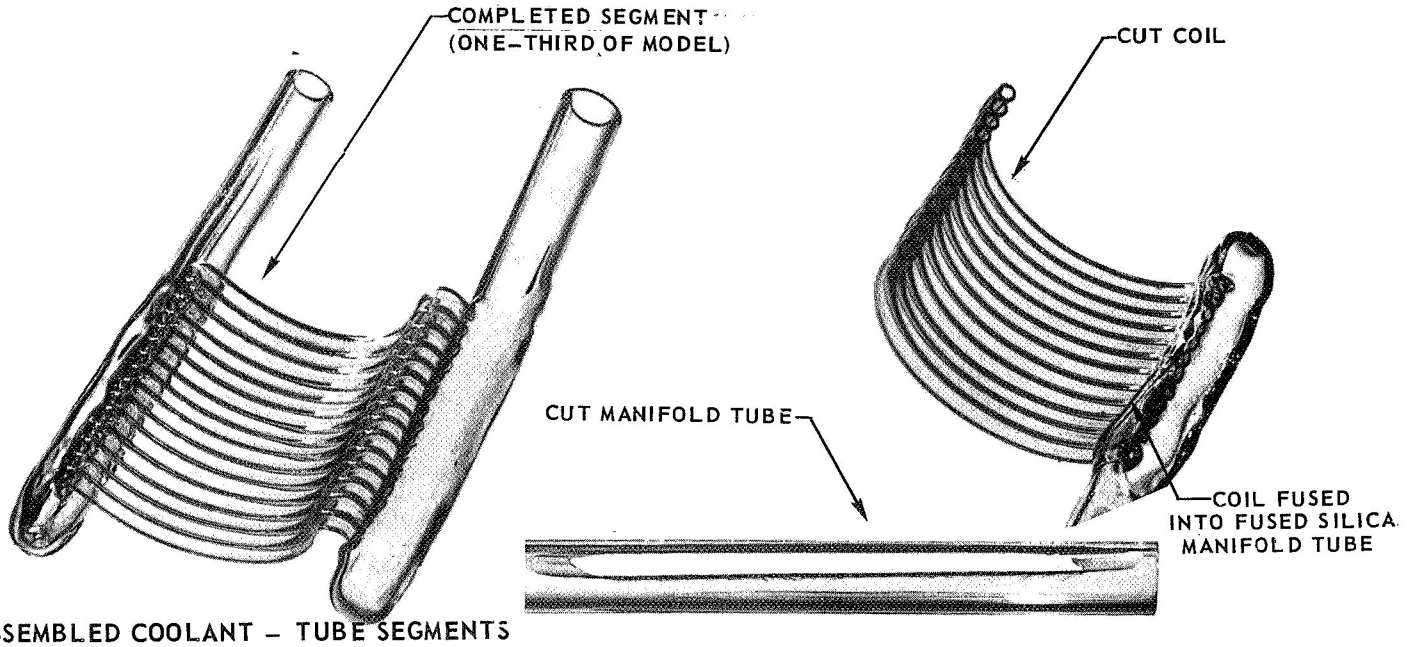

(d) ASSEMBLED COOLANT – TUBE SEGMENTS

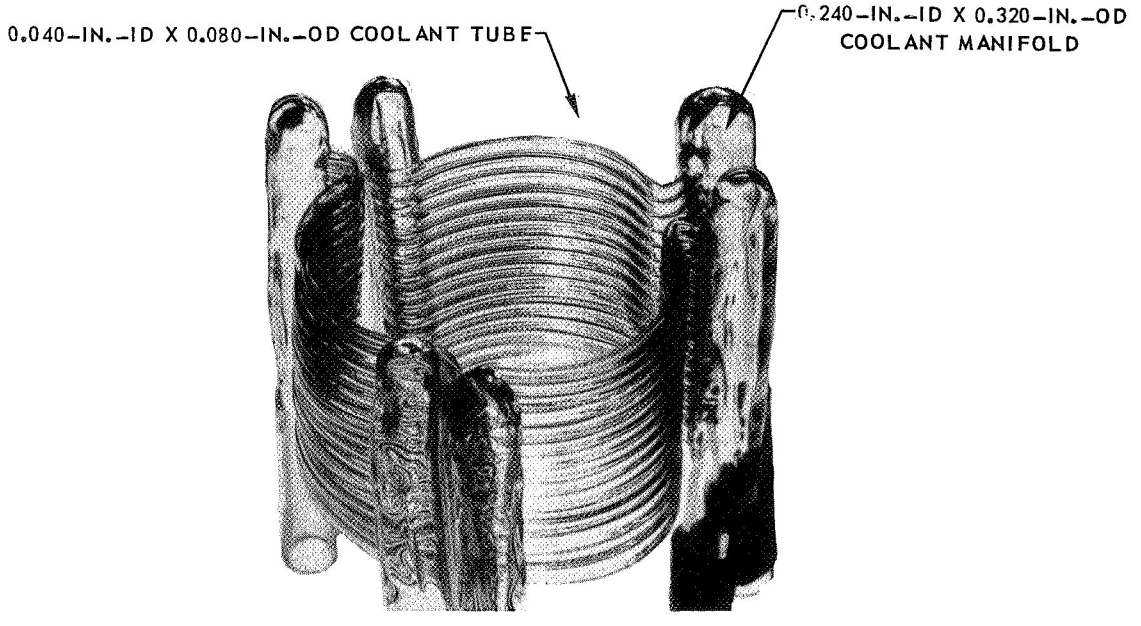

FABRICATION OF CIRCUMFERENTIALLY SHAPED FUSED SILICA TUBES BY THE SAGGING TECHNIQUE

(a) FABRICATION OF LOWER MOLD

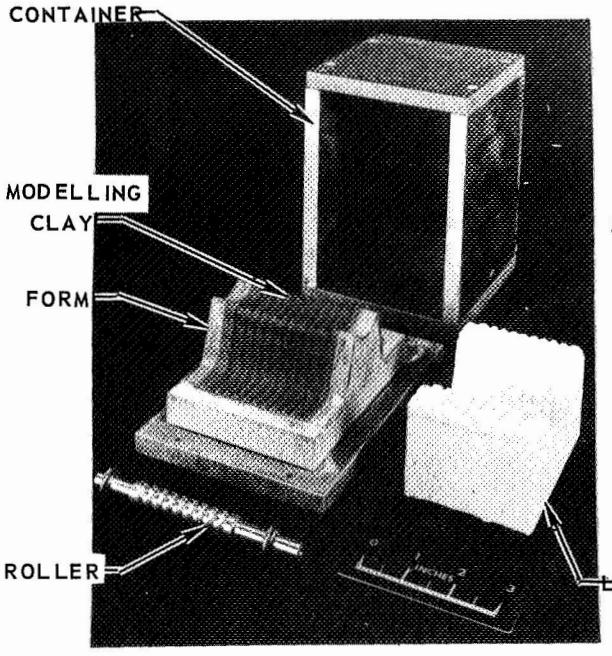

(b) FABRICATION OF UPPER MOLD

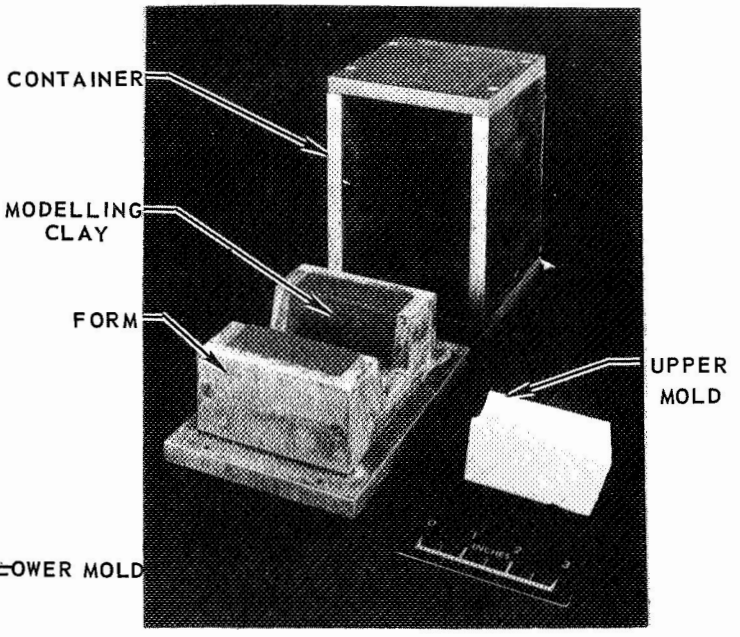

(c) FUSED SILICA TUBES LOCATED ON MOLD BEFORE HEATING

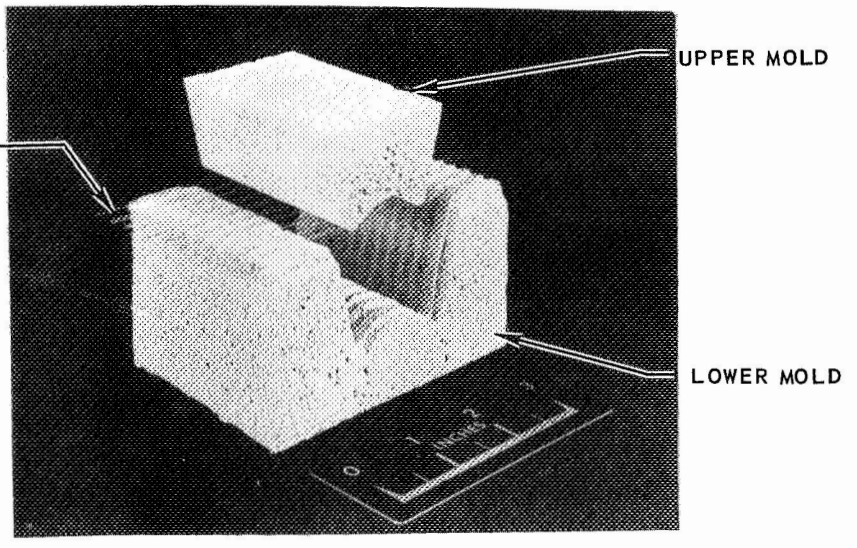

FIG. 9

VORTEX INJECTOR CONFIGURATIONS FOR AXIAL – COOLANT – TUBE MODELS

(a) ULTRASONICALLY DRILLED FUSED SILICA TUBE INJECTOR

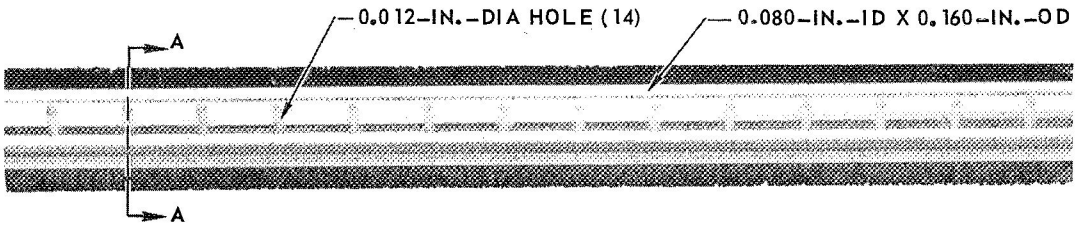

SECTION A–A

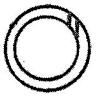

(b) DRILLED COPPER TUBE INJECTOR

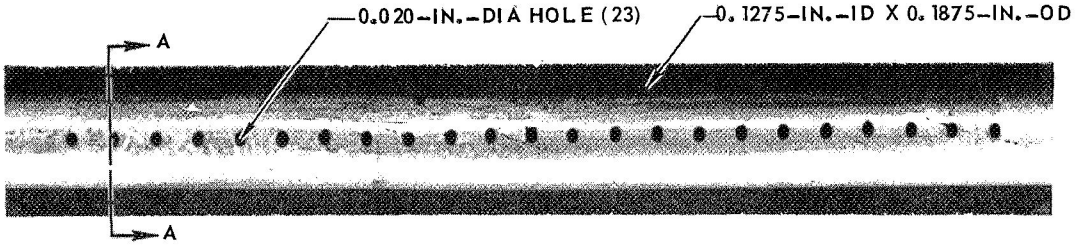

SECTION A–A

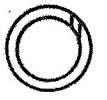

(c) COPPER HYPO-TUBE INJECTORS SOLDERED INTO COPPER MANIFOLD TUBE

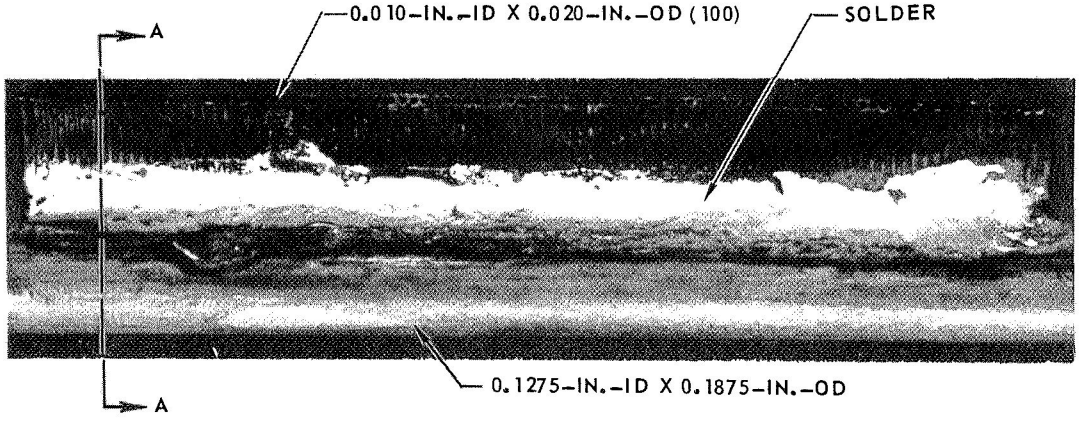

SECTION A–A

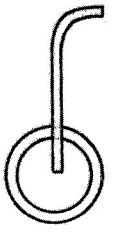

(d) FUSED SILICA HYPO-TUBE INJECTORS POTTED INTO COPPER MANIFOLD TUBE

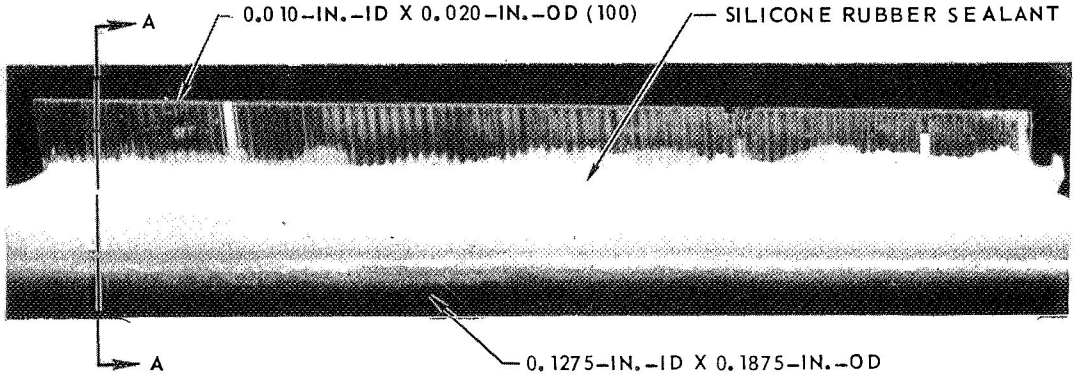

SECTION A–A

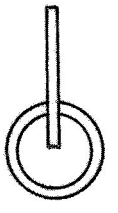

PHOTOGRAPHS OF FLOW CONTROL AND RECORDING EQUIPMENT USED IN TESTS

(a) EQUIPMENT USED IN COLD-FLOW TESTS

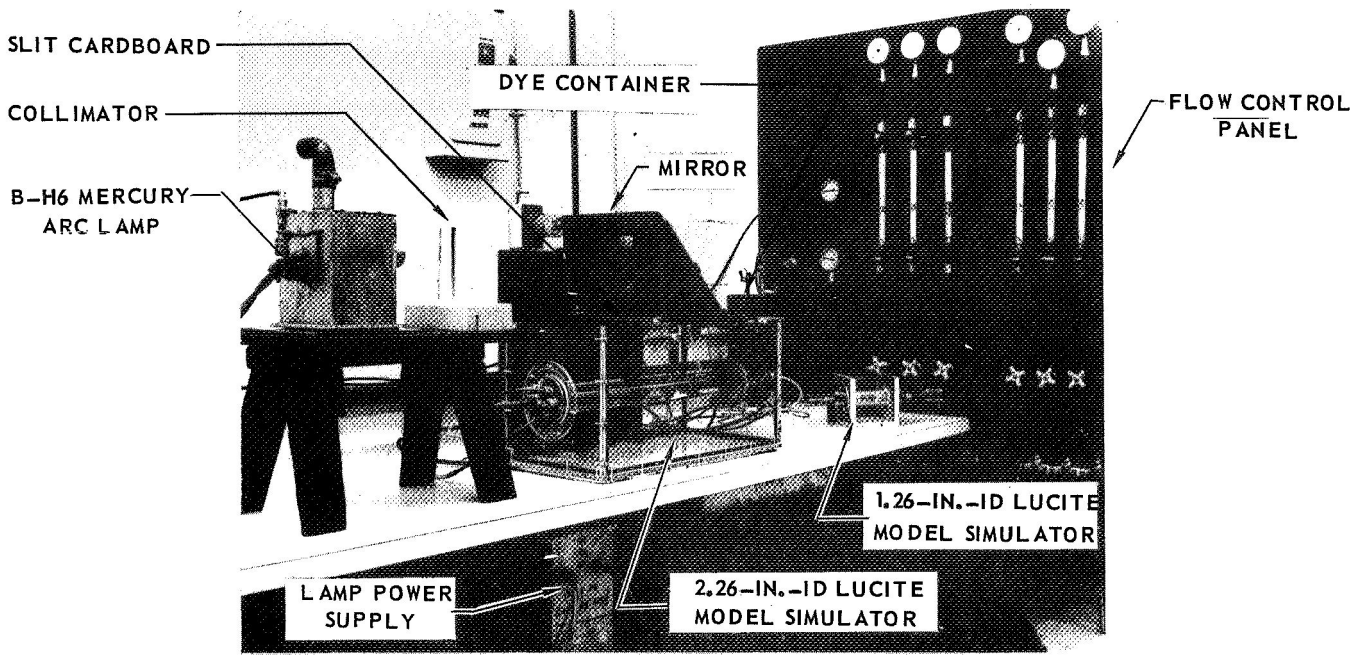

(b) EQUIPMENT USED IN HOT-FLOW TESTS

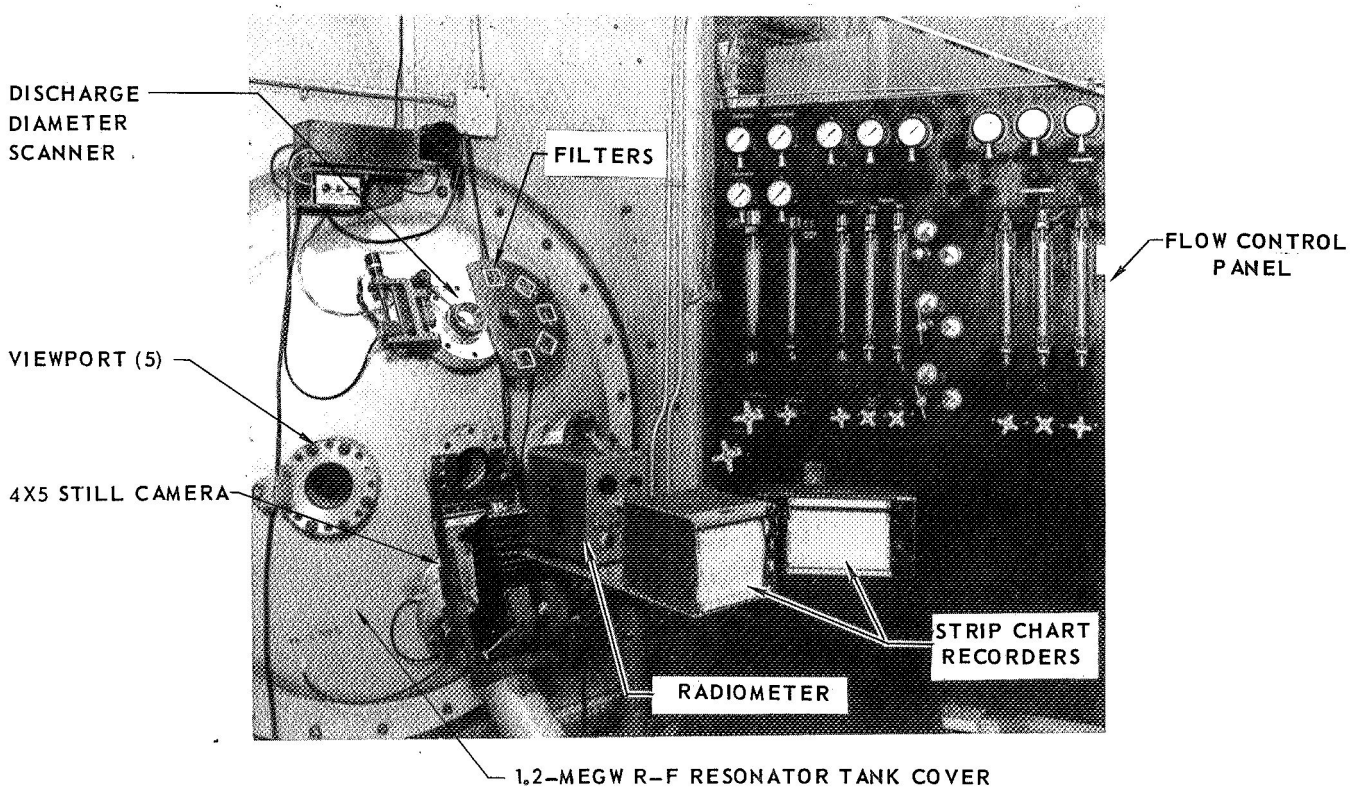

PHOTOGRAPHS OF THE 1.2-MEGW R-F INDUCTION HEATER

(a) DETAILS OF TEST SECTION

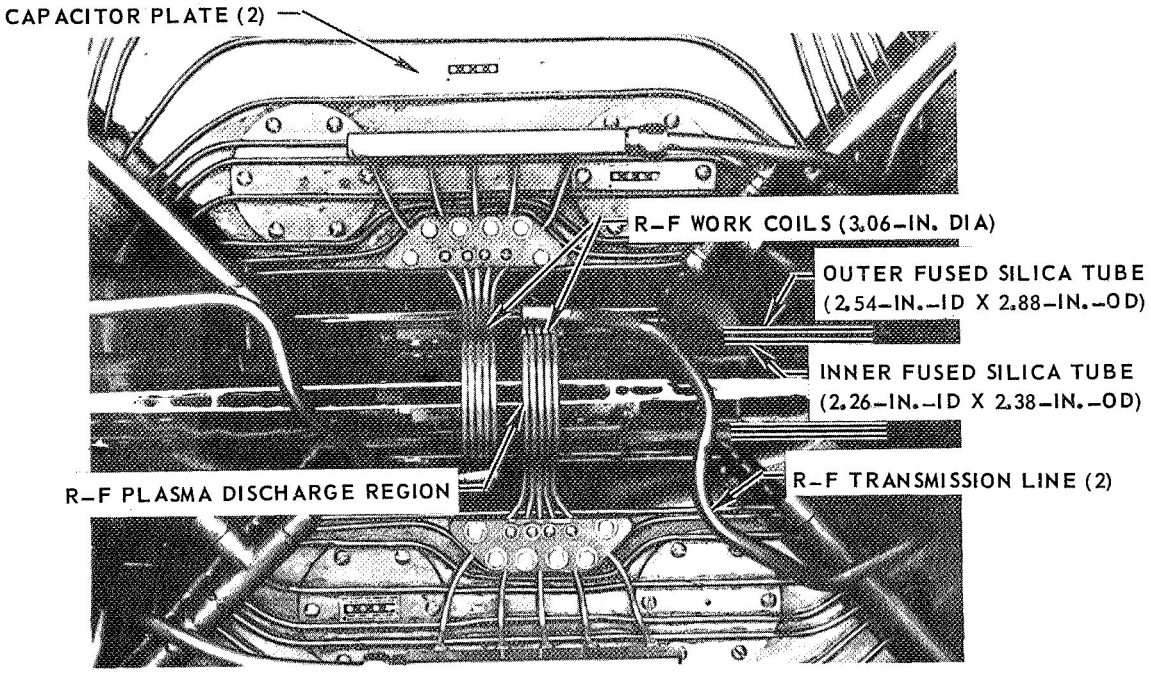

(b) DETAILS OF CONTROL PANELS

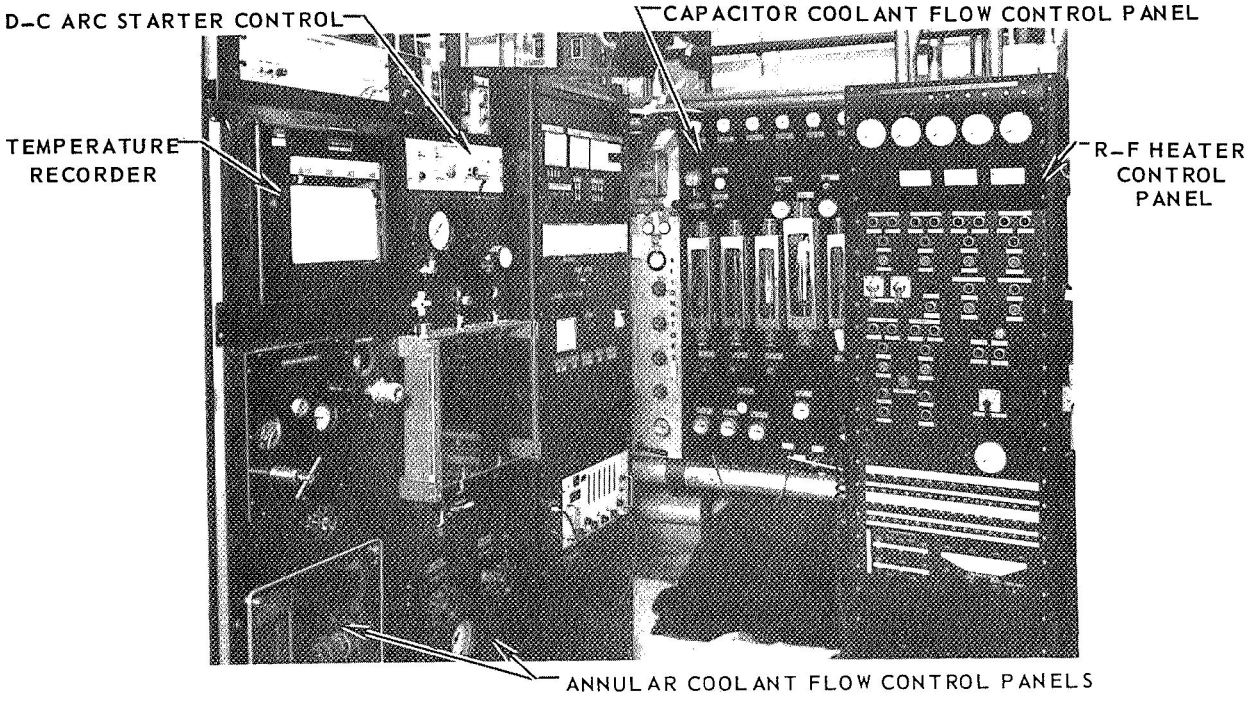

PHOTOGRAPHS OF AXIAL – COOLANT – TUBE MODEL TEST CONFIGURATION FOR USE IN 1.2–MEGW R–F INDUCTION HEATER

(a) CLOSE–UP VIEW OF MODEL ON END WALLS

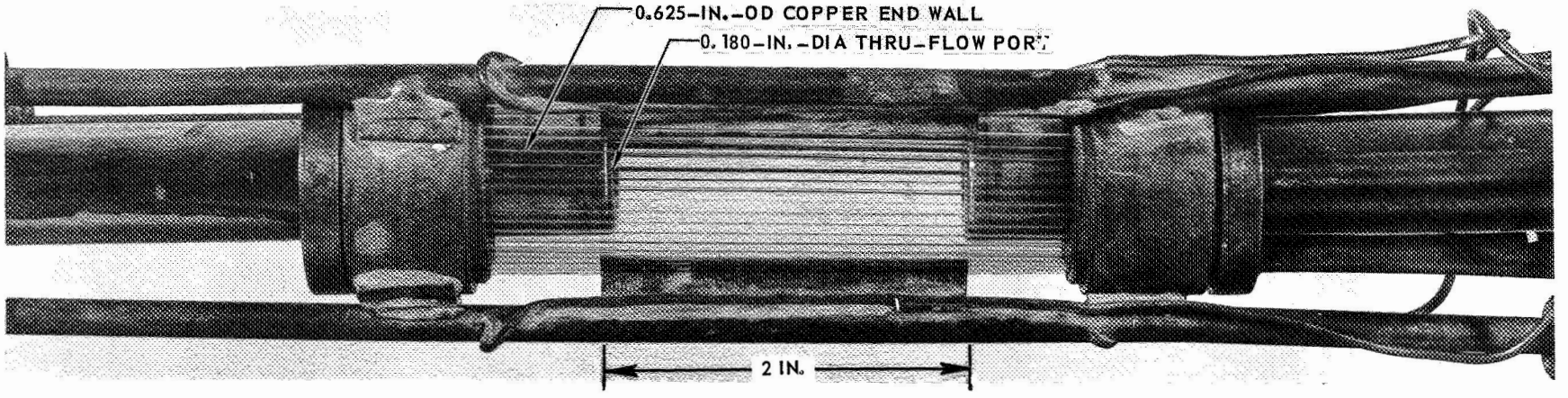

(b) BENCH MOCKUP OF MODEL LOCATION IN 1.2–MEGW R–F HEATER

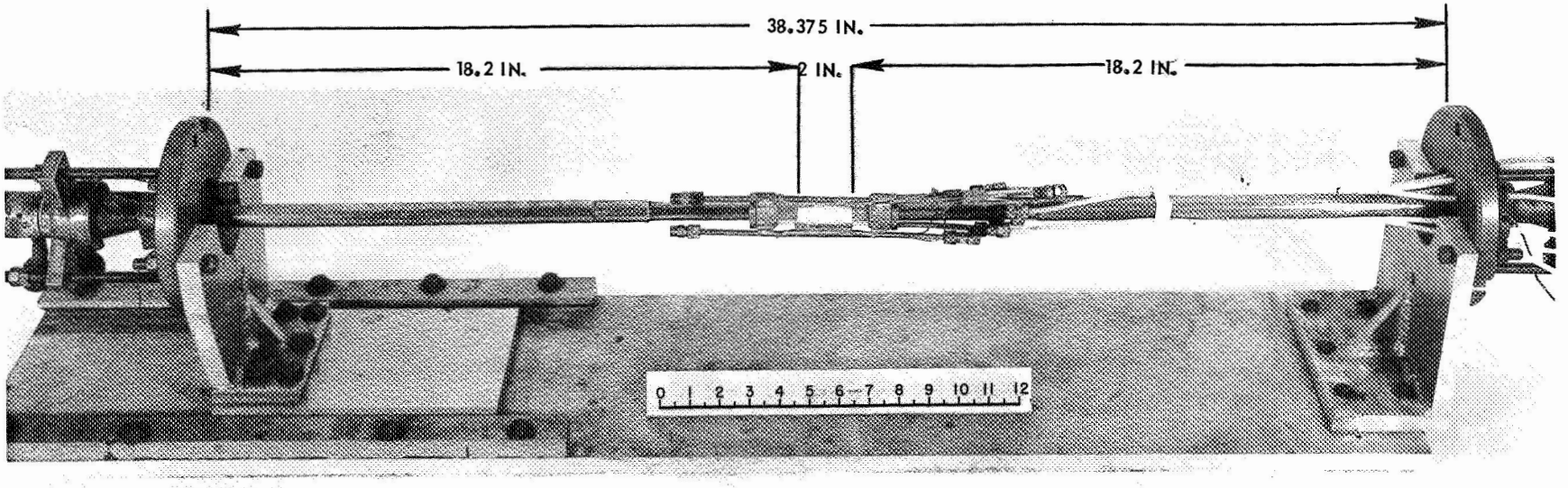

J–910900–3

FIG. 12

FIG. 13

PHOTGRAPHS OF DYE PATTERNS OBTAINED IN COLD-FLOW TESTS WITH MODELS HAVING DIFFERENT VORTEX INJECTOR GEOMETRIES

DYE ADDED FROM BOTH ENDS

REFER TO APPENDIX C FOR DERIVATION OF β_t

(a) MODEL WITH DRILLED COPPER TUBE INJECTORS (β_t = 23)

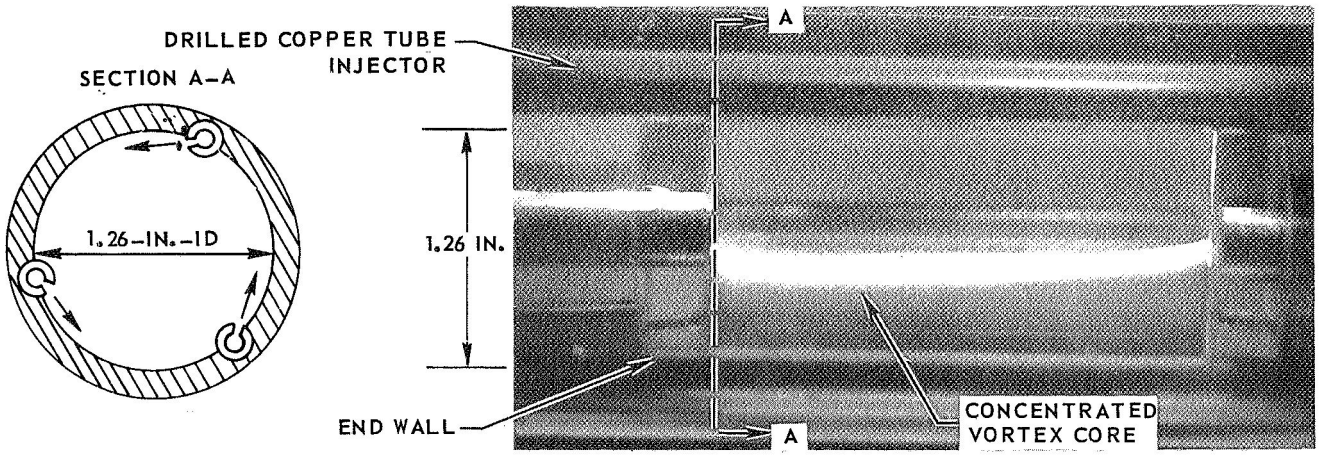

(b) MODEL WITH COPPER HYPO-TUBE INJECTORS (β_t = 23)

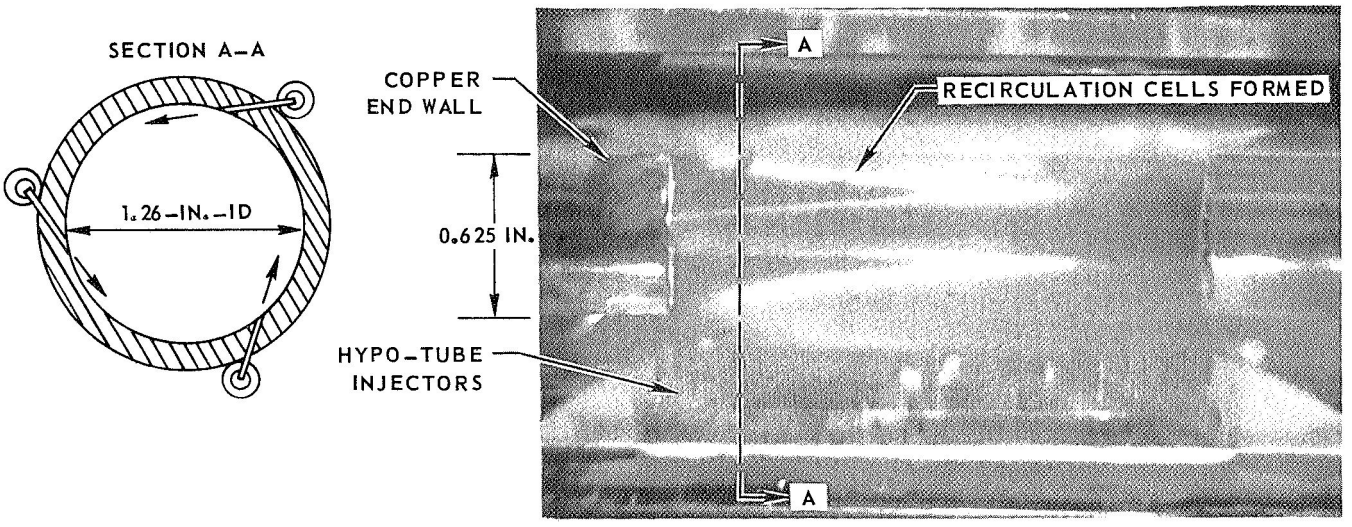

(c) AXIAL-COOLANT-TUBE MODEL WITH COPPER HYPO-TUBE INJECTORS (β_t = 14)

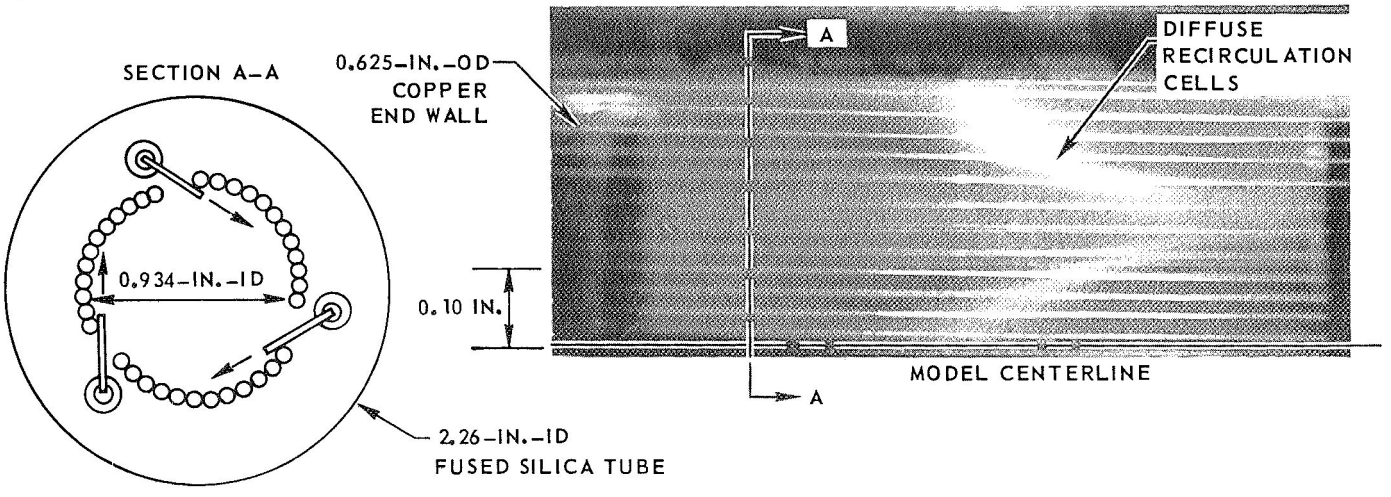

FIG. 14

SKETCHES OF INJECTOR AND COOLANT TUBE CONFIGURATIONS FOR AXIAL-COOLANT-TUBE MODELS EMPLOYED IN HOT-FLOW TESTS

SEE FIG. 5 FOR ADDITIONAL MANIFOLD DETAILS

CROSS-SECTION OF MODELS EMPLOYED IN INITIAL TESTS (SEE REF. 10)

(a) INDIVIDUAL-HOLE MANIFOLD WITH DRILLED INJECTOR TUBES

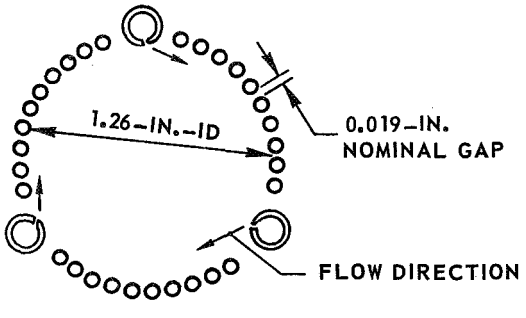

(b) ANNULAR MANIFOLD WITH DRILLED INJECTOR TUBES

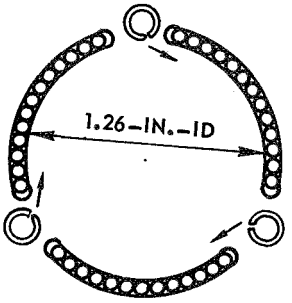

CROSS-SECTION OF MODELS EMPLOYED IN CURRENT TESTS

(c) ANNULAR MANIFOLD WITH STRAIGHT HYPO-TUBE INJECTORS

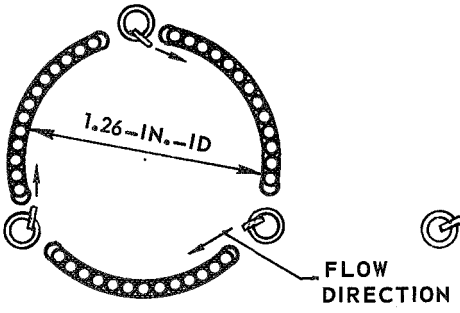

(d) ANNULAR MANIFOLD WITH CURVED HYPO-TUBE INJECTORS

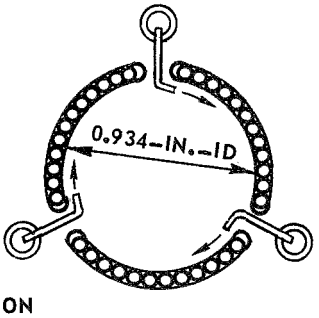

(e) OFFSET ANNULAR MANIFOLD WITH CURVED HYPO-TUBE INJECTORS

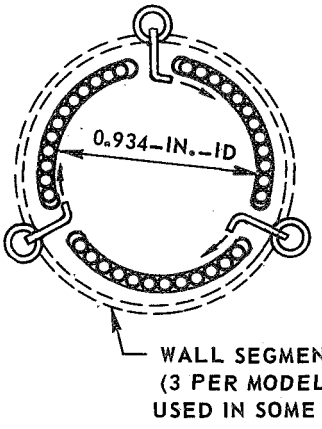

PHOTOGRAPHS SHOWING DETAILS OF ONE AXIAL-COOLANT-TUBE MODEL WITH OFFSET MANIFOLD EMPLOYED IN HOT-FLOW TESTS

SEE FIG 14(e) FOR SKETCH OF CROSS-SECTION

(a) VIEW OF COMPLETE MODEL

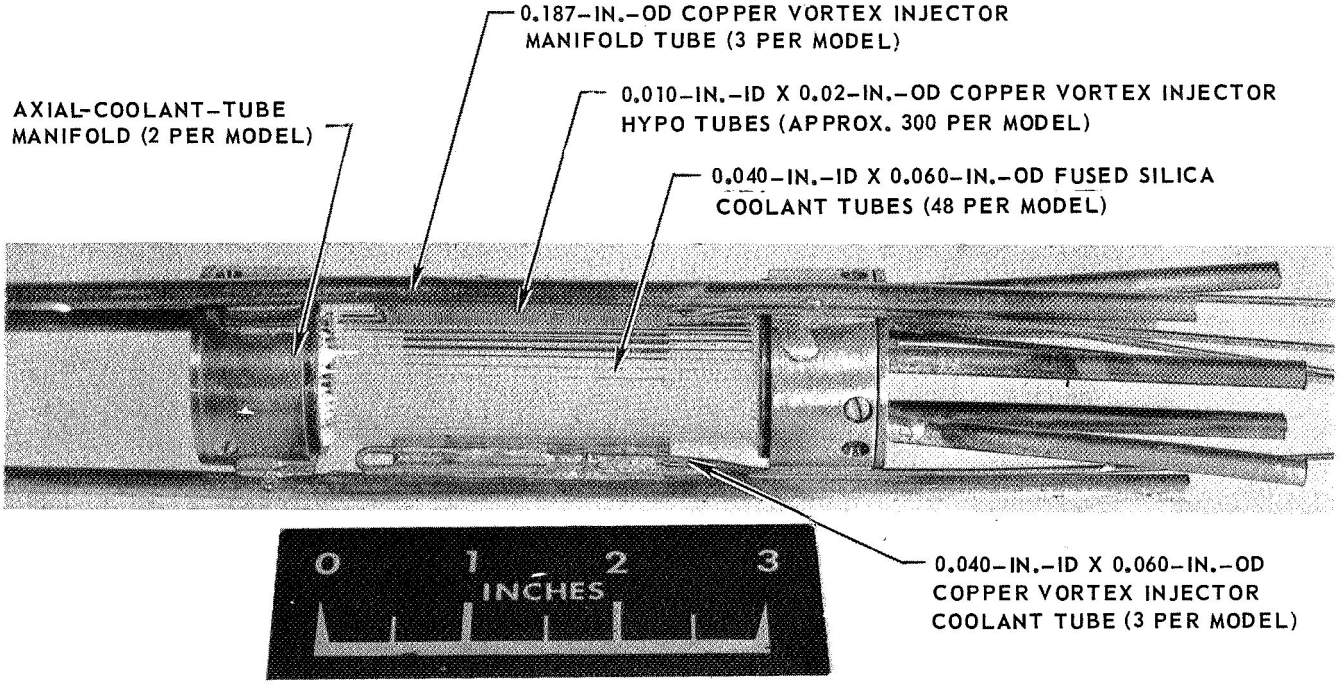

(b) VIEW SHOWING MANIFOLD DETAILS

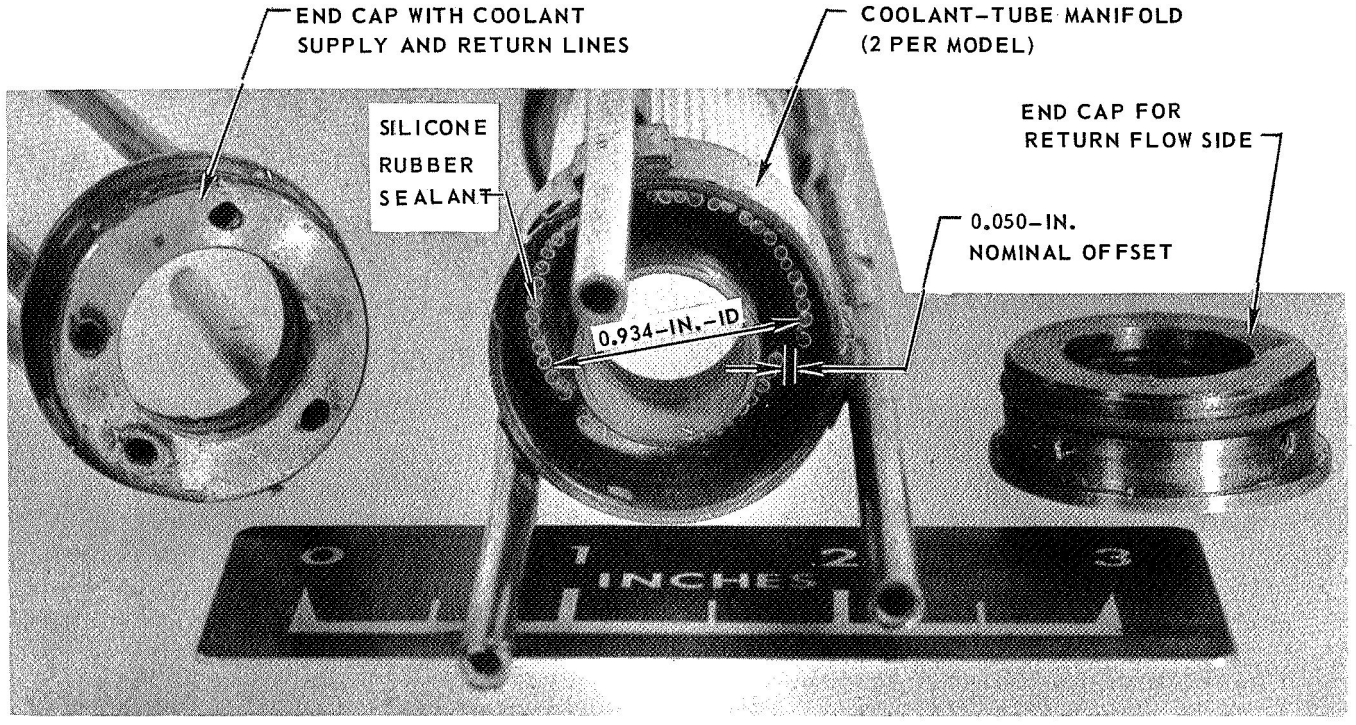

PHOTOGRAPHS SHOWING 0.934 – IN. – ID AXIAL – COOLANT – TUBE MODEL EMPLOYED IN HOT-FLOW TESTS

REFER TO FIG. 15 FOR MODEL DETAILS

(a) PHOTOGRAPH OF MODEL INSTALLED IN 1.2-MEGW R-F INDUCTION HEATER

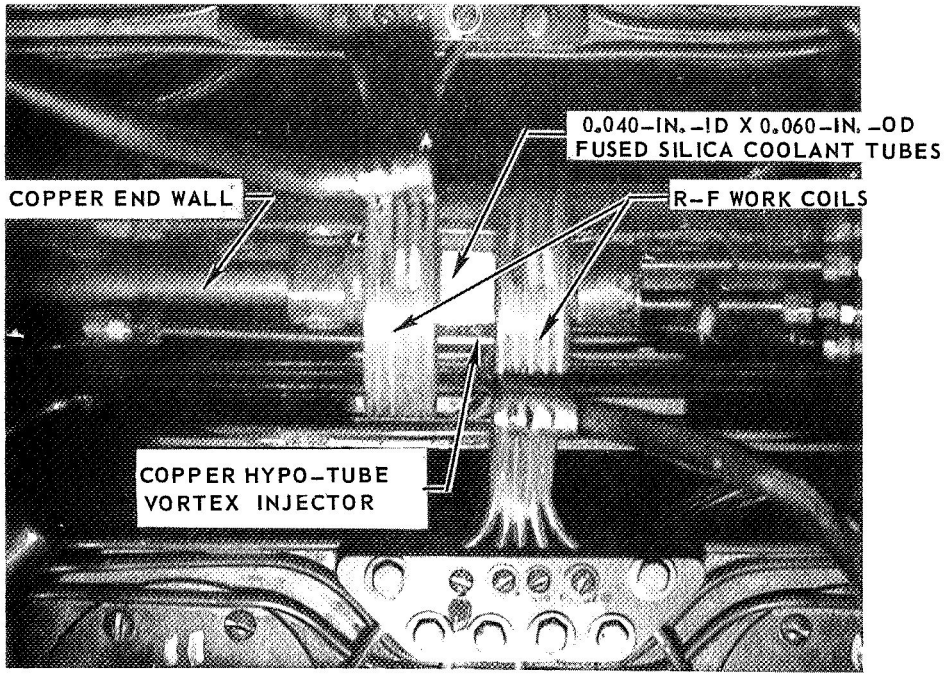

(b) PHOTOGRAPH OF R-F PLASMA

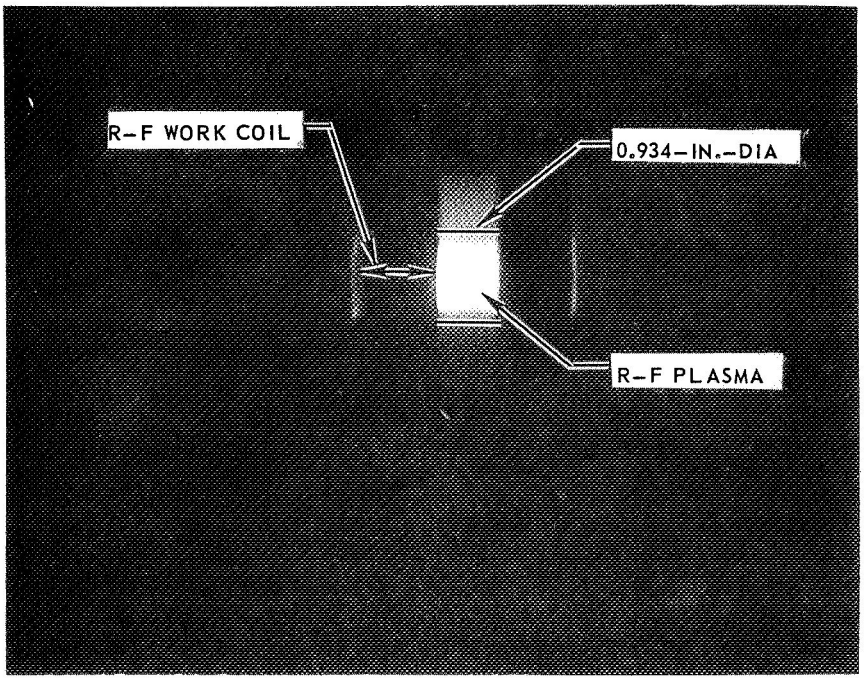

PHOTOGRAPHS SHOWING R-F PLASMA START-UP AND R-F BREAKDOWN DURING AXIAL-COOLANT-TUBE MODEL TEST

REFER TO FIG. 15 FOR MODEL DETAILS

a) MODEL INSTALLED IN 1.2-MEGW R-F INDUCTION HEATER

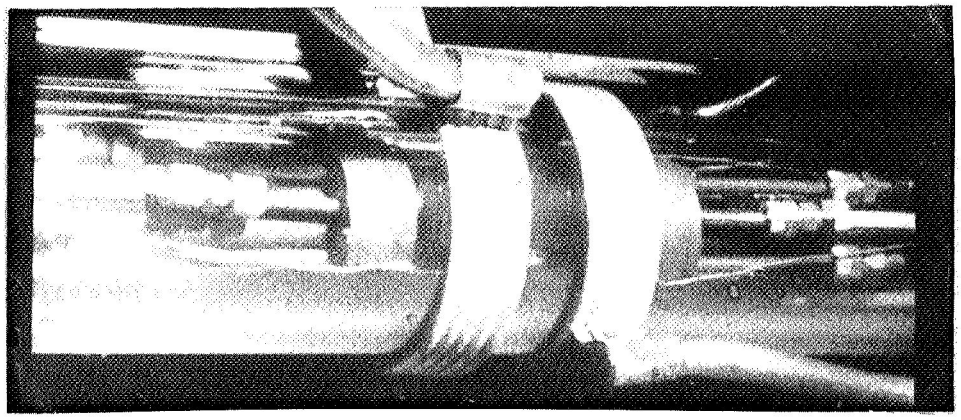

b) TYPICAL R-F PLASMA START-UP (AT t = 0, D-C ARC INITIATED)

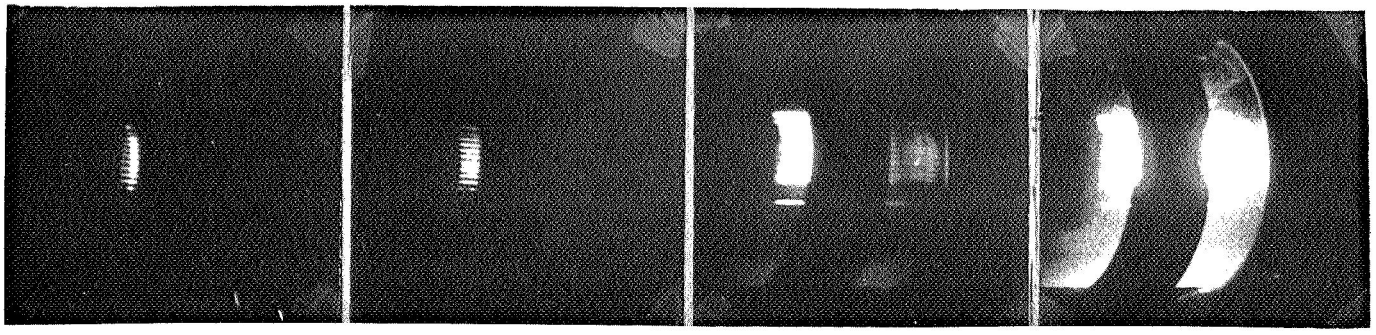

t = 0.083 SEC 0.167 SEC 0.208 SEC 0.292 SEC

c) R-F BREAKDOWN OUTSIDE OF MODEL (SEE TEXT) (AT t = 0, DISCHARGE IN NORMAL MODE)

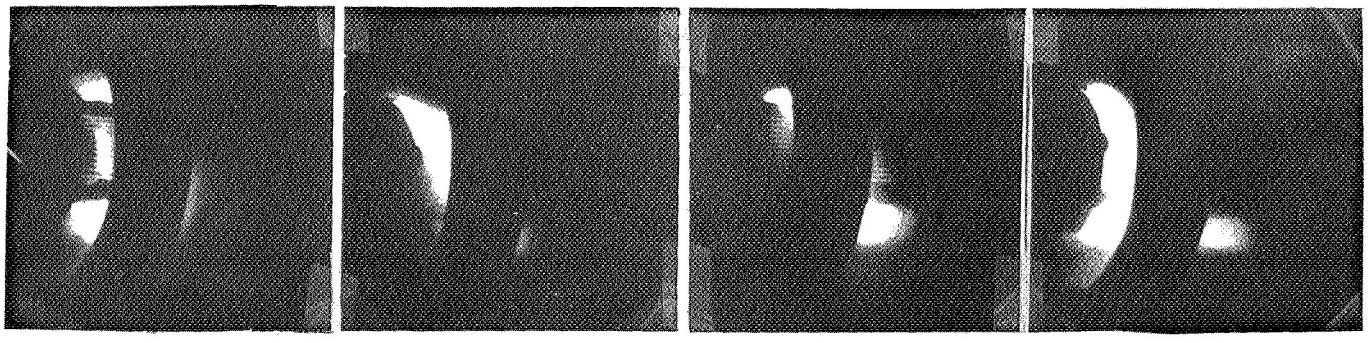

t = 0.004 SEC 0.006 SEC 0.008 SEC 0.010 SEC

POWER BREAKDOWN FOR A TYPICAL TEST WITH 0.934 – IN.– ID AXIAL–COOLANT–TUBE MODEL

TESTED IN 1.2–MEGW R–F INDUCTION HEATER
REFER TO FIG. 15 FOR MODEL DETAILS

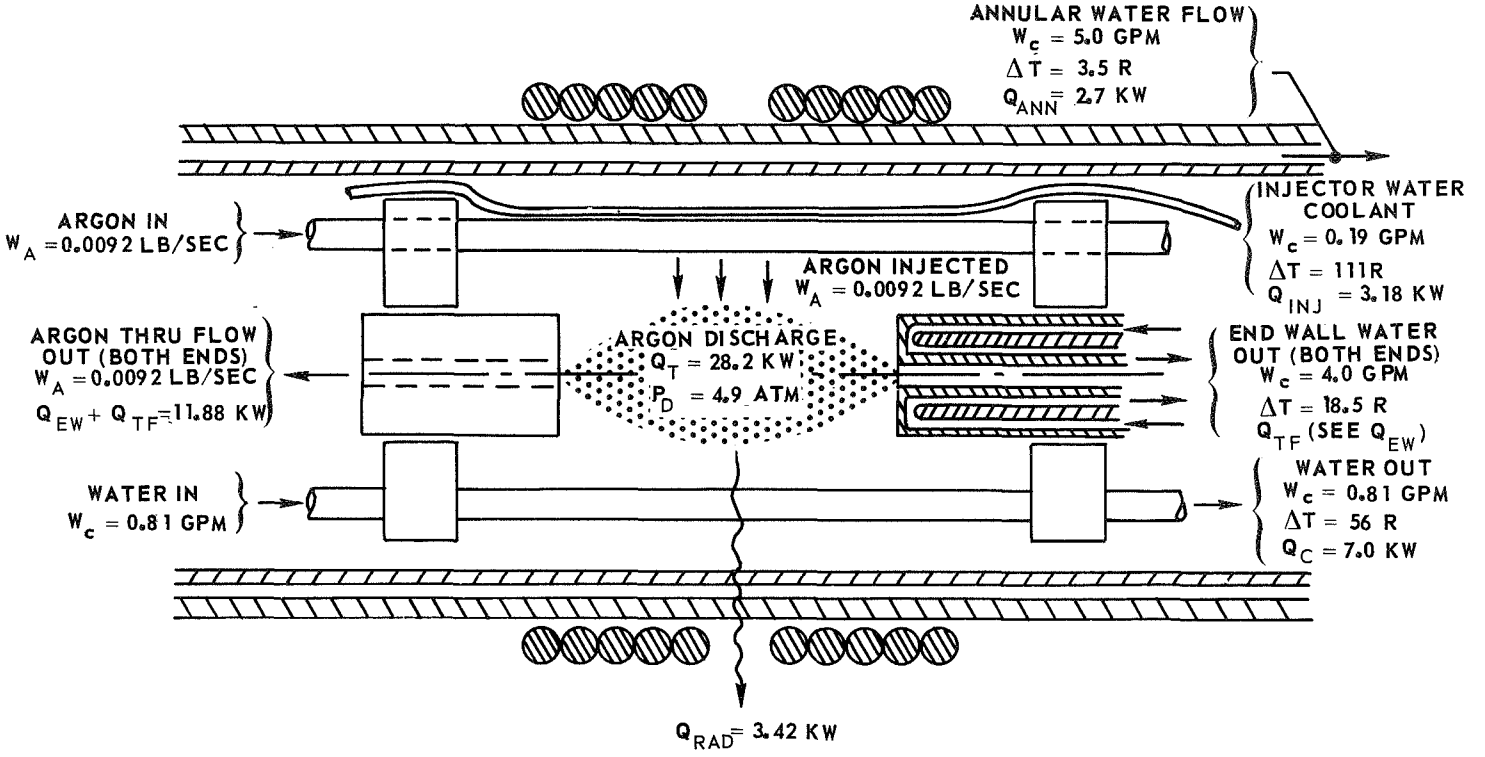

TOTAL POWER RADIATED/TOTAL DISCHARGE POWER, $Q_{RAD,T}/Q_T$:

$$\frac{Q_{RAD,T}}{Q_T} = \frac{Q_{RAD}+Q_{ANN}}{Q_T} = \frac{3.42 + 2.70}{28.2} = 0.217$$

WHERE:

$$Q_T = Q_C + Q_{INJ} + Q_{RAD} + Q_{ANN} + (Q_{EW} + Q_{TF})$$

$$= 7.0 + 3.18 + 3.42 + 2.70 + 11.88$$

$$Q_T = 28.2 \text{ KW}$$

$$Q_C, Q_{ANN}, (Q_{EW} + Q_{TF}) = (0.146)(GPM)(\Delta T)$$

$$Q_{RAD} = (311)(MV)$$

EFFECT OF OPERATING PARAMETERS ON POWER BREAKDOWN FOR A TYPICAL AXIAL – COOLANT – TUBE MODEL TEST

TESTED IN 1.2-MEGW R-F INDUCTION HEATER

NUMBERS ON CURVE DENOTE FLOW CONDITIONS FOR WHICH DATA WERE OBTAINED

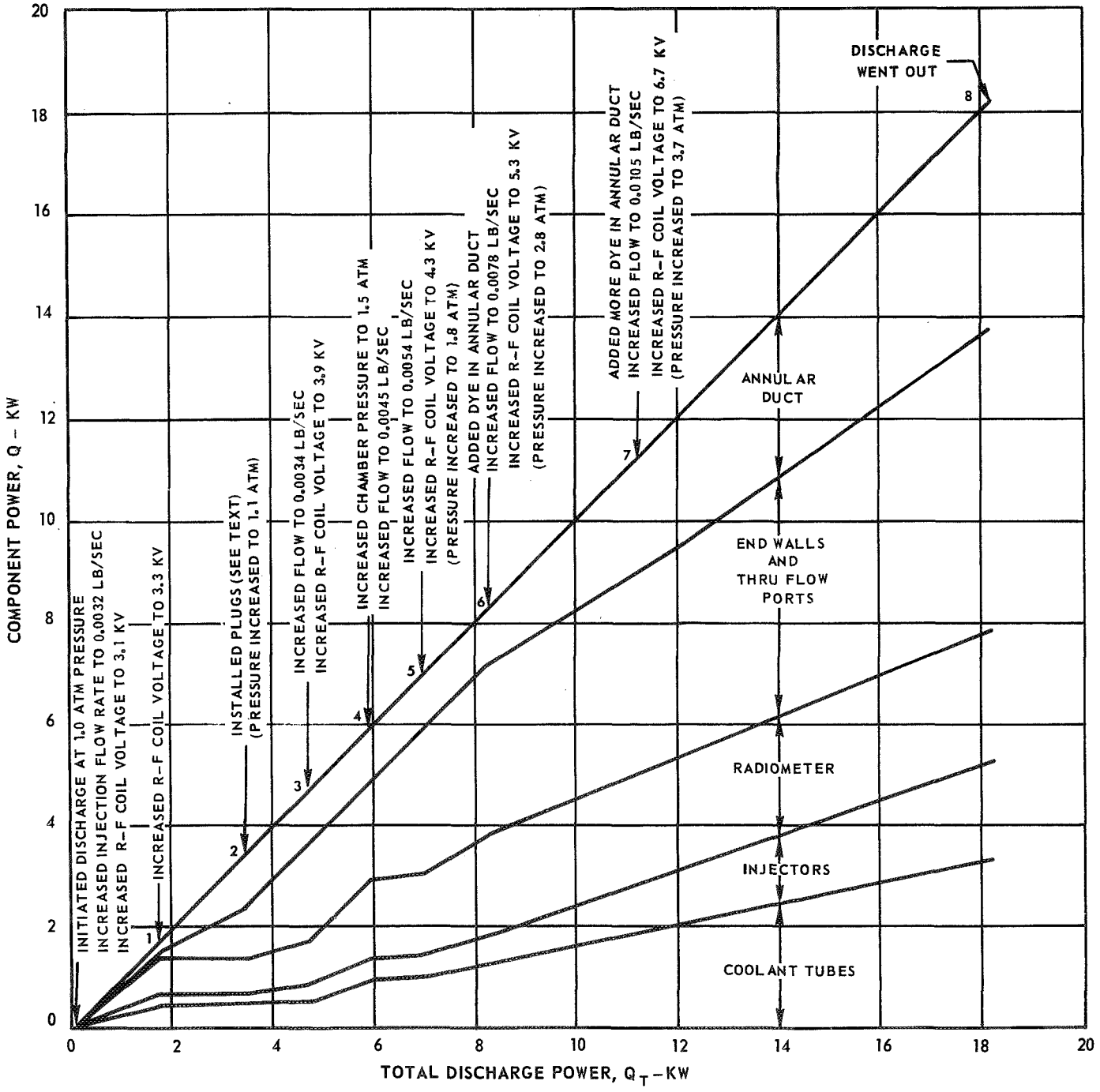

FIG. 20

EXPERIMENTALLY DETERMINED OPERATING CORRIDOR FOR AXIAL – COOLANT – TUBE MODEL TESTS

TESTED IN 1.2-MEGW R-F INDUCTION HEATER

NUMBERS ON CURVE REFER TO TEST DESCRIBED IN FIG. 19

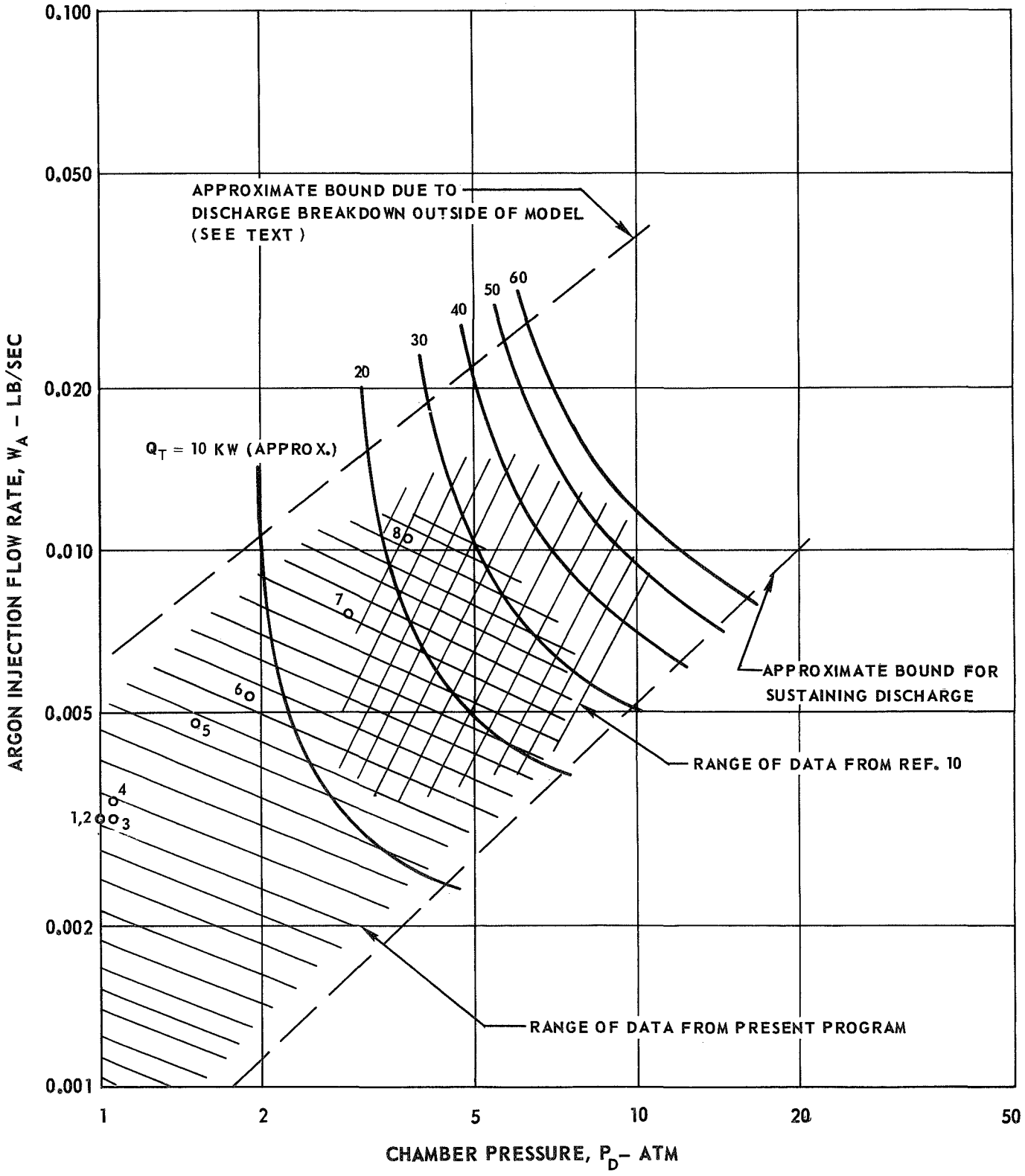

VARIATION OF POWER DEPOSITED INTO COOLANT TUBES WITH TOTAL DISCHARGE POWER IN AXIAL – COOLANT – TUBE MODEL TESTS

TESTED IN 1.2–MEGW R–F INDUCTION HEATER
SEE FIG. 5 FOR MANIFOLD DETAILS

OPEN SYMBOLS DENOTE DATA FROM REF. 10
RANGE OF CHAMBER PRESSURE, P_D = 2.2 TO 9.2 ATM
RANGE OF ARGON INJECTION FLOW RATE, W_A = 0.0032 TO 0.012 LB/SEC

SOLID SYMBOLS DENOTE DATA FROM PRESENT PROGRAM
RANGE OF CHAMBER PRESSURE, P_D = 1 TO 6.6 ATM
RANGE OF ARGON INJECTION FLOW RATE, W_A = 0.005 TO 0.0254 LB/SEC

SYMBOL	MODEL DIA, IN.
○	0.845
⊿	0.934 (OFFSET)
△	0.934
□	1.26
◇	1.55

INCLUDES RADIATION DEPOSITED INTO WATER COOLANT

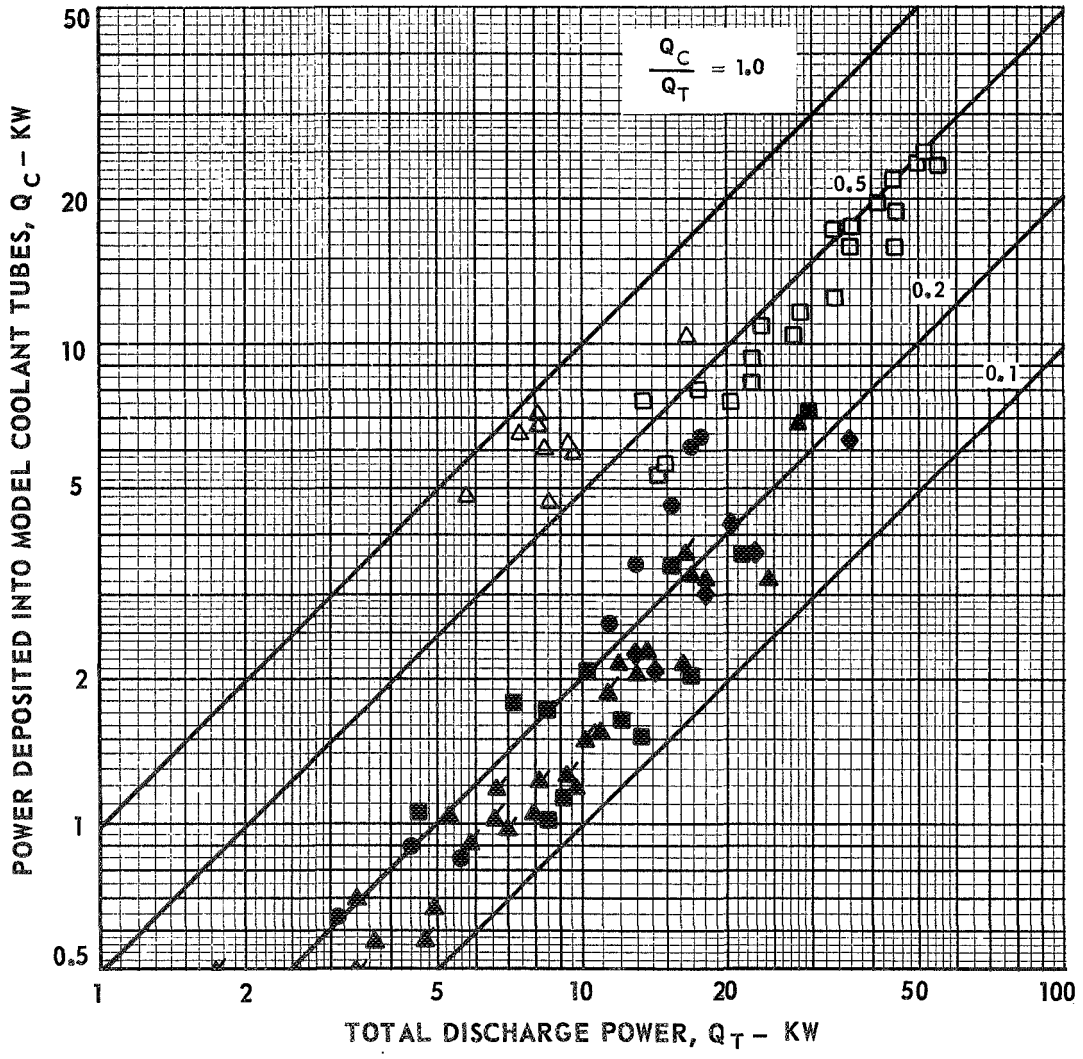

VARIATION OF POWER DEPOSITED INTO INJECTOR TUBES WITH TOTAL DISCHARGE POWER IN AXIAL – COOLANT – TUBE MODEL TESTS

TESTED IN 1.2-MEGW R-F INDUCTION HEATER
SEE FIG. 5 FOR MANIFOLD DETAILS

OPEN SYMBOLS DENOTE DATA FROM REF. 10
RANGE OF CHAMBER PRESSURE, P_D = 2.2 TO 9.2 ATM
RANGE OF ARGON INJECTION FLOW RATE, W_A = 0.0032 TO 0.012 LB/SEC

SOLID SYMBOLS DENOTE DATA FROM PRESENT PROGRAM
RANGE OF CHAMBER PRESSURE, P_D = 1 TO 6.6 ATM
RANGE OF ARGON INJECTION FLOW RATE, W_A = 0.0015 TO 0.0254 LB/SEC

SYMBOL	MODEL DIA, IN.
○	0.846
⊿	0.934 (OFFSET)
△	0.934
□	1.26
◇	1.55

EXCLUDES R-F HEATING OF COPPER INJECTORS (SEE TEXT)

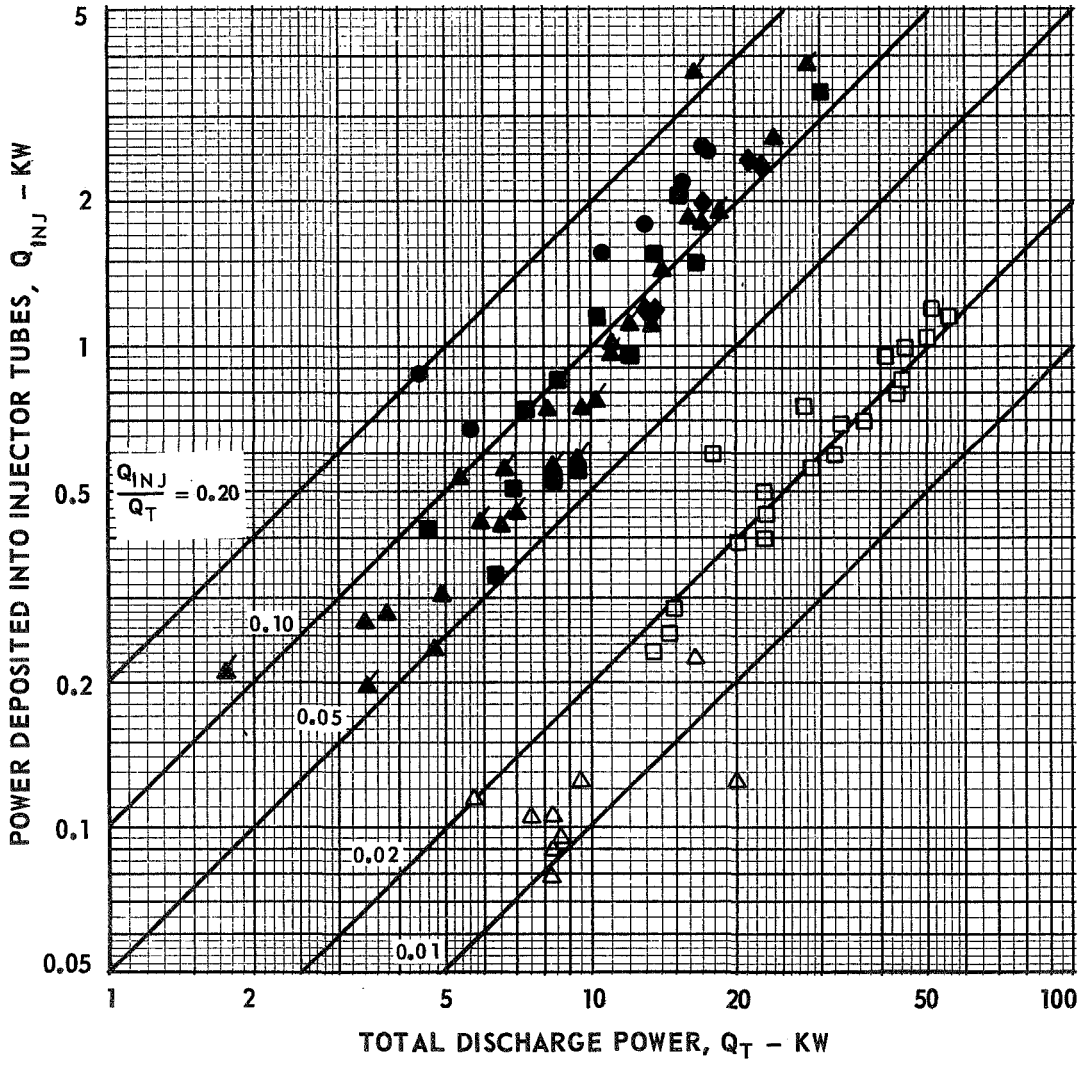

FIG. 23

VARIATION OF POWER RADIATED WITH TOTAL DISCHARGE POWER IN AXIAL – COOLANT – TUBE MODEL TESTS

TESTED IN 1.2-MEGW R-F INDUCTION HEATER
SEE FIG. 5 FOR MANIFOLD DETAILS

OPEN SYMBOLS DENOTE DATA FROM REF. 10

RANGE OF CHAMBER PRESSURE, P_D = 2.2 TO 9.9 ATM

RANGE OF ARGON INJECTION FLOW RATE, W_A = 0.0032 TO 0.012 LB/SEC

SOLID SYMBOLS DENOTE DATA FROM PRESENT PROGRAM

RANGE OF CHAMBER PRESSURE, P_D = 1 TO 6.6 ATM

RANGE OF ARGON INJECTION FLOW RATE, W_A = 0.0015 TO 0.0254 LB/SEC

SYMBOL	MODEL DIA., IN.
○	0.846
⊿	0.934 (OFFSET)
△	0.934
□	1.26
◇	1.55

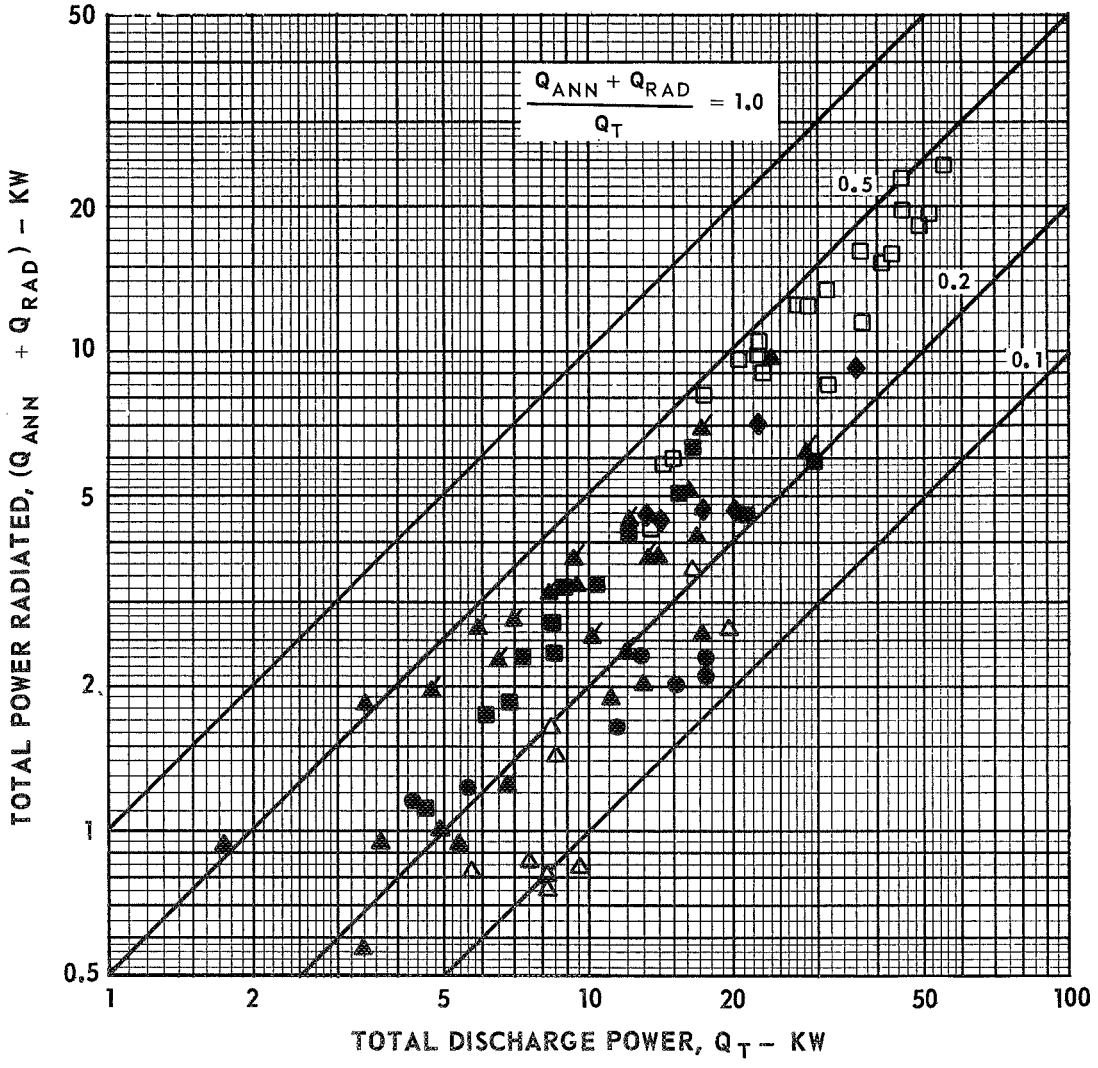

VARIATION OF POWER DEPOSITED IN END WALL AND THRU-FLOW EXHAUST WITH TOTAL DISCHARGE POWER IN AXIAL-COOLANT-TUBE MODEL TESTS

TESTED IN 1.2-MEGW R-F INDUCTION HEATER
SEE FIG. 5 FOR MANIFOLD DETAILS

OPEN SYMBOLS DENOTE DATA FROM REF. 10
RANGE OF CHAMBER PRESSURE, P_D = 2.2 TO 9.2 ATM
RANGE OF ARGON INJECTION FLOW RATE, W_A = 0.0032 TO 0.012 LB/SEC

SOLID SYMBOLS DENOTE DATA FROM PRESENT PROGRAM
RANGE OF CHAMBER PRESSURE, P_D = 1 TO 6.6 ATM
RANGE OF ARGON INJECTION FLOW RATE, W_A = 0.0015 TO 0.0254 LB/SEC

SYMBOL	MODEL DIA, IN.
○	0.846
⊿	0.934 (OFF SET)
△	0.934
□	1.26
◇	1.55

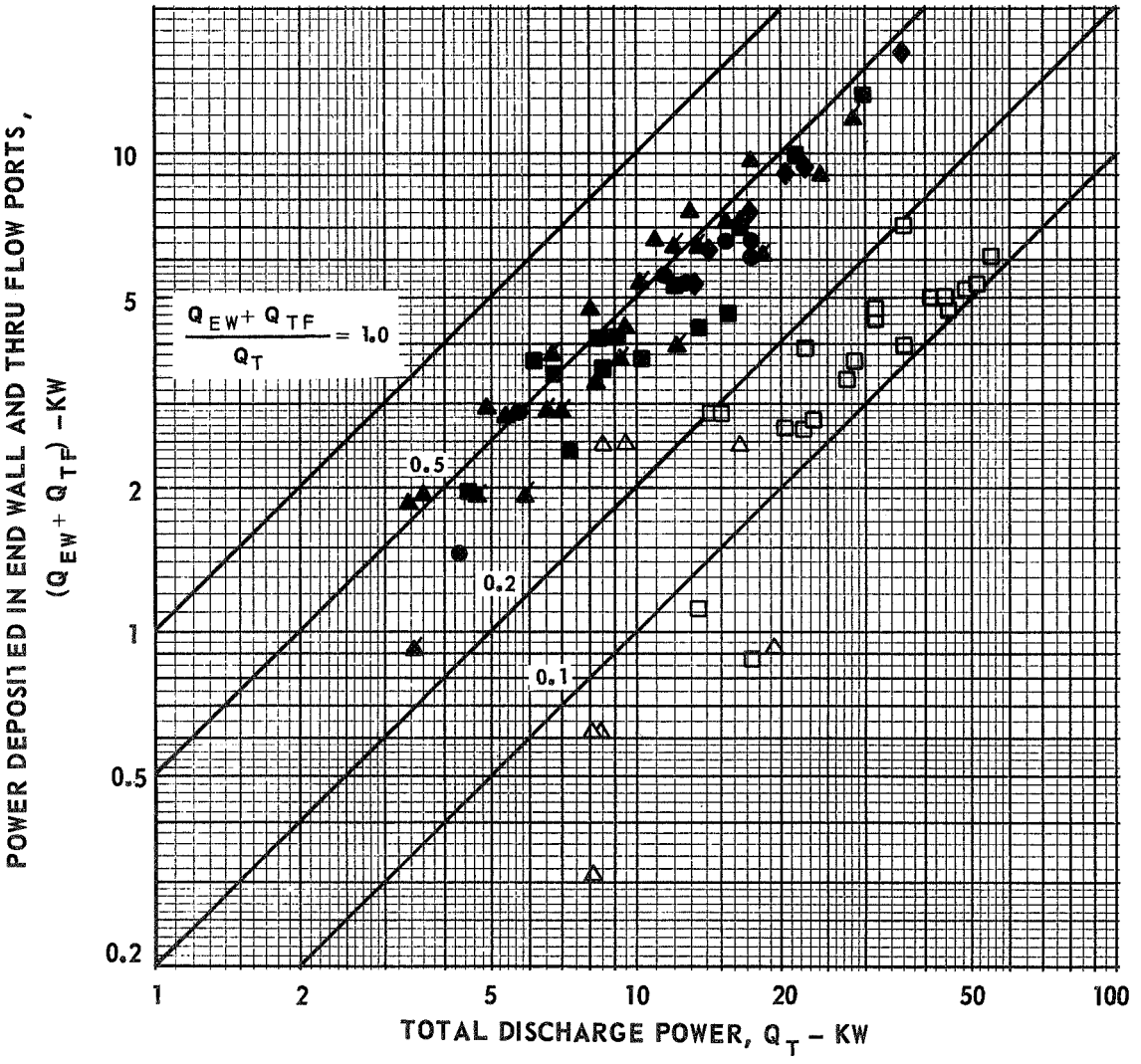

FIG. 25

SUMMARY SHOWING RATIO OF COMPONENT POWER TO TOTAL DISCHARGE POWER FOR AXIAL – COOLANT – TUBE MODEL TESTS

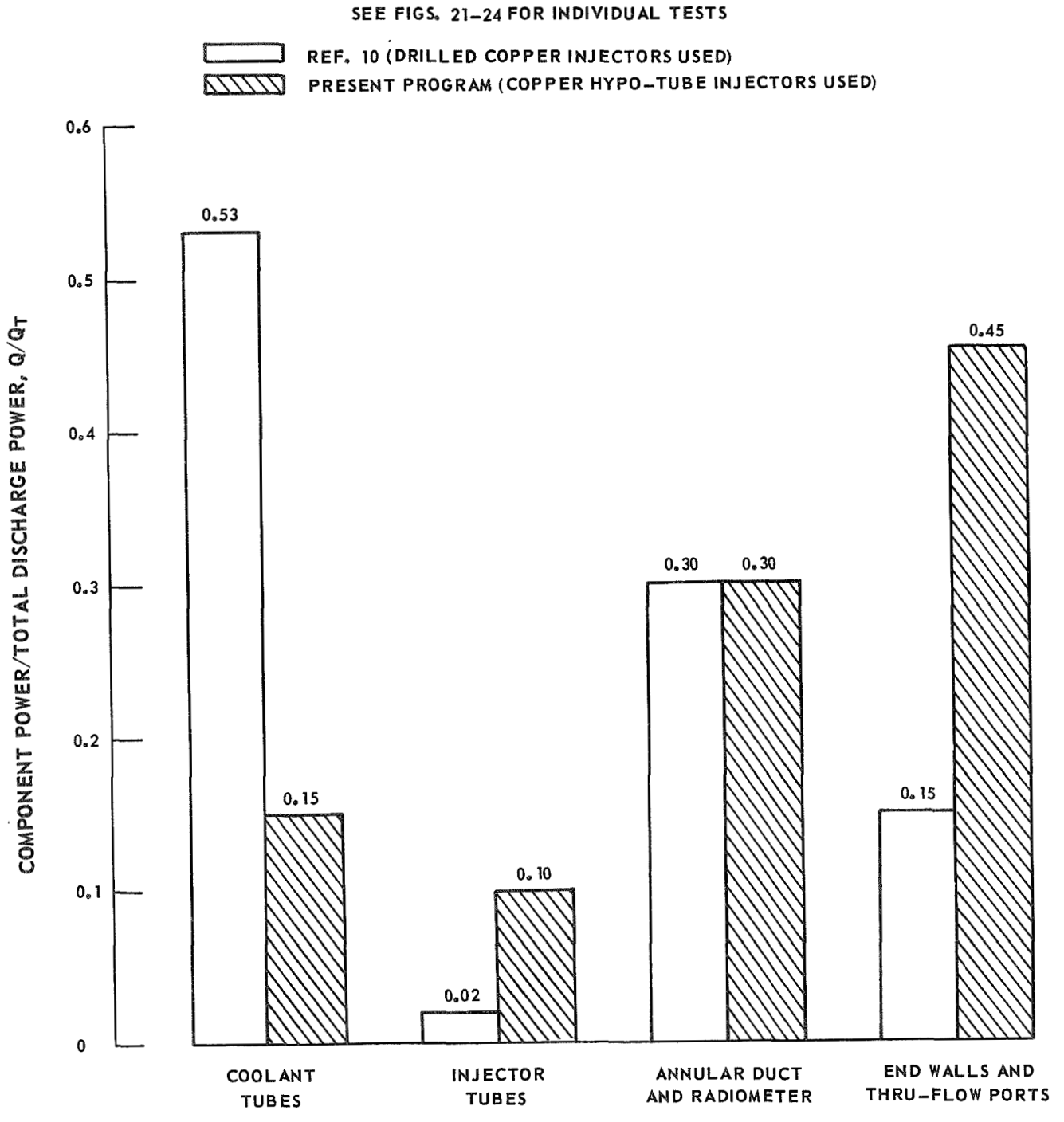

VALUES OF SECONDARY FLOW PARAMETER EMPLOYED IN COLD-FLOW AND HOT-FLOW TESTS

OPEN SYMBOLS DENOTE DATA FROM REFS. 2 AND 10

CLOSED SYMBOLS DENOTE DATA FROM PRESENT PROGRAM

○ 1.2-MEGW R-F INDUCTION HEATER

△ COLD-FLOW WATER VORTEX FACILITY

SYMBOLS DENOTE ARGON FLOW EXCEPT WHERE NOTED

SYMBOL	MODEL DIA, IN.
a	0.846
b	0.934
c	1.26
d	1.55
e	2.26

SYMBOL	FLOW RATE, LB/SEC
———	0.001
- - - - - -	0.010
— — —	0.050
— - —	0.100

NO BYPASS FLOW; $Re_t = 1 \times 10^5$ (REFER TO APPENDIX C)

VISCOSITY OF ARGON EVALUATED AT T = 685 R

MULTIPLY DATA BY 1.47 FOR ARGON AT T = 10,460 R

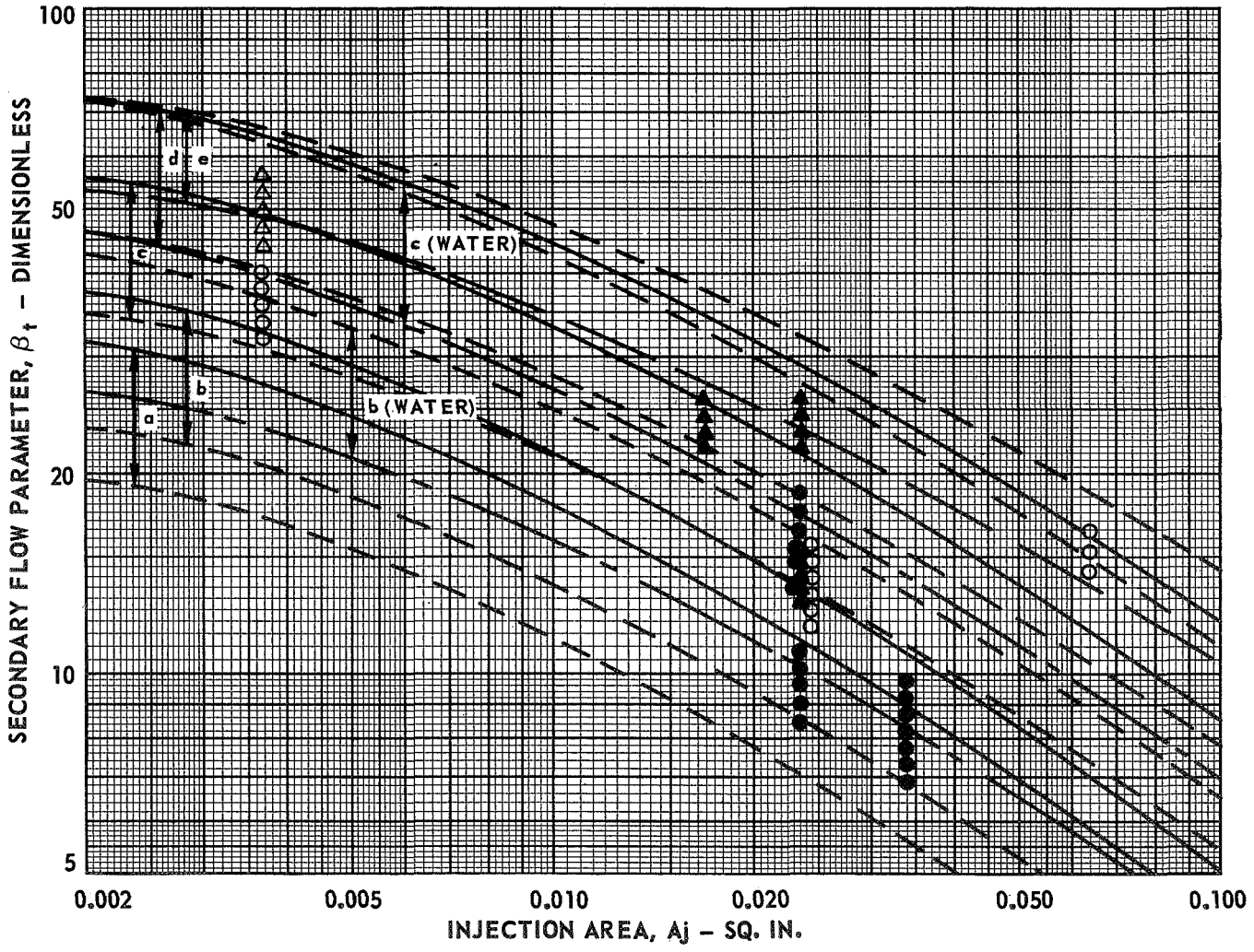

FIG. 27

PHOTOGRAPHS OF INJECTORS AFTER AXIAL-COOLANT-TUBE MODEL HOT-FLOW TESTS

(a) ULTRASONICALLY DRILLED FUSED SILICA INJECTORS (SEE FIG. 9a)

Q_T = 24 KW

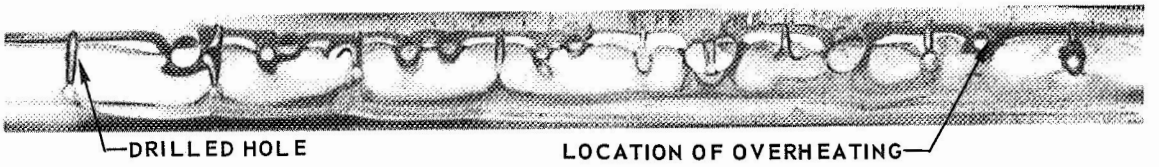

(b) DRILLED COPPER TUBE INJECTORS (SEE FIG. 9b)

Q_T = 55.3 KW

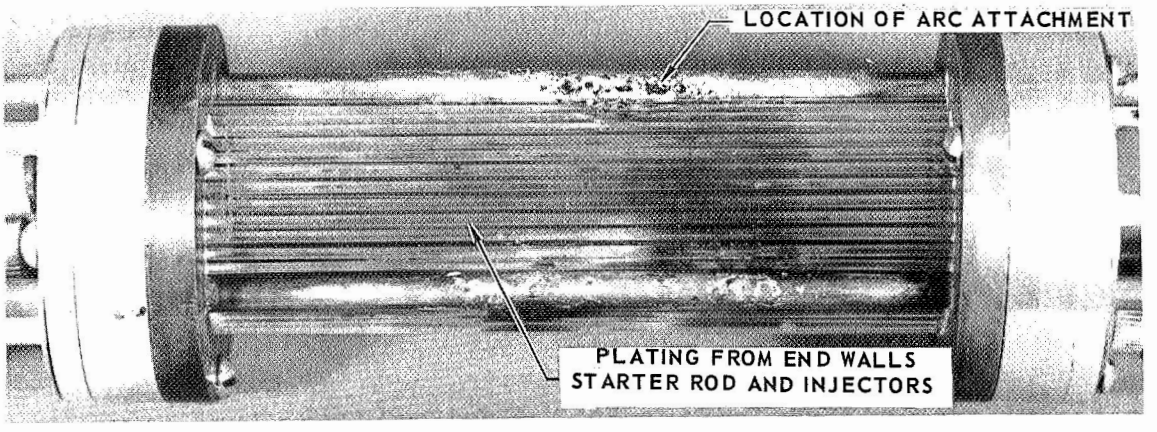

(c) COPPER HYPO-TUBE INJECTORS (SEE FIG. 9c)

Q_T = 36 KW

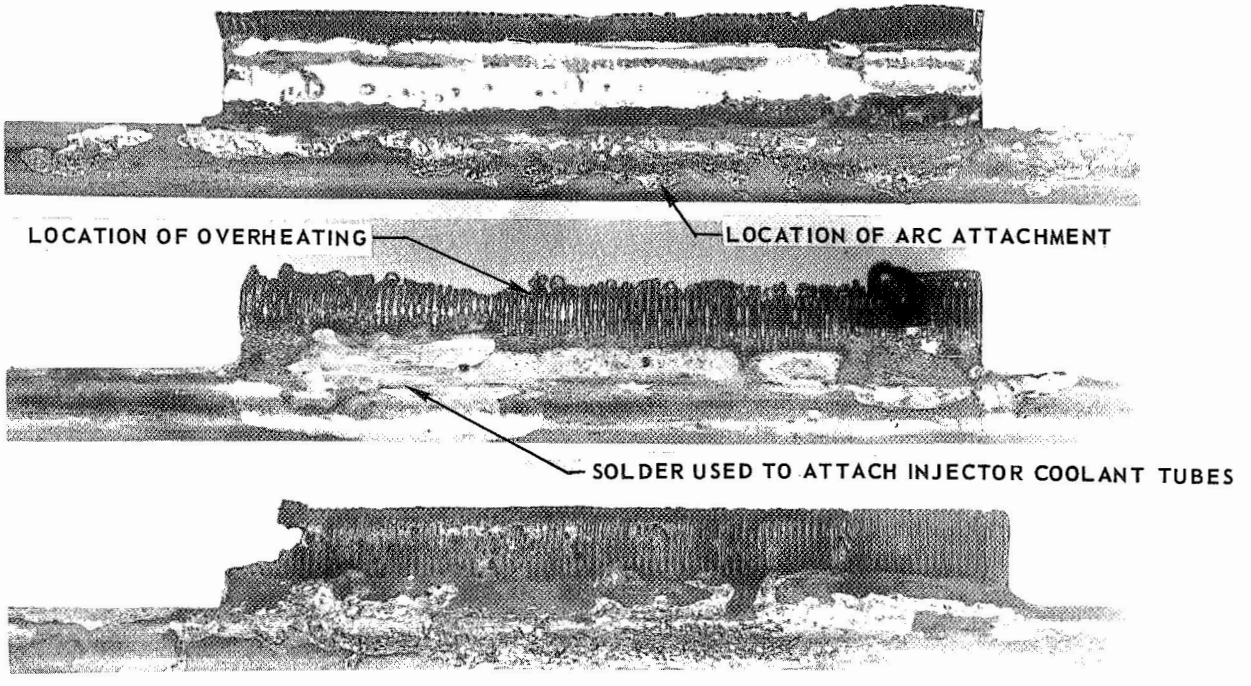

TYPICAL VARIATION WITH WAVELENGTH OF THE MEASURED INTENSITY WITH AND WITHOUT AN AXIAL – COOLANT – TUBE MODEL IN THE LIGHT PATH

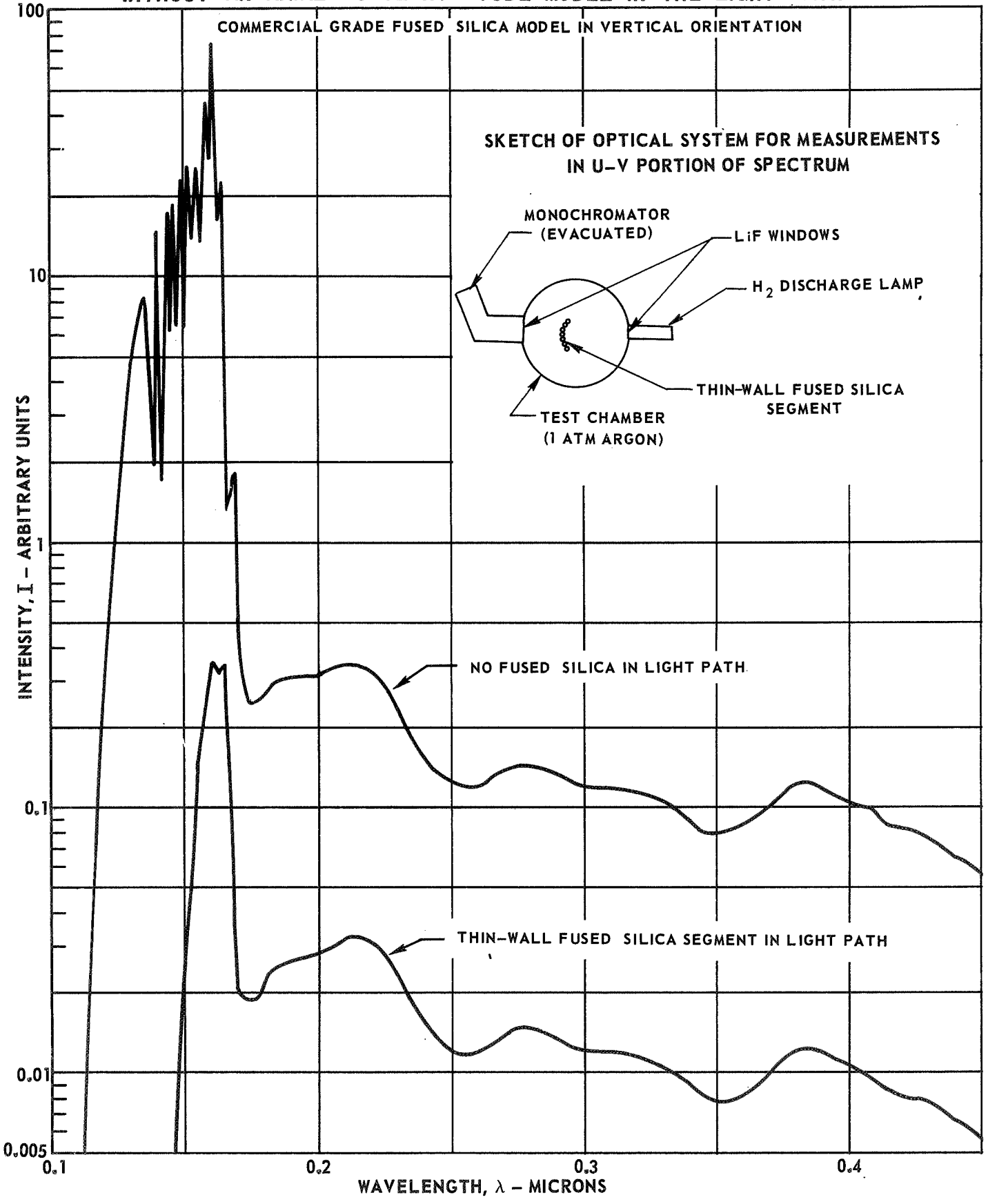

TRANSMISSION CHARACTERISTICS OF TRANSPARENT-WALL AXIAL-COOLANT-TUBE MODELS

LINE	GRADE OF FUSED SILICA	ORIENTATION	NOMINAL WALL THICKNESS
———	HIGH PURITY	VERTICAL	0.020 IN.
– – – –	COMMERCIAL	HORIZONTAL	0.005 IN.
—.—.—	COMMERCIAL	VERTICAL	0.005 IN.

INDEX OF REFRACTION ASSUMED INDEPENDENT OF WAVELENGTH

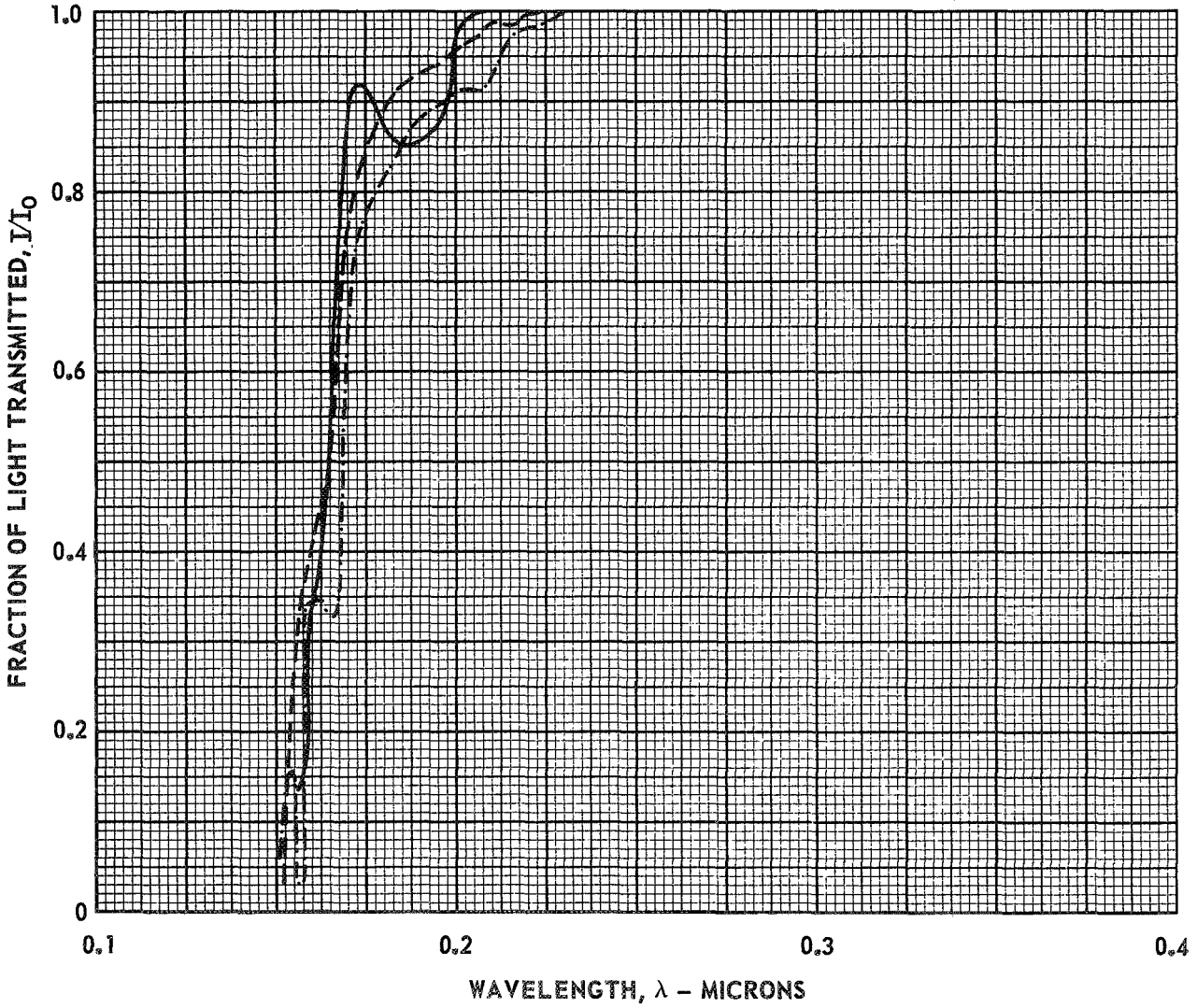

FIG. 30

TEMPERATURE VARIATIONS OF PHYSICAL PROPERTIES USED IN COOLANT TUBE HEAT TRANSFER ANALYSIS

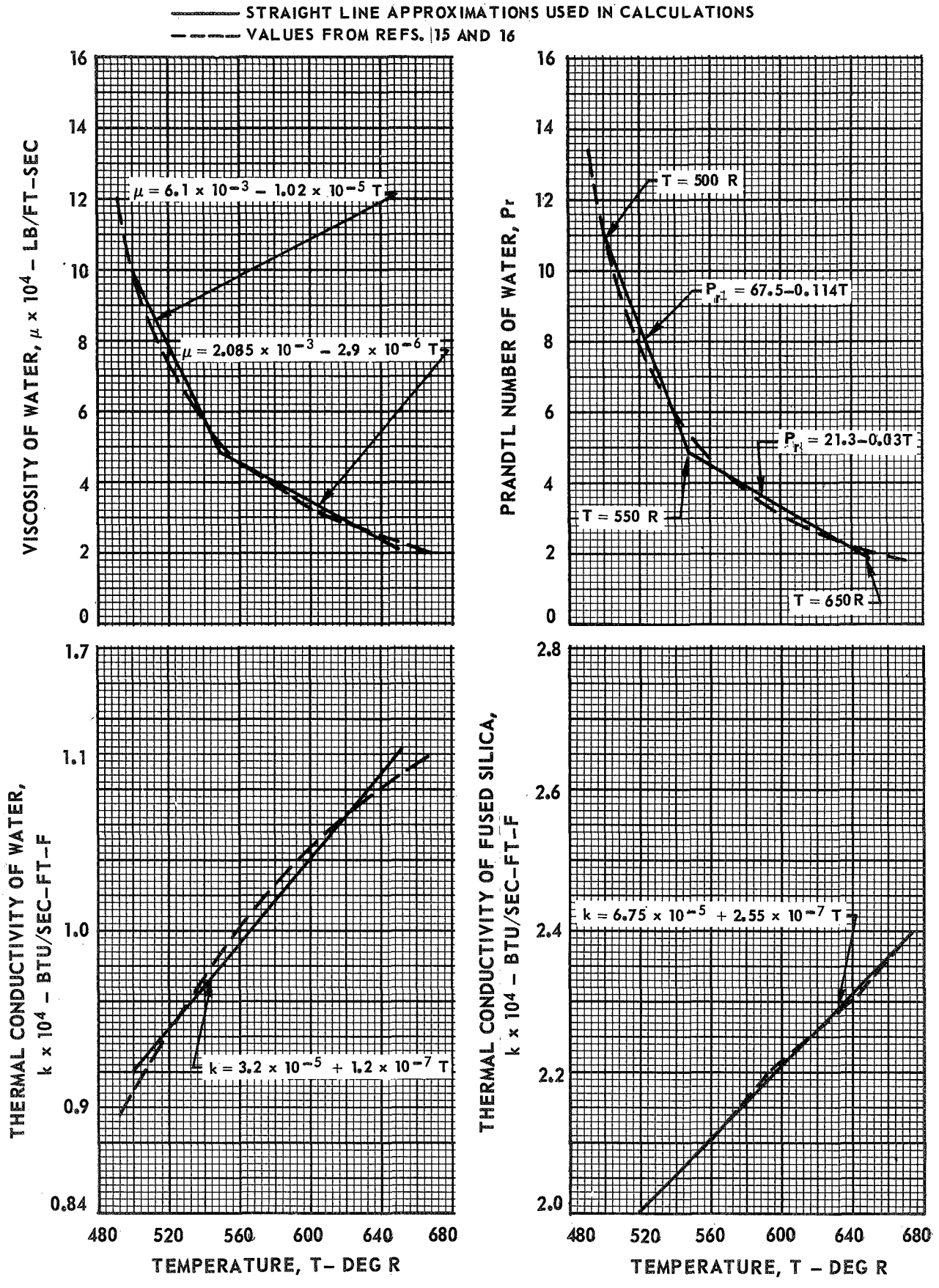

FIG. 31

CALCULATED WALL TEMPERATURE DISTRIBUTIONS ALONG A FUSED SILICA COOLANT TUBE

ASSUMES HEAT DEPOSITION IN COOLANT BY CONDUCTION THROUGH TUBE WALL ONLY

0.040-IN.-ID X 0.060-IN.-OD COOLANT TUBE (0.010-IN. WALL THICKNESS)

WATER COOLANT FLOW RATE, W_c = 1 GPM

LENGTH OF COOLANT TUBE, ℓ_c = 3 IN.

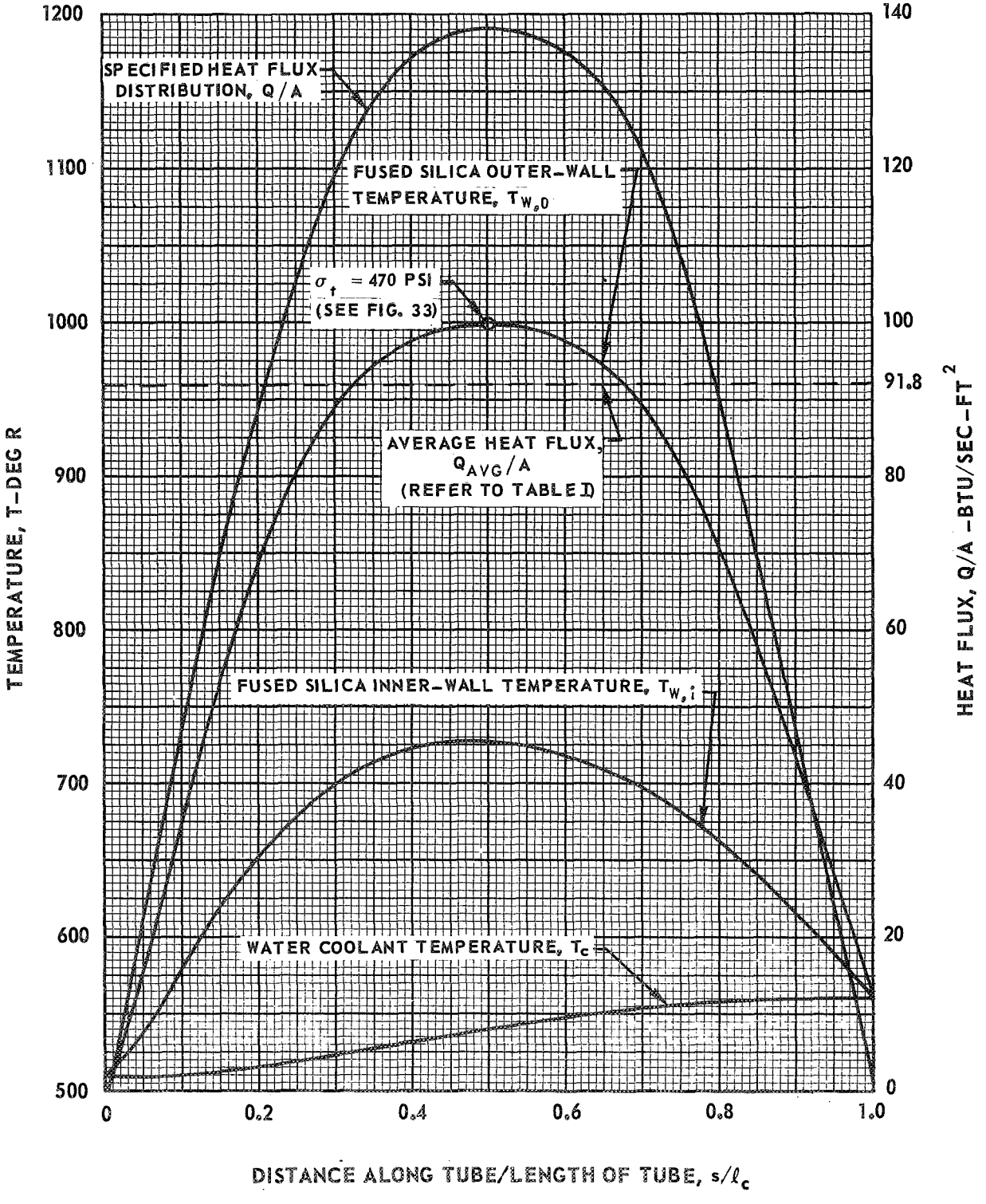

CALCULATED WALL TEMPERATURE DISTRIBUTIONS ALONG A FUSED SILICA COOLANT TUBE

ASSUMES HEAT DEPOSITION IN COOLANT BY CONDUCTION THROUGH TUBE WALL ONLY
SEE FIG. 15 FOR MODEL CONFIGURATION

WATER COOLANT FLOW RATE, W_c = 1.2 GPM
LENGTH OF COOLANT TUBE, ℓ_c = 3 IN.

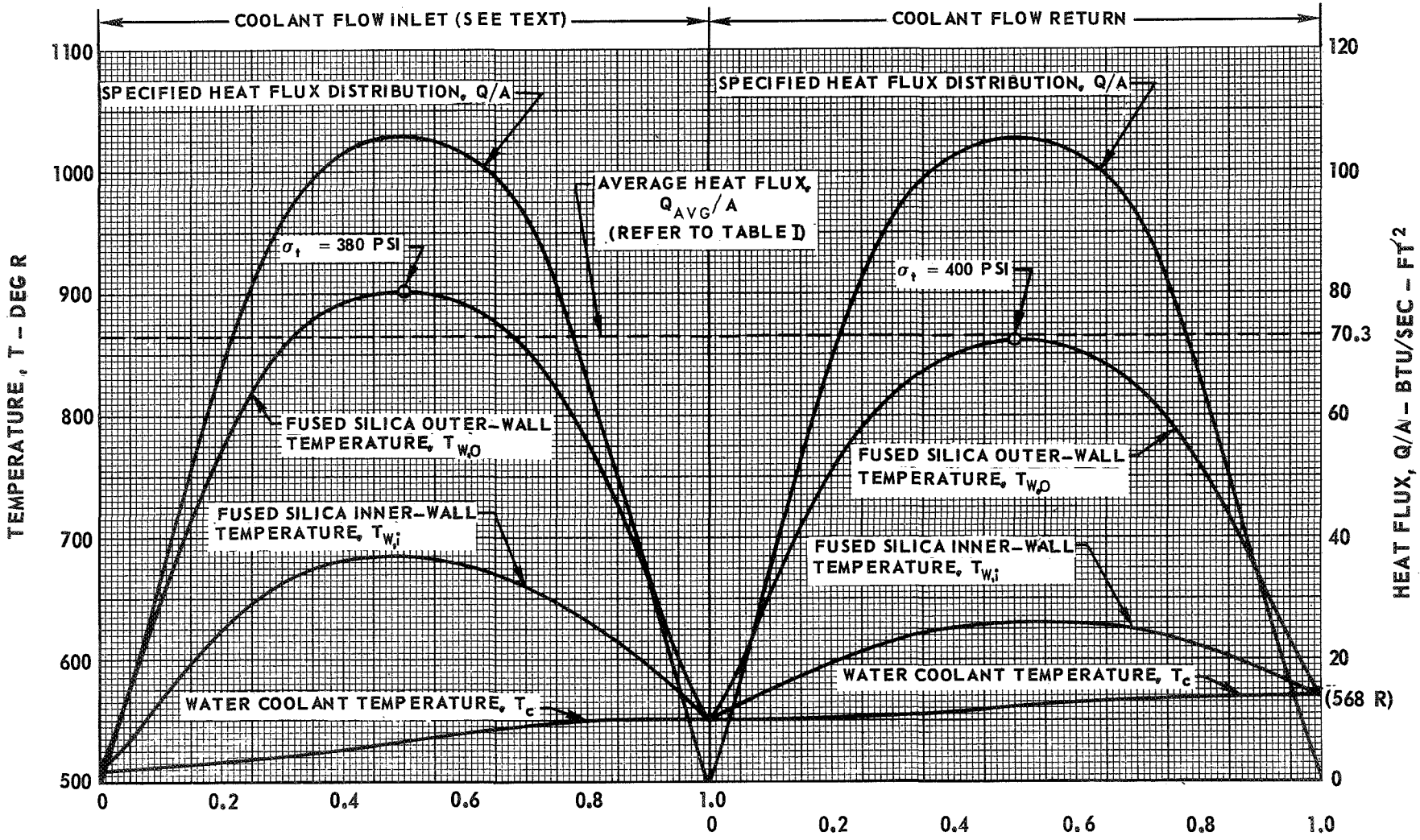

THERMAL STRESS IN FUSED SILICA TUBES

$$\sigma_t = \frac{E\alpha\Delta T}{2(1-\nu)} \quad \text{(SEE APPENDIX B)}$$

——— INCLUDES PROPERTY VARIATIONS WITH TEMPERATURE (REF. 15)

— — — EXCLUDES PROPERTY VARIATIONS WITH TEMPERATURE

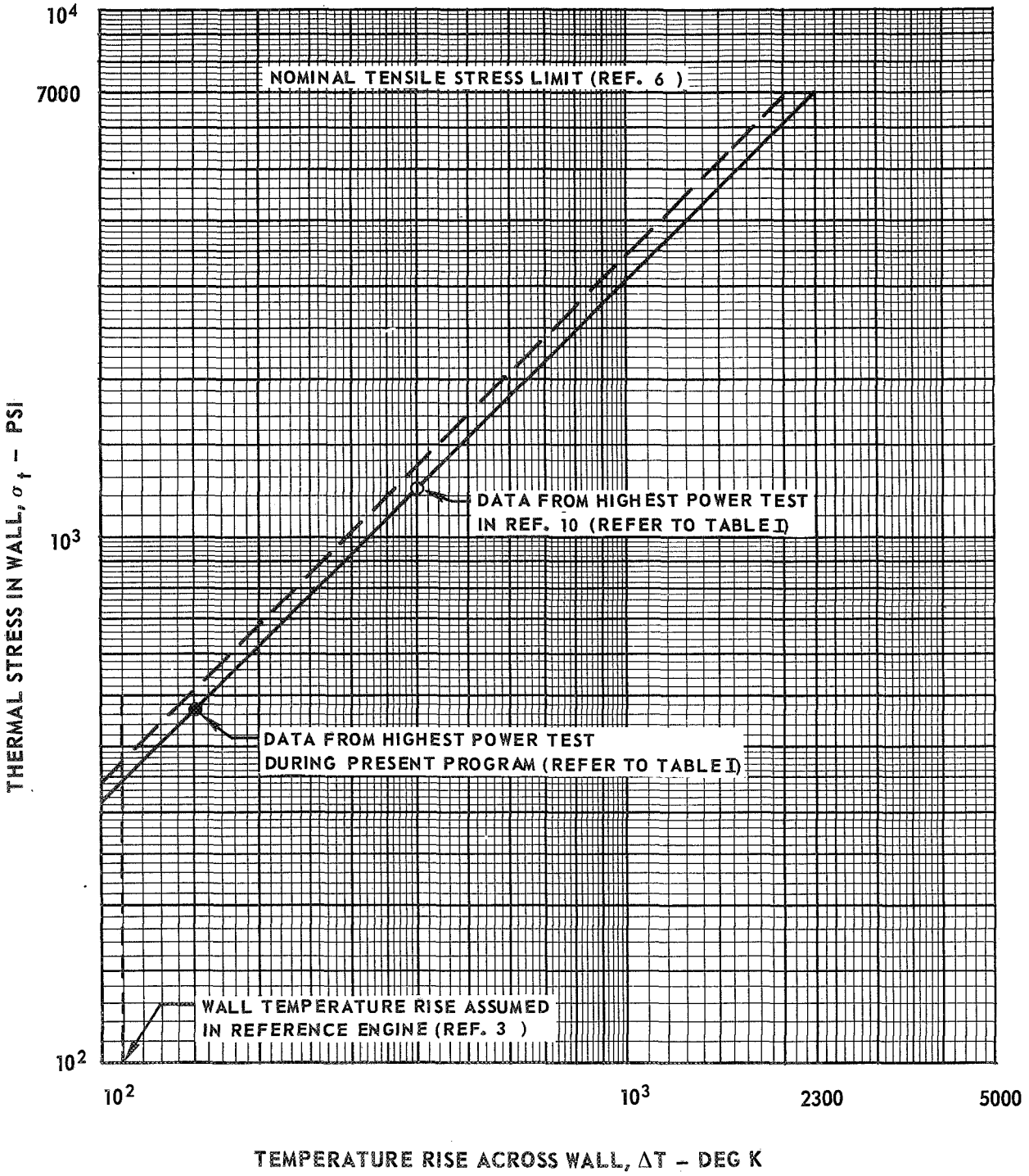

RESULTS OF HYDROSTATIC PRESSURE TESTS ON FUSED SILICA TUBES

(a) PHOTOGRAPH SHOWING TUBES BEFORE AND AFTER TESTING

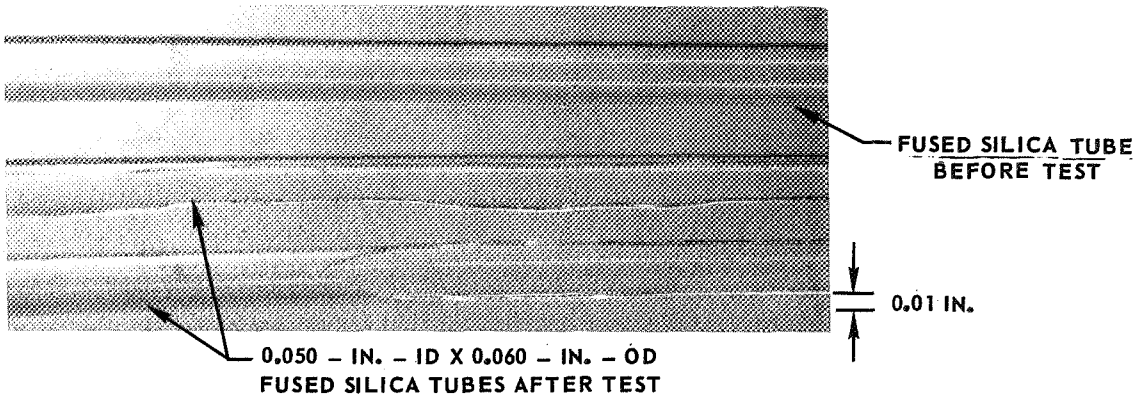

(b) PLOT OF HOOP STRESS VERSUS BURST PRESSURE

OPEN SYMBOLS DENOTE DATA FROM REF. 10
CLOSED SYMBOLS DENOTE DATA FROM PRESENT PROGRAM
— — — NOMINAL TENSILE STRESS LIMIT (REF. 6)

SYMBOL	TUBE DIMENSIONS
○	2.26–IN.–ID X 2.38–IN.–OD
△	2.22–IN.–ID X 2.38–IN.–OD
□	1.95–IN.–ID X 2.15–IN.–OD
◇	1.76–IN.–ID X 2.85–IN.–OD
◺	2.54–IN.–ID X 2.85–IN.–OD
D	0.05–IN.–ID X 0.06–IN.–OD

$$\sigma_H = \frac{P_B D}{2X}$$ (SEE APPENDIX B)

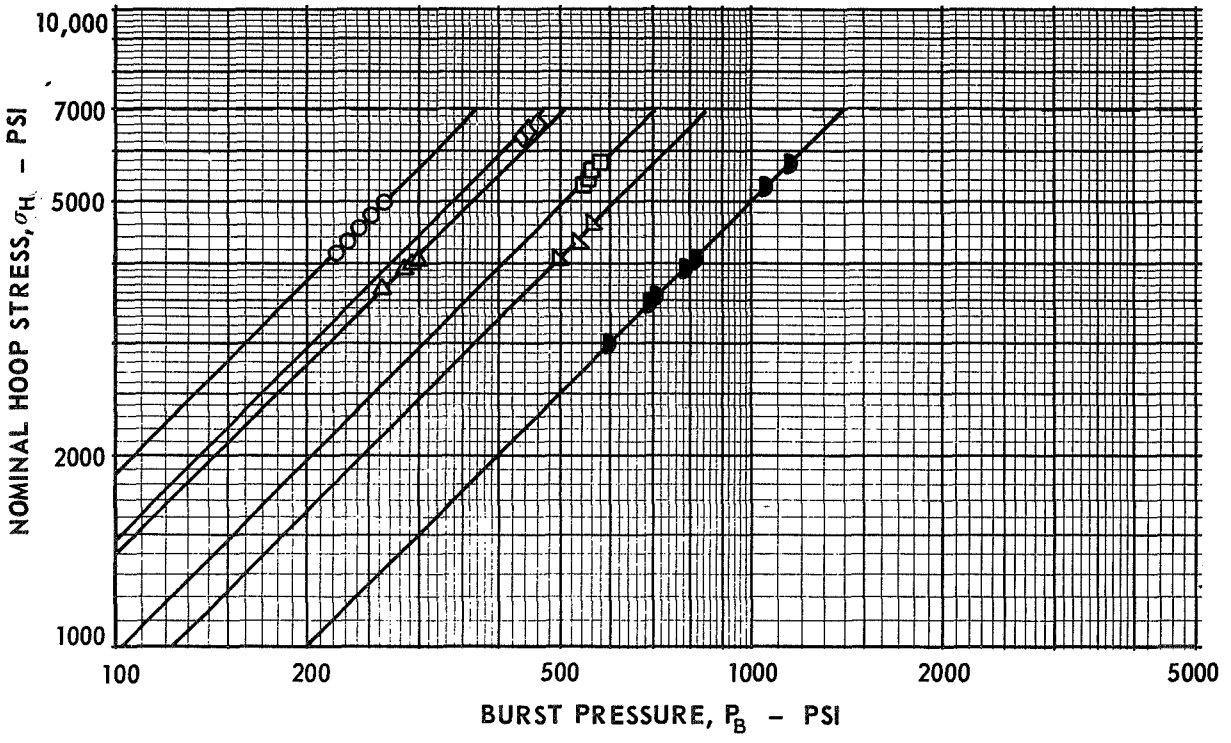

FLOW REGIMES POSSIBLE IN CONFINED VORTEX FLOWS

(a) RADIAL – INFLOW FLOW PATTERN

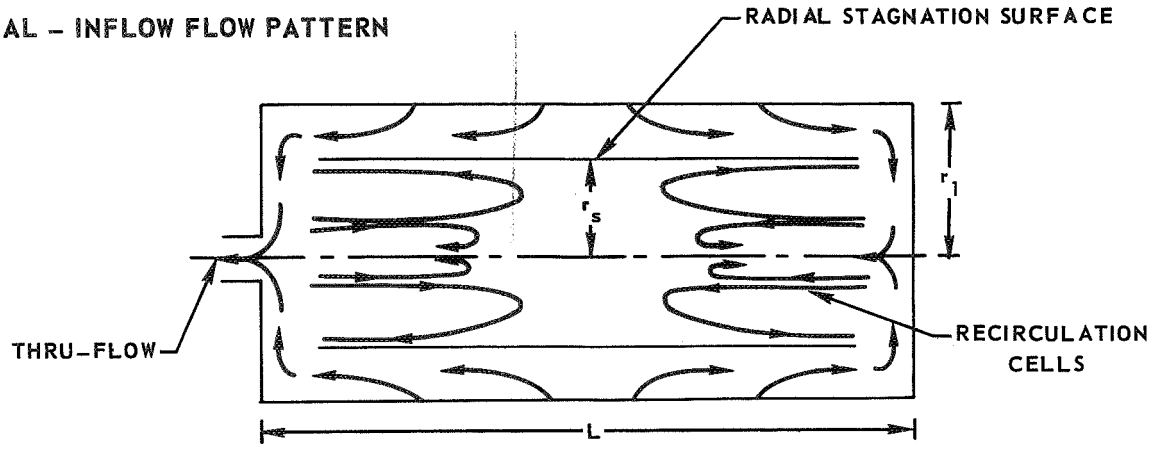

(b) SECONDARY FLOW REGIMES IN INCOMPRESSIBLE VORTEXES

FROM ANALYSIS OF REF. (20)

SECONDARY FLOW PARAMETER, $\beta_t = \frac{D}{L} \frac{Re_{t,p}^{4/5}}{Re_r}$

(RADIUS OF VORTEX TUBE)/(RADIUS OF THRU–FLOW PORT) = 10

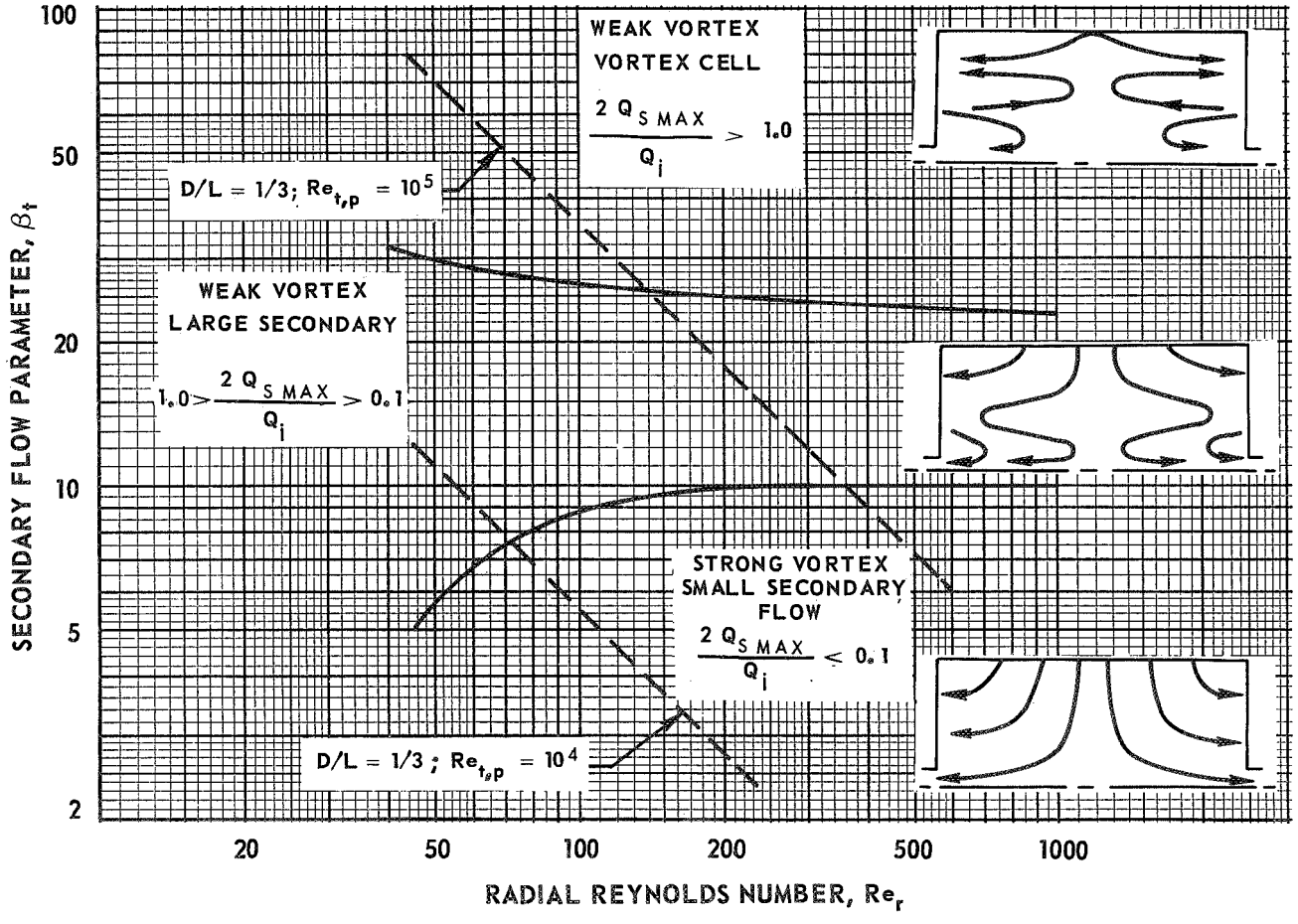

CHARTS USED TO DETERMINE INJECTOR CONFIGURATIONS FOR AXIAL – COOLANT – TUBE MODELS

(a) CHART FOR DETERMINING REQUIRED INJECTION AREA

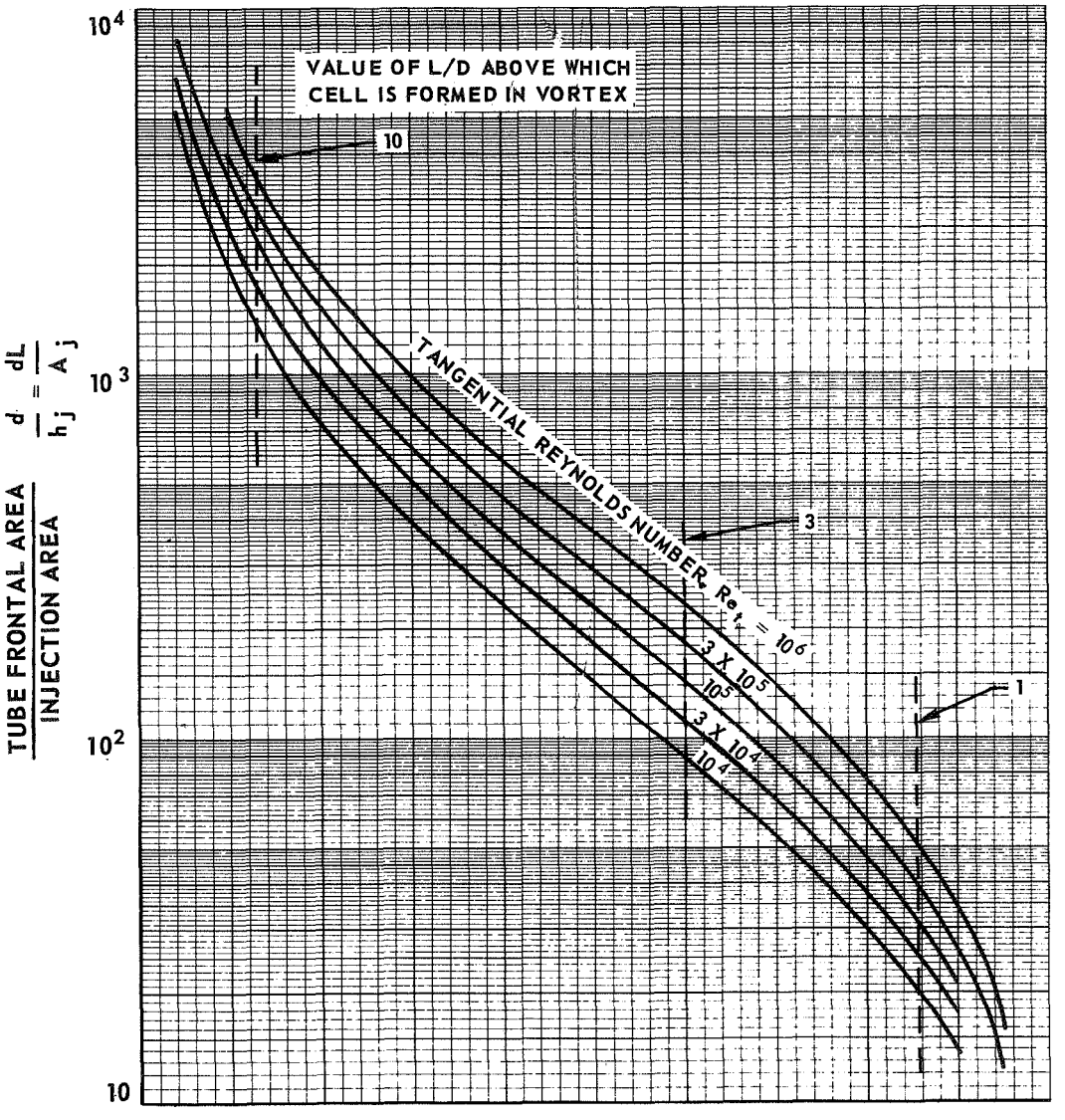

(b) CHART FOR DETERMINING APPROXIMATE POSITION OF RADIAL STAGNATION SURFACE

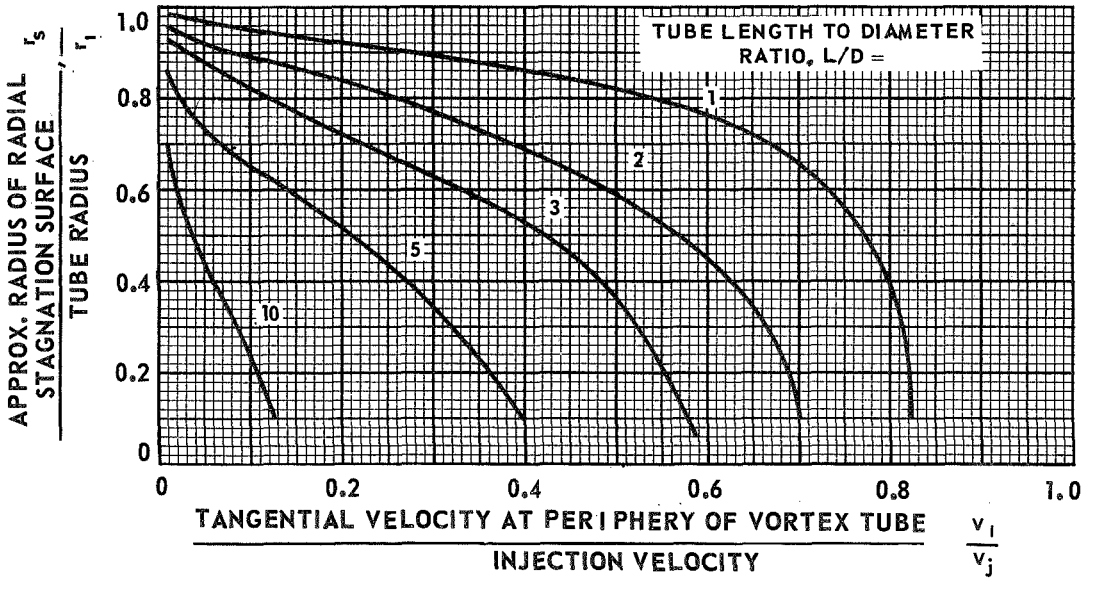


UNITED AIRCRAFT CORPORATION